LANGZEITVERHALTEN VON POLYKRISTALLINEN OXIDFASERN BEI HOHEN TEMPERATUREN

LONG-TERM BEHAVIOR OF POLYCRYSTALLINE OXIDE FIBERS AT ELEVATED TEMPERATURES

Vom Fachbereich Produktionstechnik

der

Universität Bremen

zur Erlangung des Grades

Doktor-Ingenieur

genehmigte

Dissertation

von

Dipl.-Ing. Renato Saint Martin Almeida

Gutachter:

Prof. Dr.-Ing. Kurosch Rezwan, Universität Bremen

Prof. Dr.-Ing. Dietmar Koch, Deutsches Zentrum für Luft- und Raumfahrt

Tag der mündlichen Prüfung: 27.10.2017

To the small circle of people that I call family.

Acknowledgements

A work of this extent could not have been accomplished within the time frame of four years without any help. Therefore, I believe that it is more than fair to start this thesis by acknowledging the people who were part of or helped this project in a direct or indirect way. This work was conducted in the Advanced Ceramics group of the University of Bremen (Bremen, Germany). Hence, I would like to start by thanking my supervisor and first reviewer Prof. Dr.-Ing. Kurosch Rezwan for the opportunity given to me. My second reviewer Prof. Dr.-Ing. Dietmar Koch from the German Aerospace Center (DLR, Stuttgart, Germany) is also acknowledged for the interest in my work. Additionally, I express my sincere gratitude to Prof. Dr.-Ing. Georg Grathwohl for being part of this last step of my education even after his retirement.

I extend my acknowledgments to my direct supervisor Dr.-Ing. Kamen Tushtev for all his trust and support to my work, and to the other colleagues of the CMC group who helped me a lot in the beginning of my PhD, in special to: Eike Volkmann, Jürgen Horvath, Thomas Schumacher.

This project could not have started/finished without the cooperation with other institutes. In this sense, I further thank Dr. Bernd Clauß from the German Institutes of Textile and Fibers research (DITF, Denkendorf, Germany) for supplying the test materials and important input given. I also thank Dr. Hanna Lührs from the MAPEX group of the University of Bremen for the extensive XRD analysis performed and fruitful discussions.

As it will be evidenced along the text, part of this research project was done by very motivated students, with whom I had a pleasant time and also befriended. I like to think that I have taught them an amount equivalent to their hard work in the labs. Therefore, I thank the following students: Amrit Singh, Dieter Zahn, Thomas Ganser, Lena Cramer, Mohannad Alghazawi, Bruno Eggert, Eduardo Bergmüller, João Paulo Rescala, Ernest Anyanwu Chiedozie, Jéssica Mainardi and Marcelo Rech.

Now that I think, 4 years is a long period. Therefore, I`m also grateful for the great working colleagues and friends that I had during this time as I actually spent more time with them than

with my own family. Perhaps they are not directly related to the research work, but the eventual beers after 4 p.m., dancing in the roof top, and virtually "killing" each other once a week, are all acknowledged. In this sense, I thank my colleagues (in the alphabetic order so they do not fight for it): Ana Rei, Benjamin Besser, Daniel Carmona, Gesa Hollermann, Huixing Zhang, Reshma Kadam, Silvia Abarca, Thamires Canuto, Tobias Bollhorst, Torben Halfer, Victor Lauth.

Here, I would also like to thank my family, not only for the support given to me during my PhD and all my education, but also for always encouraging me to become a better person. Hence, I`m grateful to my mother Fátima S. M. Almeida, my two brothers Alberto and Flávio, and my fiancée Daniela Weber.

Finally, I thank the "National Counsel of Technological and Scientific Development" (CNPq, Brasília, Brazil) for financing my scholarship (237936/2012-7) in the frame of the program Science without Borders (CsF).

Abstract

Ceramic matrix composites based on oxide materials have gained more attention in the last decades, because of their chemical stability, strength and considerably high toughness. The development of this class of material was only possible due to the appearance of suitable oxide fibers. Currently available fibers are based either on alumina for high strength, or on mullite for better long-term performance. However, it is well known that these fibers are prone to loss of their mechanical properties above 1000°C. Although high, these temperatures are easily reached during processing and in-field applications of composites. Therefore, the aim of this work is to study the mechanical behavior and the degradation mechanisms of oxide fibers at elevated temperatures. For that, two mullite fibers were evaluated: the well-established mullite–alumina Nextel™ 720, and the fully crystalline mullite fiber CeraFib 75. Both fibers were analyzed before and after heat treatments at temperatures ranging 1000-1400°C for 25 h. The characterization approach included microstructural analyses, as well as creep and tensile tests at room and high temperatures. For comparison, the same procedure was conducted with the alumina fibers Nextel™ 610 and CeraFib 99. As-received Nextel™ 720 fibers present a microstructure of mullite grains with smaller α-alumina grains, whereas the microstructure of CeraFib 75 consists basically of mullite with traces of γ-alumina. The higher amount of mullite in CeraFib 75 resulted in lower room-temperature strength. Still, CeraFib 75 showed higher strength retention than Nextel™ 720 at temperatures above 1200°C, while the measured creep rates were in the same order of magnitude. With the thermal treatments performed, two microstructural changes were observed: grain growth and dissociation of the mullite phase. The kinetics of these reactions were quantified and related to the mechanical performance of the fibers. Thus, a strength decrease was observed for all oxide fibers mainly due to grain growth. On the other hand, the phase transformations caused by the thermal exposures improved the thermal stability of the fibers. As a consequence, the treated fibers were more resistant to creep, *i.e.*, the creep rates decreased. In summary, this work presents a more detailed analysis on the long-term behavior of oxide fibers at high temperatures. Based on these results, it is suggested that a fiber with a chemical composition near to the stoichiometric 3/2 mullite would have higher thermal stability.

BLANK PAGE

Zusammenfassung

Oxidbasierte Keramische Verbundwerkstoffe haben in den letzten Jahrzehnten wegen ihrer chemischen Stabilität, Festigkeit und erheblichen Bruchzähigkeit an Bedeutung gewonnen. Die Entwicklung dieser Materialklasse war nur möglich aufgrund der Kommerzialisierung von geeigneten Oxidfasern. Derzeit erhältliche Fasern basieren entweder auf Aluminiumoxid für eine hohe Festigkeit, oder auf Mullit für eine erhöhte Lebensdauer. Diese Fasern verlieren allerdings zunehmend ihre mechanischen Eigenschaften bei Temperaturen über 1000°C. Obwohl diese Temperaturen vergleichsweise hoch sind, werden sie leicht während der Herstellung und in Anwendungsbereichen von Verbundwerkstoffen erreicht. Das Ziel dieser Arbeit ist es, dieses mechanische Verhalten und die Gefügeveränderung von Oxidfasern bei erhöhten Temperaturen zu untersuchen. Dafür wurden zwei unterschiedliche Mullitfasern untersucht: die bekannte Mullit-Aluminiumoxid Faser Nextel™ 720 und die kristalline Mullitfaser CeraFib 75. Beide Fasern wurden bei Temperaturen zwischen 1000-1400°C für 25 h ausgelagert und sowohl davor, als auch danach analysiert. Der Charakterisierungsansatz umfasste mikrostrukturelle Analysen, sowie Kriech- und Zugversuche bei Raum- und bei hohen Temperaturen. Zum Vergleich wurde die gleiche Prozedur mit den Aluminiumoxidfasern Nextel™ 610 und CeraFib 99 durchgeführt. Nextel™ 720 Fasern weisen eine Mikrostruktur von Mullitkörnern mit kleineren α-Aluminiumoxidkörnern auf, wohingegen CeraFib 75 eine Mikrostruktur zeigt, die hauptsächlich aus Mullit mit Spuren von γ-Aluminiumoxid besteht. Der höhere Mullitanteil in CeraFib 75 ergab eine geringere Festigkeit bei Raumtemperatur. Dennoch zeigte CeraFib 75 eine höhere Festigkeit als Nextel™ 720 bei Temperaturen über 1200°C, während die gemessenen Kriechraten in der gleichen Größenordnung waren. Bei den durchgeführten Wärmebehandlungen konnten zwei mikrostrukturelle Veränderungen beobachtet werden: Kornwachstum und Dissoziation der Mullitphase. Die Kinetik dieser Reaktionen wurde quantifiziert und auf das mechanische Verhalten der Fasern bezogen. Somit wurde eine Festigkeitsverringerung für alle Oxidfasern beobachtet, hauptsächlich verursacht durch Kornwachstum. Die Phasenumwandlungen, verursacht durch die thermische Auslagerung hingegen, resultierten in einer verbesserten thermischen Stabilität. Folglich waren die Fasern widerstandsfähiger gegen Kriechverformung, d.h. die Kriechrate nahm ab. Die hier präsentierten Ergebnisse zeigen eine detailliertere Analyse des Langzeitverhaltens von oxidkeramischen Fasern bei hohen Temperaturen. Daraus schlussfolgernd wird erwartet, dass Fasern mit einer Zusammensetzung nahe der stöchiometrischen Zusammensetzung von 3/2 Mullit eine erhöhte thermische Stabilität aufweisen.

BLANK PAGE

List of figures

List of acronyms, symbols and abbreviations

A	Creep rate proportionality constant
a, b, c	Lattice parameters
A_0	Initial area
A_B	Bundle initial area
A–D	Anderson–Darling statistic
AE	Acoustic emission
AR	As-received
C_h	Compliance of heated region
C_i	Compliance
CMC	Ceramic matrix composite
C_p	Compliance of the tensile testing machines
DDT	Duration discrimination time
Δl	Displacement
E	Elastic modulus
E_B	Bundle elastic modulus
EDX	Energy-dispersive X-ray
ε	Strain
ε_0	Characteristic strain to failure
ε_h	Strain of heated region
ε_T	Total creep strain

F	Force
F_{MAX}	Maximum force
HT	Heat treatment
L_0	Initial length
L_{eff}	Effective length of creep test
L_h	Length of heated region
m	Weibull modulus
n	Creep stress exponent
Ox-CMC	Oxide-oxide ceramic matrix composite
p	Creep inverse grain size exponent
P	Failure probability
Q	Creep activation energy
R	Universal gas constant, 8.314 J/(mol K)
RT	Rearm time
ρ	Density
ρ_l	Density of standard liquid
SEM	Scanning electron microscope
σ	Stress, Strength
σ_0	Characteristic strength
T	Temperature
T_h	Temperature of the heated region
W, W_l	Weight, Apparent immersed weight
XRD	X-ray diffraction

Table of contents

1 Introduction

Energy efficiency is a very recurrent topic nowadays. A recent example of that is the project Environmentally Responsible Aviation (ERA) from the National Aeronautics and Space Administration (NASA, Washington, USA). The project aims to reduce the fuel consumption, emissions and noise level of aircrafts that will enter in service around 2020 [1]. This can be achieved by lighter components that can operate at temperatures higher than conventional metallic alloys. Under these requirements, ceramic matrix composites (CMC) are very promising candidates since they show low density, high strength and considerable toughness [2, 3]. The concept of reinforcing a fragile matrix with ceramic fibers to produce a "non-brittle" material dates to the mid 1970s [4]. Back then, the development of CMCs was based on non-oxide systems like C/SiC due to their high strength and thermal stability. However, their application range is limited since they are prone to oxidation at intermediate temperatures [5, 6]. This is of particular concern in combustion environments, like in aircraft engines. Therefore, a great effort has been made towards the development of CMCs with all oxide materials (Ox-CMCs).

Ox-CMCs are normally based on alumina or alumino-silicates, which provide a high chemical stability, but lower strength in comparison to non-oxide materials. The development of this class of composite started only in the 1990s [7]. The "delay" on their development was due to the lack of high-strength fibers. Oxide fibers have been commercialized since the late 1970s [8]. Still, the fibers of that time were either too weak, or too fragile to be weaved [9]. This would change only in 1993 with the appearance of the alumina fiber Nextel™ 610 [10]. This fine grained fiber was developed by Minnesota Mining and Manufacturing Company (3M Co., Minnesota, USA), and presents a strength of 3100 MPa [11]. Even today, Nextel 610 is still considered the strongest oxide fiber in the market. Following the success of their alumina fiber, 3M released later the mullite–alumina fiber Nextel™ 720 for high-temperature applications. This fiber shows a strength of 2100 MPa, and is the most creep resistant oxide fiber [12]. As a consequence, current Ox-CMCs normally use either Nextel 610 or Nextel 720, and can present strength levels up to 400 MPa [13, 14]. Nowadays, Ox-CMCs are being employed in the aerospace and aircraft sectors, like in the project ERA mentioned

before, as well as other industrial applications such as hot gas filters and tools for high-temperature ovens [15].

The high strength of the current oxide fibers is based on their refined microstructure containing grains in the nanometer scale [12]. However, these microstructures are not stable at elevated temperatures. As a consequence, the fibers are susceptible to loss of their mechanical properties above 1000°C [16, 17]. This is a rather concerning fact, especially considering that temperatures as high as 1200°C can be achieved, not only in some of the aforementioned applications, but also during the processing of the composites. Therefore, several authors have studied the thermal stability of Nextel 610 and Nextel 720. This is normally accessed by performing tensile or creep tests at high temperatures [18-22], as well as analyzing the strength retention of the fibers after different thermal exposures [19, 23-25]. Here lies another problem as the results obtained by different authors are rather different and conflicting. Taking the strength retention of Nextel 720 as an example; while some authors mention that the fiber is quite stable after 100 h treatment at 1200°C [19], others report extensive degradation after only 2 h at the same temperature [24]. Nevertheless, there is normally a consensus that this degradation is possibly caused by microstructural changes like grain growth [23, 26] and thermally induced defects [16, 25]. Still, the author of this thesis acknowledges that microstructural observations and mechanical characterizations are normally studied separately. Furthermore, there is a lack of in situ experiments regarding the microstructural changes. Hence, the actual degradation mechanisms, and how they develop over time, are still uncertain.

Due to the thermal limitation of the available oxide fibers, one of the current development focuses on Ox-CMCs is the production of fibers with higher thermal stability. A good example are the two fibers developed by the German Institutes of Textile and Fiber research (DITF, Denkendorf, Germany), formerly known as ITCF Denkendorf, together with the German company CeraFib GmbH (Olbersdorf, Germany) [27]. With the trade name of CeraFib 99, this alumina fiber contains oxide dopants to inhibit grain growth. On the other side, CeraFib 75 is a fully crystalline fiber developed to overcome the thermal stability of the current oxide fibers. Nonetheless, there is still little information regarding their long-term performance at elevated temperatures. Here it is important to highlight that the understanding of these properties is crucial for the further development on oxide fibers, and therefore, improvement of Ox-CMCs.

1.1 Aim of the work

Given the problematic described above, the objective of this work is to study the mechanical behavior and microstructural evolution of oxide fibers at elevated temperatures. For this purpose, two mullite fibers, Nextel 720 and CeraFib 75, and two alumina fibers, Nextel 610 and CeraFib 99, were investigated. During the analyses, a higher focus was given to the mullite fibers, because they are designed for high-temperature applications. This could be evaluated with tensile and creep tests at temperatures ranging from 900°C to 1400°C. To access the thermal stability of the fibers, they were also characterized after thermal exposures to 1000-1400°C for 25 h. This investigation aimed to identify and understand the degradation mechanisms on oxide fibers at high temperatures. Thus, changes in the microstructure of the fibers were quantified with microscopy observations and X-ray diffraction analyses at room and elevated temperatures. These changes were then related to the room-temperature tensile properties of the fibers. In addition, the creep behavior of the treated fibers was also studied in detail. With the results of this research project, three peer-reviewed papers were published in international journals.

1.2 Structure of the thesis

To help the reader, this thesis is divided in eight chapters, starting with this general introduction to the topic. In Chapter 2, a proper contextualization and review of previous works in this research area are given. Chapter 3 describes the fibers and characterization methods employed, as well as the reason for their use and applicability. As previously mentioned, the main findings of this project were published elsewhere, and are adapted in Chapters 4, 5 and 6. Within these chapters, only the results of the mullite fibers are discussed. The main results obtained with the alumina fibers are summarized in Appendix A.1. The initial results of the as-received mullite fibers are detailed in Chapter 4. This includes microstructural characterizations, and the study of the mechanical behavior and deformation mechanisms at room and elevated temperatures by tensile and creep tests [28]. Chapter 5 discusses the influence of thermal exposures on the microstructure, strength retention and load redistribution capability of the treated fibers [29]. The long-term behavior of the fibers is further evaluated in Chapter 6. Within this chapter, the kinetics of crystal phase transformation at 1200°C is quantified, and the creep performance of fibers previously heat

treated is analyzed [30]. In the end, a summary of the project and ideas for its continuation are given in Chapters 7 and 8, respectively.

1.3 References

[1] F. Collier, R. Thomas, C. Burley, C. Nickol, C.-M. Lee, M. Tong. “Environmentally responsible aviation – Real solutions for environmental challenges facing aviation”, pp. 1-16 in *Proceedings of 27th International Congress of the Aeronautical Sciences*. Optimage Ltd. on behalf of the International Council of the Aeronautical Sciences, 2010.

[2] F. W. Zok. “Developments in oxide fiber composites”. Journal of the American Ceramic Society, vol. 89 (11), pp. 3309-3324, 2006.

[3] D. Koch, K. Tushtev, G. Grathwohl. “Ceramic fiber composites: Experimental analysis and modeling of mechanical properties”. Composites Science and Technology, vol. 68 (5), pp. 1165-1172, 2008.

[4] R. Naslain. “Design, preparation and properties of non-oxide CMCs for application in engines and nuclear reactors: an overview”. Composites Science and Technology, vol. 64 (2), pp. 155-170, 2004.

[5] N. S. Jacobson. “Corrosion of silicon-based ceramics in combustion environments”. Journal of the American Ceramic Society, vol. 76 (1), pp. 3-28, 1993.

[6] R. C. Robinson, J. L. Smialek. “SiC recession caused by SiO_2 scale volatility under combustion conditions: I, experimental results and empirical model”. Journal of the American Ceramic Society, vol. 82 (7), pp. 1817-1825, 1999.

[7] A. Evans, D. Marshall, F. Zok, C. Levi. “Recent advances in oxide-oxide composite technology”. Advanced Composite Materials, vol. 8 (1), pp. 17-23, 1999.

[8] A. K. Dhingra, N. Peacock, A. R. Ubbelohde, C. Manfre. “Alumina Fibre FP”. Philosophical Transactions of the Royal Society of London A: Mathematical, Physical and Engineering Sciences, vol. 294 (1411), pp. 411-417, 1980.

[9] A. R. Bunsell, M. H. Berger. “Fine diameter ceramic fibres”. Journal of the European Ceramic Society, vol. 20 (13), pp. 2249-2260, 2000.

[10] D. M. Wilson, D. C. Lueneburg, S. L. Lieder. “High temperature properties of Nextel 610 and alumina-based nanocomposite fibers”, pp. 609-621 in *Proceedings of 17th Annual Conference on Composites and Advanced Ceramic Materials: Ceramic Engineering and Science*, J. B. Wachtman Jr. (Ed.). John Wiley & Sons, Inc., 2008.

[11] D. Wilson. “Statistical tensile strength of Nextel™ 610 and Nextel™ 720 fibres”. Journal of Materials Science, vol. 32 (10), pp. 2535-2542, 1997.

[12] D. M. Wilson, L. R. Visser. “High performance oxide fibers for metal and ceramic composites”. Composites Part A: Applied Science and Manufacturing, vol. 32 (8), pp. 1143-1153, 2001.

[13] R. A. Jurf, S. C. Butner. “Advances in oxide-oxide CMC”. Journal of Engineering for Gas Turbines and Power, vol. 122 (2), pp. 202-205, 2000.

[14] H. G. Halverson, W. A. Curtin. “Stress rupture in ceramic-matrix composites: Theory and experiment”. Journal of the American Ceramic Society, vol. 85 (6), pp. 1350-1365, 2002.

[15] A. Noeth, A. Rüdinger, W. Pritzkow. “Oxide ceramic matrix composites – Manufacturing, machining, properties and industrial applications”. Ceramic Applications, vol. 3, pp. 48-54, 2015.

[16] P. E. Cantonwine. “Strength of thermally exposed alumina fibers – Part I. Single filament behavior”. Journal of Materials Science, vol. 38 (3), pp. 461-470, 2003.

[17] M. Schmücker, F. Flucht, P. Mechnich. “Degradation of oxide fibers by thermal overload and environmental effects”. Materials Science and Engineering: A, vol. 557 (0), pp. 10-16, 2012.

[18] J. A. DiCarlo. “Creep limitations of current polycrystalline ceramic fibers”. Composites Science and Technology, vol. 51 (2), pp. 213-222, 1994.

[19] D. M. Wilson. “New high temperature oxide fibers”, pp. 1-12 in *High Temperature Ceramic Matrix Composites*, W. Krenkel, R. Naslain, H. Schneider (Eds.). Wiley-VCH Verlag GmbH & Co. KGaA, 2002.

[20] F. Deléglise, M. H. Berger, A. R. Bunsell. “Microstructural evolution under load and high temperature deformation mechanisms of a mullite/alumina fibre”. Journal of the European Ceramic Society, vol. 22 (9–10), pp. 1501-1512, 2002.

[21] C. J. Armani, M. B. Ruggles-Wrenn, G. E. Fair, R. S. Hay. “Creep of Nextel™ 610 fiber at 1100°C in air and in steam”. International Journal of Applied Ceramic Technology, vol. 10 (2), pp. 276-284, 2013.

[22] C. J. Armani, M. B. Ruggles-Wrenn, R. S. Hay, G. E. Fair. “Creep and microstructure of Nextel™ 720 fiber at elevated temperature in air and in steam”. Acta Materialia, vol. 61 (16), pp. 6114-6124, 2013.

[23] F. Deléglise, M. H. Berger, D. Jeulin, A. R. Bunsell. “Microstructural stability and room temperature mechanical properties of the Nextel 720 fibre”. Journal of the European Ceramic Society, vol. 21 (5), pp. 569-580, 2001.

[24] C. Milz, J. Goering, H. Schneider. “Mechanical and microstructural properties of Nextel™ 720 relating to its suitability for high temperature application in CMCs”, pp. 191-198 in *Proceedings of 23rd Annual Conference on Composites, Advanced Ceramics, Materials, and Structures*, E. Ustundag, G. Fischman (Eds.). John Wiley & Sons, Inc., 2008.

[25] R. S. Hay, G. E. Fair, T. Tidball. “Fiber strength after grain growth in Nextel 610 alumina fiber”. Journal of the American Ceramic Society, vol. 98 (6), pp. 1907-1914, 2015.

[26] M. D. Petry, T.-I. Mah. “Effect of thermal exposures on the strengths of Nextel™ 550 and 720 filaments”. Journal of the American Ceramic Society, vol. 82 (10), pp. 2801-2807, 1999.

[27] S. Petzold, M. Morche, J. Taesler. “Oxide-ceramic continuous fibres and ceramic fibre reinforced composites – Innovative materials for the firing process”. ZI International, vol. 64, pp. 24-31, 2011.

[28] R. S. M. Almeida, K. Tushtev, B. Clauß, G. Grathwohl, K. Rezwan. “Tensile and creep performance of a novel mullite fiber at high temperatures”. Composites Part A: Applied Science and Manufacturing, vol. 76 (0), pp. 37-43, 2015.

[29] R. S. M. Almeida, E. L. Bergmüller, B. G. F. Eggert, K. Tushtev, T. Schumacher, H. Lührs, B. Clauß, G. Grathwohl, K. Rezwan. “Thermal exposure effects on the strength and microstructure of a novel mullite fiber”. Journal of the American Ceramic Society, vol. 99 (5), pp. 1709-1716, 2016.

[30] R. S. M. Almeida, E. L. Bergmüller, H. Lührs, M. Wendschuh, B. Clauß, K. Tushtev, K. Rezwan. “Thermal exposure effects on the long-term behavior of a mullite fiber at high temperature”. Journal of the American Ceramic Society, vol. 100 (9), pp. 4101-4109, 2017.

2 State of the art

The objective of this chapter is to give the reader an overview on the topic of oxide fibers for high-temperature applications. In this sense, the literature review written below brings to the reader the explanation of terms, contextualization and extensive summary of the past works on this research topic. The chapter starts with an introduction to the main application area of oxide fibers, ceramic matrix composites. Then, an historical overview of the oxide fibers development is given. In the end, the state of the art of the main oxide fibers, Nextel 610 and Nextel 720, is described in relation to their mechanical properties. Within this review, the problematic and further research interests on oxide fibers are evidenced, which are mainly concerning the thermal stability of the fibers above 1000°C.

2.1 Ceramic matrix composites

Engineering materials are traditionally divided in three categories: polymers, metals and ceramics. These categories go along with the different chemical bonds that form these materials, and their resultant physical properties. For instance, the "weak" intermolecular bonds of polymers lead to materials that are flexible and easy to process. The bonding energy of metallic materials is higher, and therefore, metals are stronger than polymers, but still ductile. On the other side, ceramics have covalent or ionic bonds, resulting on materials with high strength and fragility. As it can be seen, each of these materials has very distinct properties and limitations. In order to combine the advantages of these different groups, the concept of composite materials has been studied. Basically, a composite consists of two or more materials that retain their characteristics, and yet, can achieve unique properties when they are combined. This concept has been extensively applied for structural materials since the 1940s [1]. In this sense, a composite normally consists of a continuous and softer phase, the matrix, which is strengthened by some type of reinforcement. Different geometries of reinforcements can be used such as fibers, whiskers, particles, etc. In many cases, the interface between the matrix and the reinforcements is also considered as a constituent of the composite, given the importance of this part on the proper load distribution between matrix and reinforcements [1].

In general, composites are classified depending on the type of matrix used [2]: polymer matrix composites (PMC), metal matrix composites (MMC) and ceramic matrix composites (CMC). As one can imagine, the concept of each of these composites differs depending on the properties of their base materials, and so are their limitations. Thus, CMCs are the ones that exceed on high-temperature applications given the superior thermal stability of ceramics.

CMCs are considered the newest class of composite materials. As mentioned before, ceramics show high strength and hardness, but suffer from catastrophic failure, *i.e.*, low toughness. The concept of reinforcing a ceramic matrix with ceramic fibers to achieve higher toughness was first investigated in the mid 1970s [3]. This might sound contradicting, since both constituents of a CMC are essentially brittle. Still, the idea is that the material will slowly crack at different regions while the whole component can still bear load through the fibers [4]; instead of the abrupt failure seen in monolithic ceramics. As a result, CMCs show a non-linear, quasi-plastic, behavior when they are stressed. As exemplified in Figure 2.1, CMCs might have lower strength in comparison to highly dense monolithic ceramics. Nevertheless, their higher damage tolerance compensates it for mechanical applications. After decades of development, and several efforts on reducing processing costs, CMCs are now present in different industrial sectors like aerospace, motor sport, power generation, kilns, etc [5-9]. For these applications, the composites are normally based on non-oxide, carbon (C) and silicon carbide (SiC), or oxide ceramics, alumina (Al_2O_3) and silica (SiO_2) [10].

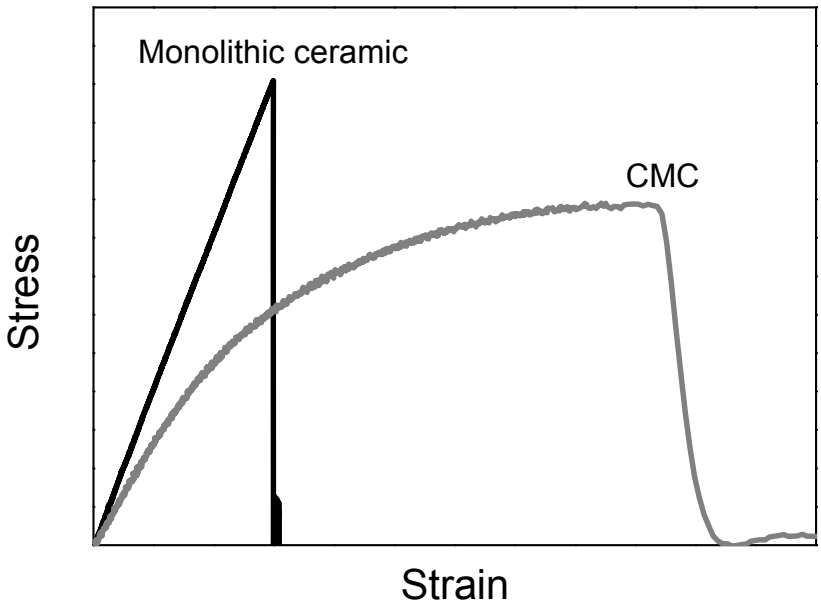

Figure 2.1: Example of stress *vs.* strain curve typical of monolithic ceramics and CMCs.

The non-linear behavior of CMCs, seen in Figure 2.1, is the result of different crack deflection mechanisms that act when the composite is stressed [10, 11]. During loading, it is presumed that the cracks are generated in the matrix, since it is the weakest part of the composite. To avoid the catastrophic failure of the whole component, the matrix cracks should not propagate through the fibers. Therefore, it is necessary to adjust the properties of fiber and matrix, as well as the interface resistance between them [12]. In this sense, He and Hutchinson [13] proposed different criteria for crack deflection to happen. In summary, if the matrix is sufficiently weak, micro-cracking will happen throughout the matrix, and the cracks can be deviated close to the fiber-matrix interface. When the stiffness of the matrix is similar to the fibers, *i.e.*, dense matrices, the interface between them should be weak enough so that the cracks do not propagate to the fibers [14]. Considering those criteria, crack deflection can be then achieved by producing a porous matrix [15], Figure 2.2b, or a weak interface, either with a weak coating [11] or by leaving a gap between fiber and matrix [16], Figure 2.2c and Figure 2.2d, respectively. In both cases, considerable mechanical energy is released during crack deflection, which in turn, relieves the concentrations of stress in the fibers by debonding and pull-out, cf. Figure 2.2a. The "failure" of the composite, maximum stress of Figure 2.1, will then happen only after a considerable amount of fibers have failed.

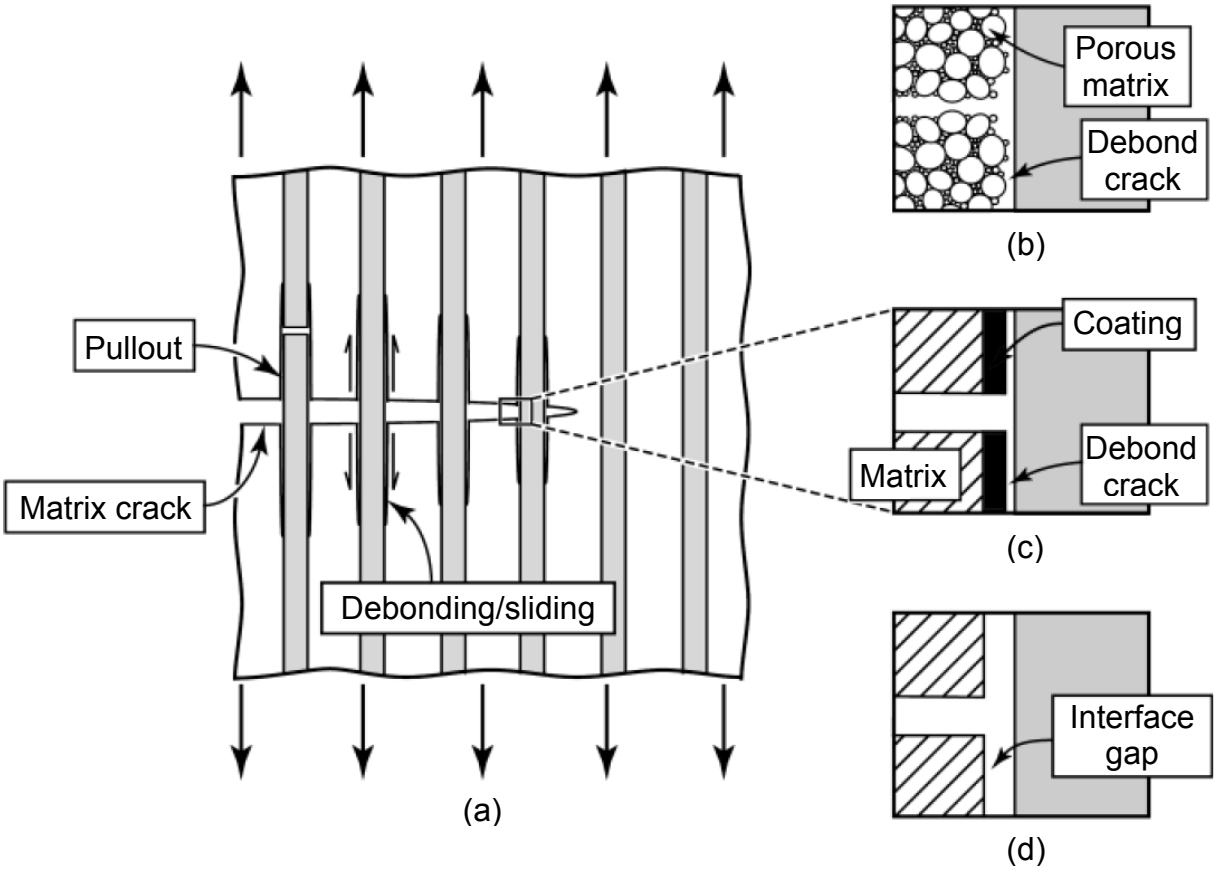

Figure 2.2: Microstructural concepts for enabling crack deflection in continuous-fiber ceramic composites. Adapted from [10].

2.2 Oxide CMCs

As the name implies, the most interesting feature of making a CMC only with oxide materials (Ox-CMCs) is their natural oxidation resistance. Depending on the application, this chemical resistance makes up for the lower strength of oxide ceramics in comparison to non-oxide CMCs. Examples of oxides for composites are alumina, zirconia (ZrO_2) and different alumino-silicates like mullite ($Al_2O_3 \cdot SiO_2$). Before talking in more detail about the development of Ox-CMCs however, it is important to mention the earlier development of non-oxide CMCs. As mentioned before, the first investigations on CMCs date back to the mid 1970s. At that time, the main focus was on the development of composites based on C or SiC [3]. This preference is understandable given the high thermal stability of these materials; not to mention the lack of high-strength oxide fibers at that time [17]. Nevertheless, with the increasing interest on components that can operate at oxidizing atmospheres and high temperatures, non-oxide CMCs became less suitable because they are prone to oxidation [18,

19]. One solution found was to protect these CMCs with coatings [20], but that would increase the already high cost of CMCs. Hence, a more viable option would be the development of all-oxide CMCs. Still, this was only possible in the 1990s with the appearance of suitable oxide fibers [10].

Nowadays, Ox-CMCs are mature enough to be present in different industrial applications. This is the result of the efforts from different universities and research centers from USA, Germany and France. A few companies that produce Ox-CMCs in a commercial scale can also be cited: COI Ceramics Inc. (California, USA), Walter E.C. Pritzkow Spezialkeramik (Filderstadt, Germany) and WPX Faserkeramik GmbH (Troisdorf, Germany). Current composites show high strength, see Table 2.1, and fracture toughness higher than 10 MPa $m^{0.5}$ [21]. It has been shown that 1D composites can even exceed 400 MPa of strength [22]. In addition, the crack-deflection in Ox-CMCs is commonly achieved by porous matrices [15, 23-25], although investigations using weak coatings, like La-monazite, can also be found [26, 27].

Table 2.1: Mechanical properties of several commercial 2D oxide composites under in-plane tensile loading.

Composite	Manufacturer	Fiber volume (%)	Tensile strength (MPa)	Elastic modulus (GPa)	Ref.
N312/AS	COI	48	125	31	[28]
N610/A	WPX	37	170	145	[29]
N610/AS	COI	51	366	124	[28]
N610/AZ	Pritzkow		190	123	[30]
N720/A	COI	44	169	60	[31]
N720/AM	COI	40	165	67.5	[32]
N720/AS	COI	48	179	77	[28]

Fibers: Nextel 312 (N312); Nextel 610 (N610); Nextel 720 (N720);
Matrices: Alumina (A); Silica (S); Zirconia (Z); Mullite (M).

Originally designed for aero and power turbines [33], the further development of Ox-CMCs allowed them to gain space in several industrial applications. Naturally, the main application area of Ox-CMCs is in components of gas turbine engines for aircraft [34], aerospace [35], power generation [36, 37]. As mentioned before, recent examples of this application were

seen in the frame of the project ERA, in which several companies are betting on oxide components for aircraft engines [38, 39]. An example of such component can be seen in Figure 2.3. The aerospace industry also benefits from Ox-CMCs for the thermal protection of re-entry vehicles due to the telemetry properties of oxide materials [40, 41]. More recently, the German Aerospace Center (DLR, Germany) developed an Ox-CMC capsule that can survive the re-entry temperature of 2000°C [41]. With the different processing techniques available, which allow the production of complex shape components at a reasonable cost, several other industrial applications can be mentioned. Examples that can be given are: hot gas exhaust systems [28, 42], industrial burners [9], combustor liners [43], thermal protection [44] and tools for furnaces [9, 45]. In these cases, temperatures of 600-1200°C at oxidizing atmospheres are expected [9]. Hence, the higher cost of Ox-CMCs in comparison to conventional alloys is justified, since they enable higher efficiency and longer lifetime of the components, see Figure 2.4.

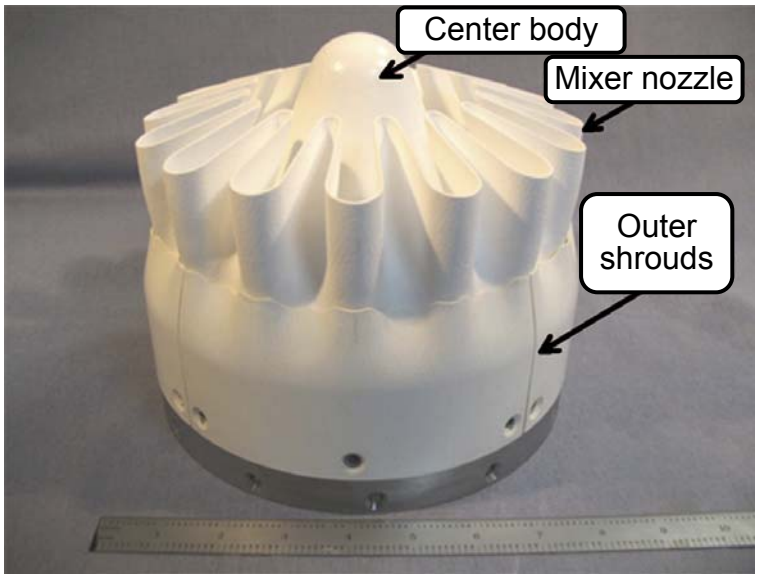

Figure 2.3: Subscale oxide/oxide CMC mixer nozzle assembly from NASA. Adapted from [46].

Figure 2.4: Ox-CMC flame tube as-processed (a) and after more than 20000 h of operation (b), in comparison to metallic flame tube (c) after only 1000 h of operation (d). Adapted from [9].

The current production of Ox-CMCs can be done by several processing techniques. In most cases, fiber fabrics or pre-forms are impregnated with a pre-ceramic fluid. This can be done by different ceramic slurry infiltration methods [17, 46], or even techniques based on polymer infiltration [47, 48]. This step is followed by the consolidation of the oxide matrix, either by pressureless sintering [49] or hot pressing [50, 51]. Usual sintering temperatures used are around 1200-1300°C for some hours. However, attention should be given to the processing parameters as it is known that the oxide reinforcements can degrade under such conditions [29, 52]. More details about the oxide fibers degradation and loss of strength are given in Section 2.4.3.

2.3 Oxide fibers

No one can argue that the development of oxide fibers was crucial for the research on Ox-CMCs. Fibers are used as the reinforcements in composites, and consequently, the mechanical properties of the composite highly depend on the fibers used. In the case of Ox-CMCs, the fibers also have an historical meaning. The development of Ox-CMCs in the mid 1990s was only possible after the commercialization of high-strength oxide fibers. In this sense, the current fibers are normally based on polycrystalline alumina. High strength is achieved by producing a nano-sized microstructure, while the necessary flexibility is obtained by reducing the diameter of the fibers to about 10 μm. Since it is hard to control grain growth and porosity in such small-diameter fibers, they are usually mixed with other oxide compounds like silica, zirconia, iron oxide (Fe_2O_3) or magnesium peroxide (MgO_2). Nonetheless, the addition of these compounds also reduces the stiffness of the fiber [53].

2.3.1 Fiber development

Although the development of Ox-CMCs was driven only in the 1990s, oxide fibers have been produced since the 1970s. These fibers, however, were not suitable for mechanical applications. The first pure alumina fiber to be produced for composites appeared in the late 70s [54]. Fibre FP was a fiber developed by DuPont (Delaware, USA) using the spinning technology. The fiber showed a microstructure of 500 nm corundum (α-alumina) grains, resulting in a strength of 1380 MPa and an elastic modulus of 379 GPa [55]. The main problem of that fiber was related to its relatively big diameter of 20 μm, which made the fiber too fragile to be weaved or braided. DuPont released later a fiber with the addition of 20 wt.% of tetragonal zirconia to improve the flexibility, the Fibre PRD-166. The addition of zirconia increased the fiber strength to 2070 MPa. This increase was related to the transformation toughening mechanism of the partially stabilized zirconia [56]. Still, Fibre PRD-166 was also too fragile to be handled without breaking. Thus, the company ceased the production of both fibers later.

From that point on, a higher focus was given to the increase of flexibility of alumina fibers for mechanical applications. This could be achieved either by reducing the fibers diameter, or by adding different compounds to the chemical composition of the fiber. In this sense, different companies started developing two-phase fibers like Altex [57], Nextel 312 [58], Nextel 440 [59], Nextel 480 [60]. Nonetheless, the applicability of these fibers was restricted to moderate/low temperatures. The presence of glassy phases severely reduced the strength and

creep resistance of the fibers at high temperatures [59, 61-63]. At the same time, other alumina [64] and sapphire (single alumina crystal) [65] fibers were developed. Then again, they were limited to isolation purposes and not for mechanical applications, because of their diameter [66]. One of the first α-alumina fibers suitable for weaving appeared in 1992 under the name of Almax. This fiber was developed by Mitsui Mining Co. (Tokyo, Japan), and has a diameter of 10 μm [67]. Unfortunately, the fiber presented a strength of only 1020 MPa, relatively low for a reinforcement. This low strength was associated to the grain size and high residual porosity of the fiber [68]. Nevertheless, the fiber is still commercialized nowadays.

Only in 1993 that 3M Co. released an alumina fiber suitable for CMCs, the Nextel 610 [69]. First investigations with the fiber pointed out a strength of 2100 MPa and elastic modulus of 380 GPa. After further development, the fiber shows now the outstanding strength of 3100 MPa [70]. The high strength of Nextel 610 is credited to its fine microstructure of 100 nm α-alumina grains, and the flexibility is guaranteed by its small diameter of 12 μm, cf. Figure 2.5. The refined microstructure of the fiber is achieved by the addition of grain growth inhibitors, SiO_2 and Fe_2O_3. Still, the main limitation of the fiber is regarding creep deformation and grain growth at temperatures higher than 1000°C [69]. Therefore, 3M developed the mullite–alumina fiber Nextel 720 in the following years [71]. This fiber has a microstructure of slightly miss-oriented mullite grains, forming 500 nm mosaics, and elongated α-alumina grains [72]. As a result, the strength of the fiber is of around 2100 MPa, and the elastic modulus of 260 GPa [70]. Yet, this fiber aims for high-temperature applications, and is considered the most creep resistant oxide fiber up to date [73, 74]. These two fibers had a great importance for the development of Ox-CMCs as their appearance called the attention back to oxide materials.

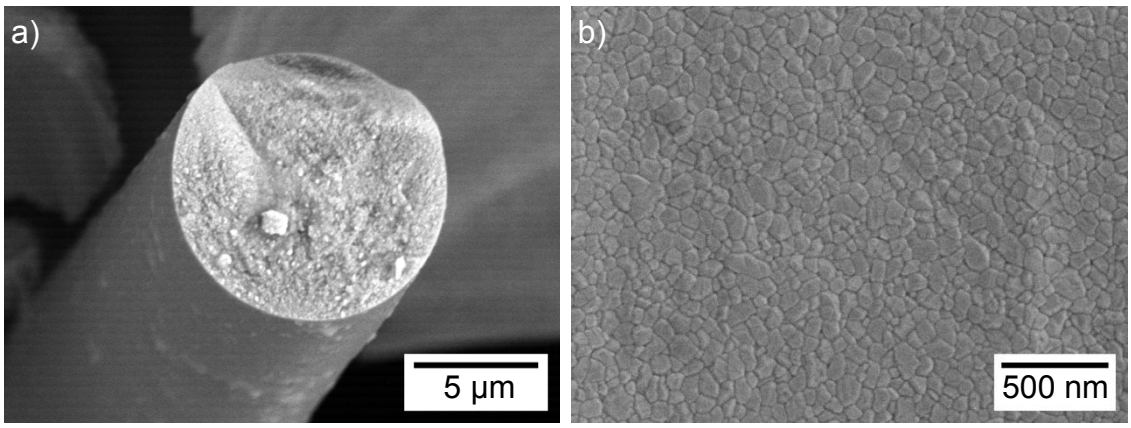

Figure 2.5: (a) Fracture surface of a Nextel 610 fiber with a diameter of approximately 12 µm. (b) Microstructure of as-received Nextel 610 showing approximately 100 nm alumina grains. Adapted from [17].

The current development of oxide fibers goes in the direction of producing fibers with higher thermal stability. As it will be evidenced in Section 2.4.2 and Section 2.4.3, creep and thermal degradation are important issues for oxide materials. In this sense, several works can be found in the literature about the production of new fibers that can overcome these temperature limitations. Attention is given to different chemical compositions like: alumina–silica [75], alumina–zirconia [76], mullite [77-79], zirconia [80, 81] and yttrium aluminum garnet (YAG) [82, 83]. It should be noted, however, that most of these studies face the problems of going from laboratory research to commercial production.

2.3.2 Currently available fibers

Several oxide fibers have been produced during the course of time. Therefore, there are quite some options for oxide fibers in the market nowadays. Table 2.2 presents a summary of the currently commercial oxide fibers. Due to their distinct properties, each one aims for different application areas. Still, the great majority of works on Ox-CMCs use either Nextel 610 or Nextel 720 as the reinforcement. This preference is somewhat understandable considering the high strength of Nextel 610, and the good creep performance of Nextel 720. More detailed information about the mechanical performance of both fibers is given in Section 2.4. Nonetheless, the mechanical performance is not the only parameter to be considered during fiber selection. Due to the high production costs of CMCs, the actual price of the fibers can also be a deciding factor for cases in which a high mechanical resistance is not necessary. For instance, the price per kilo of Nextel 312 can be up to three times cheaper than Nextel 610 or Nextel 720 [84].

Table 2.2: General properties of commercial oxide fibers, according to their manufacturers [85-87].

Fiber	Manufacturer	Composition (wt.%)	Diameter (μm)	Strength (MPa)	Elastic modulus (GPa)
Almax	Mitsui	>99 Al_2O_3	10	1020	330
Almax-B	Mitsui	70 Al_2O_3 30 SiO_2	7	-	-
Nextel 312	3M	62.5 Al_2O_3 24.5 SiO_2 13 B_2O_3	10-12	1700	150
Nextel 440	3M	70 Al_2O_3 28 SiO_2 2 B_2O_3	10-12	2000	190
Nextel 610	3M	>99 Al_2O_3	12	3100	380
Nextel 720	3M	85 Al_2O_3 15 SiO_2	12	2100	260
Nitivy ALF	Nitivy	72 Al_2O_3 28 SiO_2	7	1916	167

Besides Nextel 610 and Nextel 720, other single phase alumina and alumina–silica fibers should be mentioned. From the current alumina fibers, Almax was one of the first to be developed. The fiber is produced by a dry-spinning process using refined alumina particles, which results in a microstructure of 500 nm α-alumina grains [67]. As seen in Table 2.2, Almax has a much lower strength in comparison to Nextel 610. The considerably low strength of Almax is due to the presence of transgranular porosity, which is related to the rapid grain growth during processing [66]. More recently, Mitsui Co. also started the production of an alumina–silica fiber known as Almax-B. The fiber consists of δ-alumina and silica [88], but not that many details have been published about the fiber besides the manufacturer datasheet. Several examples of alumina–silica fibers can be found under the Nextel line from 3M. These fibers are produced by a special sol-gel process [89], hence their refined microstructure. Nextel 312 is considerably cheaper than the other oxide fibers [84]. However, its microstructure is predominantly amorphous [58], which results in low thermal stability due to the volatilization of boron compounds [53]. For higher thermal stability, Nextel 440 has a lower amount of B_2O_3. Nevertheless, the fiber also suffers from thermal degradation above

1200°C. This goes by the fact that its microstructure consists of γ-alumina and amorphous silica, which are unstable phases at such conditions [59]. In this sense, both fibers have a much lower thermal stability than the crystalline Nextel 720. Another alumina–silica fiber that was more recently developed is the Nitivy ALF from Nitivy Co., Ltd. (Tokyo, Japan). Also using a dry-spinning technique, the microstructure of the fiber is of γ-alumina grains and amorphous silica. After thermal exposures above 1100°C, the microstructure evolves to mullite and a decrease in strength is observed [75]. Still, this fiber has been reported in the production of 3D composites [90].

2.3.3 Fiber processing

There is not much information published about the processing of the currently available oxide fibers. This goes by the fact that the main parameters, *e.g.*, solution composition and processing temperatures, are confidential to the respective manufacturers. Nevertheless, it is generally known that ceramic fibers are produced by different spinning techniques. These processing routes use the production method of polymers to produce green fibers, which are later converted to ceramics. Practically speaking, spinning consists in extruding a solution with high viscosity, spin dope, through a multi-orifice spinneret [91]. The main disparity between the available spinning techniques is in relation to the dope composition. In the case of oxide fibers, there are two main approaches, which are frequently termed as dry-spinning and sol-gel [92]. The dry-spinning method is used by many companies. For this technique, the dope contains fine ceramic particles and inorganic binders [67]. Therefore, the initial solution has a high ceramic yield, reducing the shrinkage during processing [92]. In the case of the Nextel fibers, the spinning technique resembles the sol-gel process. Hence, the dope is formed by a solution of organic pre-cursor salts and polymers. The use of pre-cursors allows for better control and refinement of the fiber microstructure, leading to higher strength [89]. Several other spinning techniques can also be found in the literature. One example is the electro-spinning for the production of small diameter fibers [79]; although none of the current commercial fibers use this method.

For a better understanding of the spinning processes in general, Figure 2.6 shows the scheme of a dry-spinning facility for the production of endless oxide fibers. Here it should be highlighted that the equipment used for spinning using the sol-gel process is normally very similar to the one presented below, and therefore, it will not be shown. At the first stage, the spin dope is prepared and extruded through the holes of the spinneret. This is done with a

pressure high enough so that the dope behaves like a Newtonian fluid [93]. The spinned dope is normally blown, for the solution to solidify into a green body [81]. The green fibers are then heat treated in order to convert them into ceramic fibers. Normally, the fibers are slowly cured at moderate temperatures, and then pyrolyzed/sintered at higher temperatures [89]. Typical sintering temperatures are around 1300-1400°C [72, 94]. At this stage, it should be accounted that the composition of the fibers deviates from the initial composition due to volatilization [89]. After sintering, it is also common to size the fibers to protect them from dust and to help during the post-processing handling. The fibers can be then winded in bundles or braided in the desired fabrics.

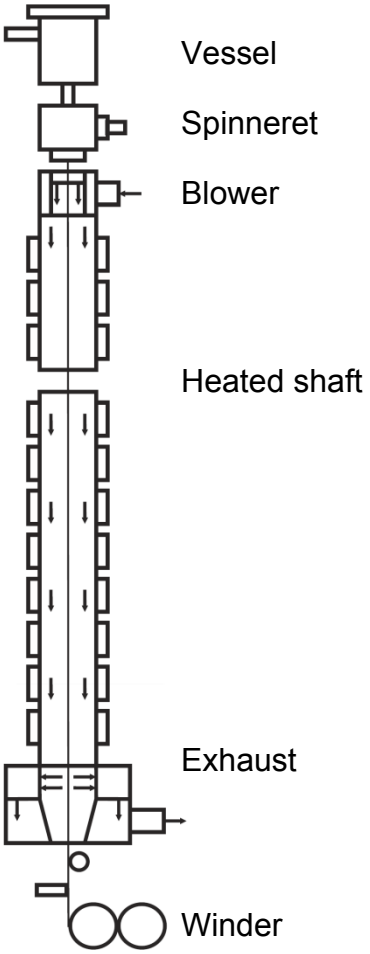

Figure 2.6: Scheme of a dry-spinning facility for spinning of endless oxide fibers. Adapted from [92].

2.4 Fiber properties

2.4.1 Tensile properties

Being the reinforcement of a composite, it is of particular importance the study of the tensile properties of the fibers. As previously discussed, the high strength of oxide fibers at room temperature rely on the control of the nano-sized microstructure. At the same time, these fibers are also quite flexible due to their small diameter. Like most ceramics however, oxide fibers fail in a fragile way when loaded, *i.e.*, no plastic deformation. This also implies that the strength of the fibers depend on their distribution of defects, which can deviate. Therefore, it is generally accepted that the strength distribution of ceramic fibers can be described by the Weibull distribution [95]. Although some authors criticize the methods for the estimation of the Weibull parameters and state that the strength data can also be fitted fairly good by the normal distribution [96]. Still, the Weibull distribution is the most used distribution for ceramic fibers. The Weibull distribution relates the failure of a material with the weakest-link theory [97]. It basically compares the material to a chain formed by several links. If the load applied to the chain is big enough to break one of its links, the whole chain will fail. In this sense, the failure probability of one link, and therefore of the whole material, is given by:

$$P = 1 - \exp\left(\frac{\sigma}{\sigma_0}\right)^m \quad (1)$$

where P is the failure probability, σ is the applied stress, σ_0 is the characteristic strength of the material, and m is the Weibull modulus. σ_0 is normally used to characterize the strength of the fibers, and represents the stress at which 63.21% of the fibers will fail. The Weibull modulus m is a shape parameter that describes the variability of results. In other words, a high value of m means a low scatter of results.

Fibers like Nextel 610 and Nextel 720 show a considerably high Weibull modulus [70, 94]. This is a reflection their narrow defect distribution and almost absence of big flaws [70]. Defects encountered in the fibers can be in the surface (weld-line, crack, nodule and blister) or internal (spherical and non-spherical pore) [94, 98]. In some cases, the critical flaw is even considered to be the junction between the biggest grains [99]; thus the importance of the fiber grain size. Furthermore, the measured m is considered to be underestimated due to the

variance of fiber diameter, *i.e.*, variation of tested volume and probability of finding critical defects [70]. Some authors suggest the use of a three-parameter distribution to account for fiber diameter variations, but these observations were made studying polymeric fibers [100, 101].

Nevertheless, the measured strength of Nextel 610 and Nextel 720 can be somewhat different depending on the source. To illustrate this matter, Table 2.3 and Table 2.4 bring a summary of the results from room-temperature tensile tests by different authors on both fibers. A possible explanation for the discrepancy of results is the variance between the tested fibers. Wilson [70] suggested that the flaw distribution between the fibers in a bundle is not random. That is to say that the flaw distribution of one fiber is narrow, but the distributions of different fibers are rather different. Besides, even the handling of the fibers can impair the results. For instance, fiber preparation can damage the fibers. If these external flaws are bigger than the fibers intrinsic defects or grains, the measured strength will be influenced by the external flaws [102]. The type of test used also has a high influence on the results, but this will be discussed in Section 3.4.1 and Section 3.4.2.

Table 2.3: Results of room-temperature tensile tests of Nextel 610 from different authors.

Fiber	Author	Length (mm)	Strength (MPa)	Weibull modulus	E-modulus (GPa)	Ref.
Nextel 610						
	Wilson, 1993		2400		380	[69]
	Xu, 1993	40	1651	6.6		[103]
	Wilson, 1995	215	1875			[71]
	Das, 1995	25.4	2300			[104]
	He, 1997	25.4	2580*	5.3		[105]
	Wilson, 1997	25	3080	10.9	373	[70]
			3030	11.2		
			3500	12.1		
	Cantonwine, 2003	25	3370	11	355±25	[94]
			2380*			[98]
	Schmücker, 2012	25	3280			[106]

*Values obtained from fiber bundle tests.

Table 2.4: Results of room-temperature tensile tests of Nextel 720 from different authors.

Fiber	Author	Length (mm)	Strength (MPa)	Weibull modulus	E-modulus (GPa)	Ref.
Nextel 720						
	Wilson, 1995	25	2030	9.7	260	[71]
			2130	7.1		
			1700			
	Das, 1995	25.4	2390		307±47	[104]
	Göring, 1997	100	1510	5.0		[107]
	Hay, 1999	25.4	1995			[108]
	Milz, 1999	100	1425	4.8		[109]
	Petry, 1999	25.4	1900			[110]
	Deléglise, 2001	25	1680	2-8	252±9	[72]
		100	1550		250±10	
	Wilson, 2001	25.4	1980	7.6	260	[111]
	Dassios, 2003	75	1117*	5.6	257	[112]
	Schmücker, 2012	25	2150			[106]

*Values obtained from fiber bundle tests.

Results of high-temperature tensile tests can also be found in the literature. The mechanical behavior of Nextel 610 and other oxide fibers was studied between 800-1400°C by Wilson et al. [111, 113]. As seen in Figure 2.7, Nextel 610 has much lower strength retention in comparison to other two-phase fibers. The alumina fiber showed a strength decrease already at 800°C, while Nextel 720 is stable until 1000°C. The higher thermal stability of Nextel 720 is very interesting for applications at elevated temperatures. Therefore, many other authors have studied the mechanical performance of Nextel 720 at high temperatures. The results of several high-temperature tests performed by different authors can be seen in Table A.1 from Appendix A.2. As it can be seen, the results can be rather different as some authors reported considerable strength decrease already at 1000°C [109, 112]. Moreover, it is suggested that the high-temperature strength can be influenced by the presence of alkaline contaminants, which decrease the strength of the fibers due to the formation of liquid silica [73, 80].

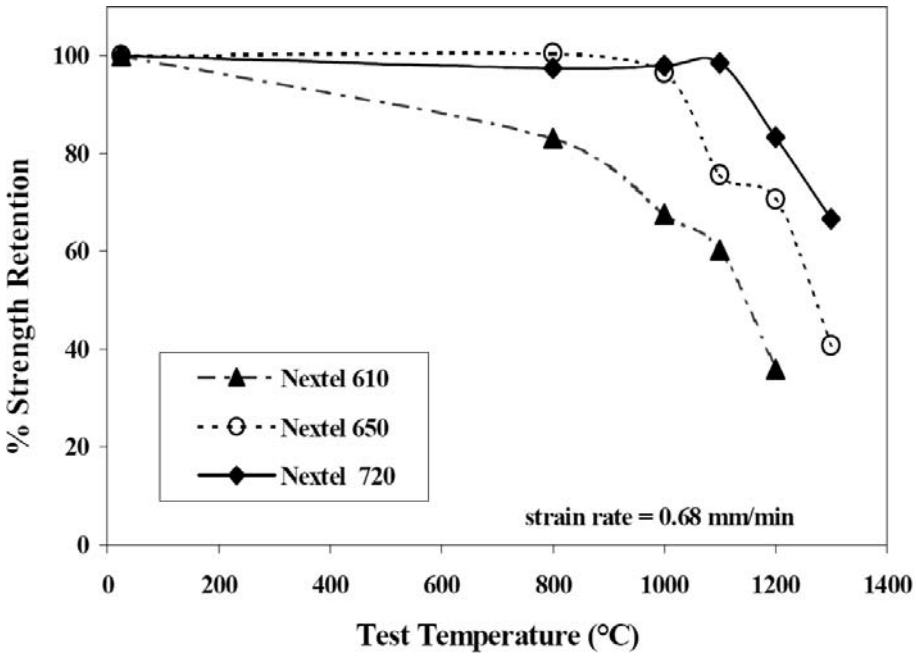

Figure 2.7: Relative strength retention, normalized to room temperature, of single filament of Nextel 610, Nextel 650 (alumina–zirconia) and Nextel 720 fibers at elevated temperatures. Adapted from [113].

In the particular case of Nextel 720 tested at high temperatures, attention should also be given to the loading rate. Studies have shown that the strength of the fiber depends on the testing speed used. In turn, this indicates that Nextel 720 suffers from subcritical crack growth under those conditions [73, 107, 109]. Deléglise et al. [73] suggested that this occurs due to the formation of silica glass phase, and growth of alumina platelets. This only happens at high temperatures under applied stress due to stress enhanced diffusion [73]. Then again, discrepancies are also reported for the temperature at which this phenomenon is observed. Some sources say that sub-critical crack growth only occurs above 1100°C [107], while others have measured it already at 1000°C [109]. As for Nextel 610, Armani et al. [114] also detected an influence of the loading rate, but only when the fiber was tested in steam at 1100°C. Therefore, sub-critical crack growth in pure alumina fibers might only be environmentally assisted.

2.4.2 Creep performance

Creep is defined as the continuous deformation over time of a material under a sub-critical stress at high temperatures [115]. This phenomenon is of particular importance for CMCs, especially considering the aforementioned mechanical applications at elevated temperatures. Under constant load, ceramics deform slowly and eventually fail at a stress lower than their strength at high temperatures. This deformation rate is high, at first, and decreases with time

until reaching a state of constant deformation rate. The first, non-linear, region is termed as primary creep stage, and is characterized by the distribution of stresses and microstructural changes in the material [115]. The secondary creep stage is said to be the steady-state regime, and represents the longest part of the creep lifetime for most materials. Therefore, creep studies on oxide fibers and composites are mainly focused on the determination of the steady-state creep rate, as well as its related parameters. In this sense, the creep rate can be described by the Arrhenius rate equation:

$$\dot{\varepsilon} = \frac{A_C\ D\ G\ b}{k\ T}\left(\frac{b}{d}\right)^p\left(\frac{\sigma}{G}\right)^n \quad ; \quad D = D_0\ \exp\left(\frac{-Q}{R\ T}\right) \tag{2}$$

where $\dot{\varepsilon}$ is the steady-state creep strain rate, A_c is a dimensionless constant, D is the diffusion coefficient, G is the shear modulus, b is the Burger`s vector, $k$ is the Boltzmann`s constant, T is the testing temperature, d is the grain size, p is the inverse grain size exponent, σ is the applied stress, n is the creep stress exponent, D_0 is a frequency factor, Q is the creep activation energy and R is the universal gas constant, 8.314 J/mol K. For most cases however, the creep rate can be simplified as a power law:

$$\dot{\varepsilon} = A\ \sigma^n \exp\left(\frac{-Q}{R\ T}\right) \tag{3}$$

where A is a creep rate proportionality constant. Thus, n and Q are usually determined to characterize the creep behavior of a material. n can be calculated by performing tests with different applied stresses at a constant temperature, while Q is obtained from tests at different temperatures and the same stress.

Under creep loading, a fiber bundle is said to behave like a collection of single filaments that deform independently. Therefore, the creep rates of bundles and single filaments are very similar, although the creep lifetime of a bundle is normally longer due to the higher amount of fibers [116]. Extending this concept to a higher scale, it can be assumed that the creep resistance of a composite will be then dependent on the creep resistance of the fibers in the direction of the load. In fact, if the volume fraction of fibers is taken into account, the creep

rates of composites are very similar to the ones of the fibers [31, 117, 118]. In this matter, attention should be given to the creep resistance of the oxide fibers, because of their small grain sizes [119]. Even though the microstructure of the fibers is refined to obtain a high tensile strength, it is well known that small grains have low creep resistance due to their higher mobility [120]. Hence, the creep resistance of single crystal fibers is higher than polycrystalline fibers like Nextel 610 [121].

The creep performance of Nextel 610 and Nextel 720 has been studied by different authors. Both fibers are prone to creep at temperatures above 1000-1100°C, although it has also been observed that they shrink, negative deformation, at low stresses [71, 73]. The most recent studies with these fibers are credited to Armani et al. [74, 114]. Figure 2.8 presents a summary of their results in terms of measured creep rates under different applied stresses. Analyzing the figure, it is evident that Nextel 720 has a much superior creep resistance than Nextel 610, *i.e.*, creep rates are up to three orders of magnitude lower. This is related to the inherent creep resistance of mullite, as well as the low mobility and complexity of the mosaic-like structure of Nextel 720 [73]. Armani et al. [74, 114] could also show that the creep lifetime of the fibers can be predicted using the Monkman-Grant relationship. Furthermore, the creep activation energy of both fibers has been measured by other authors. Q of 660 kJ/mol [69] and 702 kJ/mol [73] are reported for Nextel 610 and Nextel 720, respectively.

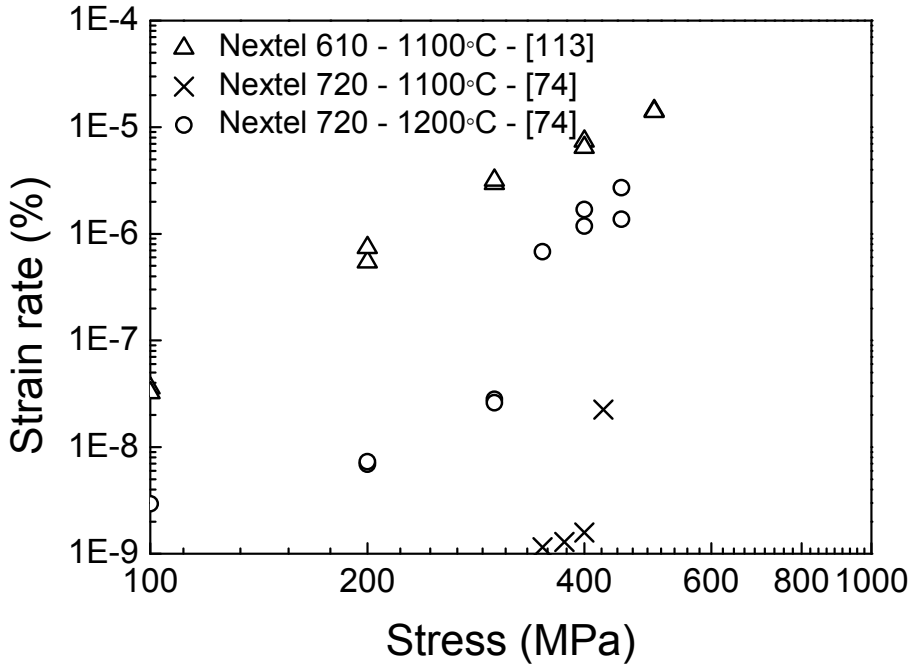

Figure 2.8: Steady-state creep rate *vs*. stress for Nextel 610 and 720 tows at 1100°C and 1200°C in laboratory air. Adapted from [74, 114].

One of the main efforts of the creep investigations is to relate the possible creep mechanisms with the stress exponent *n*. Before further observations, it is important to highlight that several creep deformation mechanism take place in oxide fibers during creep loading. Still, one phenomenon is usually dominant. Values of *n* reported for Nextel 610 are normally around 3 [69, 113, 114, 116, 122]. The observed creep mechanisms are related to interface-reactions [69], in which the coalescence of defects in the grain boundaries results in the failure of the fibers [116]. This goes along well with observations made on other alumina fibers [123] and bulky polycrystalline alumina [120, 124]. On the other hand, the analysis of creep deformation mechanisms, and its relation to *n*, is difficult for Nextel 720 due to the complexity of the fiber microstructure [71, 74]. Therefore, measured *n* for Nextel 720 is normally not comparable to other bulky polycrystalline mullite materials. The stress exponent for this fiber is around 3 under moderate stresses [71, 74]. Creep mechanisms are normally related to climb controlled interface reactions [74] and grain boundary sliding due to liquid phase formation [73]. Nevertheless, a shift in the stress exponent is seen when the fiber is tested under stresses higher than 300 MPa. For those cases, *n* changes to 5.4, presumably due to the transition to a different dislocation recovery mechanism [74]. Moreover, observations

on tested fibers have revealed that the alumina grains of Nextel 720, as well as Nextel 610, undergo extensive load-assisted grain growth prior to the failure of the fibers [73, 125].

The effect of different atmospheres on the creep performance of the fibers has also been studied. More specifically, Armani et al. [74] showed that steam is very harmful for mullite fibers since it decomposes the mullite phase, leading to a porous alumina microstructure. Hence, an increase of two orders of magnitude on the creep rates of Nextel 720 was seen when the fiber was tested in steam. In this case, the main creep mechanism was related to cavity growth [74]. The effect of steam on Nextel 610 was also observed, but not as severe as it was in Nextel 720. For Nextel 610, the creep rates increased almost one order of magnitude due to environmentally assisted sub-critical crack growth [114].

2.4.3 Thermal degradation

Thermal degradation is perhaps one of the most concerning topics on oxide materials. As evidenced before, the mechanical properties of the fibers are a reflection of their refined microstructure. The main problem is that these microstructures are not stable at high temperatures. Oxide fibers are normally sintered at temperatures around 1350°C for a few minutes, cf. Section 2.3.3. As a consequence, microstructural changes take place when the fibers are heated again to similar temperatures. Considering that temperatures as high as 1200°C can be easily reached during composites processing and target applications, see Section 2.2, thermal degradation is an important issue.

Several works about the effect of thermal exposures on the tensile properties of Nextel 610 and Nextel 720 can be found in the literature. These works normally report the room-temperature strength of the fibers after short heat treatments [72, 94, 98, 99, 103, 106, 107, 109, 110] simulating the processing of composites, or after long treatments [72, 99, 104, 108, 113] simulating application uses. Strength decreases is measured for Nextel 610 after exposures to 900°C [103], while the strength of Nextel 720 remains somewhat constant up to 1000°C [108, 110]. Nonetheless, there is a big conflict in relation to the measured strength retention of the fibers. While some authors report only minimal strength decrease after several hours at high temperatures [104, 113], others describe a severe degradation of the mechanical properties after a few hours at similar temperatures [103, 109, 110]. Due to the high amount of works in this matter, Table A.2 from Appendix A.2 shows the reader a compilation of strength retention results for Nextel 720 after different thermal exposures. In the table, it is evident the high discrepancy between the results from different sources. Still, most authors

agree that the strength decrease seen in oxide fibers is due to grain growth [72, 110] and micro grooving [94, 108]; although most of these works lack in deep microstructural investigations. In addition, it has been observed that the fracture mode of treated fibers change from transgranular to intergranular [103].

Grain growth kinetics has been studied in more detail by Schmücker et al. [77, 106, 126]. In general, grain growth is observed above 1200°C for oxide fibers. Nextel 610 is more susceptible to grain growth due to the higher mobility of its alumina grain, and the formation of a thin silica film in the grain boundary. In the case of Nextel 720, the mobility is hindered by the mosaic mullite grains [106]. Above 1300°C however, changes in morphology, from mosaic-like structure to faceted grains, are observed [77]. Furthermore, it has been found that the grain growth follows an empirical law. In this sense, grain growth kinetics is rather low below 1600°C, and much faster at temperatures beyond [126]. Then again, the works from Schmücker do not present detailed mechanical characterizations. In one of the last publications [126], grain growth was briefly compared to the strength retention of the fibers, see Figure 2.9. Still, grain growth and tensile strength follow a slightly different trend, and a relation between other mechanical properties was not presented. Other investigations on the grain growth of Nextel 610 have been published by Hay et al. [127]. It was shown that if grain analyses are conducted based on 3D models, the measured grain growth can be higher. In addition, it was proved that the heat treatments cause a broadening of the grain size distribution, meaning that Nextel 610 suffers from abnormal grain growth.

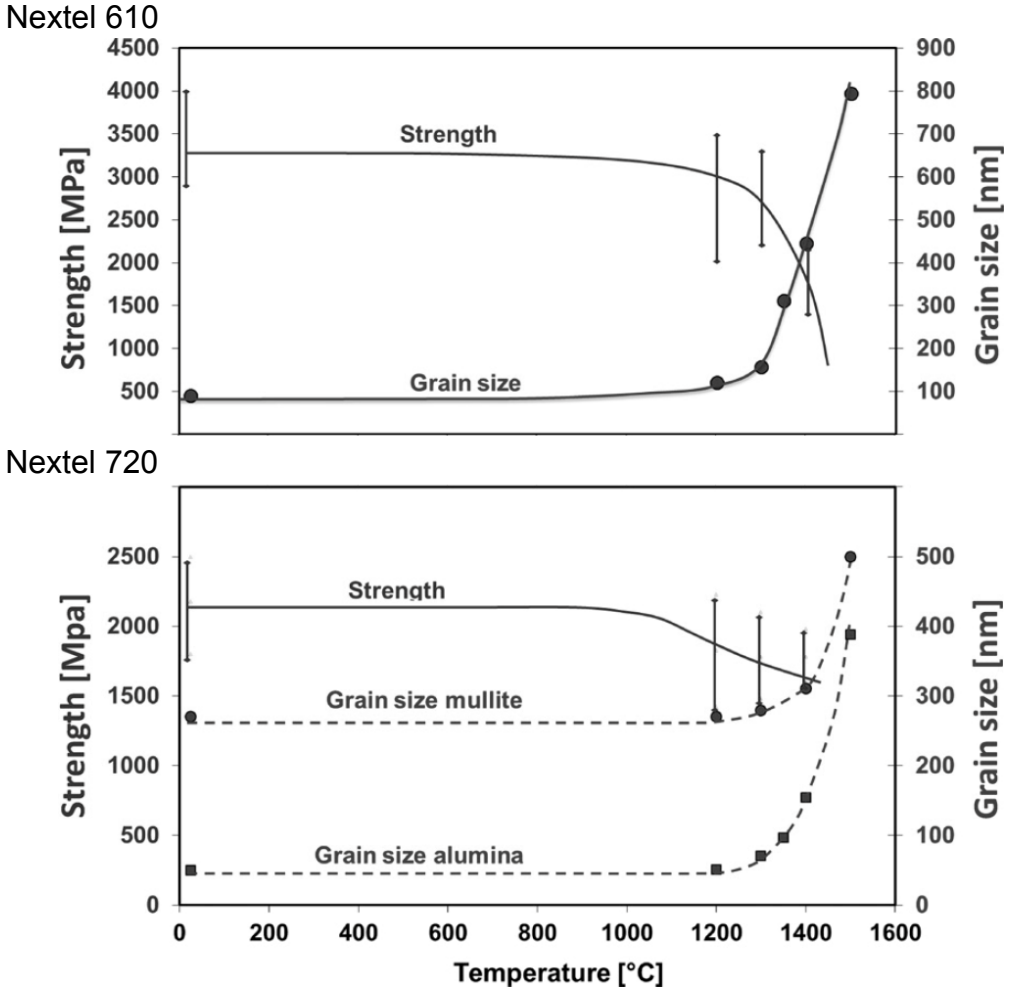

Figure 2.9: Grain size and strength development of commercial oxide fibers Nextel 610 and Nextel 720 after heat treatment between 1200°C and 1500°C for 1 h. Adapted from [106].

Besides grain growth, other microstructural changes caused by thermal exposures also influence the mechanical properties of the fibers. In reality, it has been proposed that the fiber strength after heat treatment is not dependent on grain growth when the fiber grains are smaller than 250 nm [99]. Strength loss is then caused by the appearance and coalescence of thermally induced defects. Defects observed on treated fibers include grain boundary grooving [94, 99] and surface weld-lines, caused by the sintering between the fibers of a bundle [94, 98]. These new defects are more severe than pre-existing fiber flaws, and therefore, reduce the strength of the treated fibers. This explains why Nextel 610 shows strength decrease already at 900°C [128], although grain growth is not observed at such temperature.

Nevertheless, thermal exposures can also have a positive effect on the properties of the fibers. For instance, it has been reported that the micro-porosity of Nextel 720 fibers is reduced after

thermal exposures, which in turn, increases the stiffness of the fibers [72]. Also considering Nextel 720, crystal phase transformations are detected after the treatments. This goes by the fact that the microstructure of Nextel 720 is considered to be metastable. As-received Nextel 720 fibers have an alumina-rich mullite phase due to the short processing time of the fiber. In this sense, the mullite phase slowly transforms into a more stable microstructure when the fiber is exposed again to high temperatures [72]. Similar observations have also been made for other two-phase fibers [59, 62, 75, 110]. Therefore, it is expected that the thermal stability of the fibers increase. Additionally, creep tests on treated fibers have been conducted using Nextel 610. Long and short thermal treatments are beneficial for the creep resistance of the fibers, *e.g.*, a decrease of one order of magnitude on the creep rate was observed [116, 118, 129]. Figure 2.10 illustrates this matter by showing the creep rates of Nextel 610 bundles before and after the exposure to 1400°C for only 1 min. A change in n was also observed and attributed to the formation of filament clusters [116].

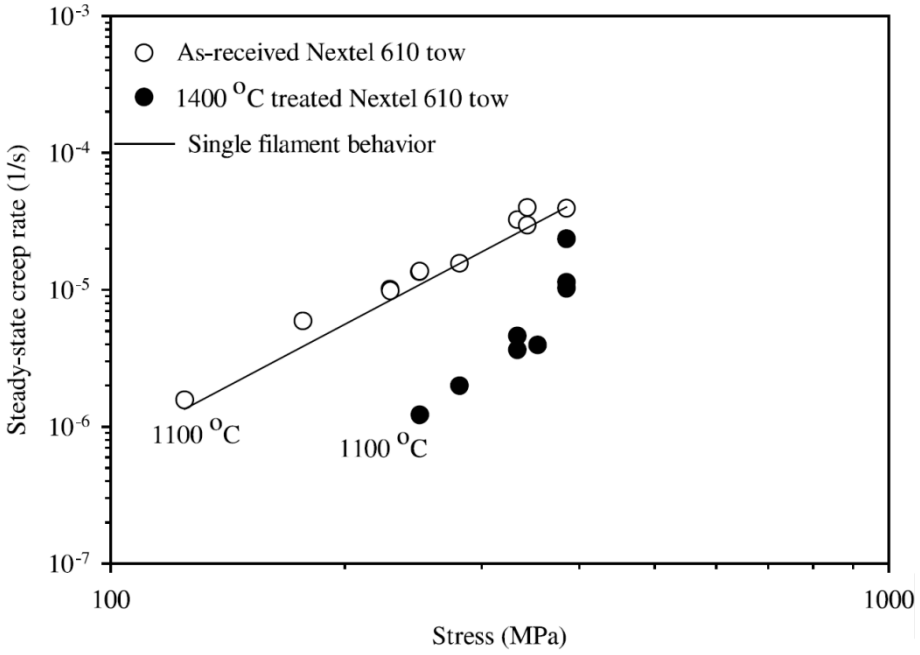

Figure 2.10: Comparison of experimental steady-state creep rates of Nextel 610 tows and single filaments. Adapted from [116].

Nonetheless, most of the analyses presented above were conducted on fibers alone. Special attention should be given when the fibers are in a composite as different fiber-matrix interactions might happen at the same temperatures. These interactions are normally driven by

the chemical composition gradient between the fibers and the matrix [130, 131]. Therefore, it will also vary depending on the CMC system. For instance, Nextel 610 shows a much severer grain growth when embedded in a pure alumina matrix [130]. In this case, it has been observed an outward-diffusion of the SiO_2 dopants from the fiber to the matrix. Since SiO_2 is used as a grain growth inhibitor in Nextel 610, this out-diffusion leads to a higher grain growth of the fiber, see Figure 2.11. Naturally, this out-diffusion, and consequently higher grain growth, can be avoided by doping the matrix with SiO_2 as well [131]. In more extreme cases, *e.g.*, when the matrix is rich in SiO_2, the opposite is observed. For instance, Volkmann et al. [132] showed that Nextel 610 fibers embedded in a mullite–SiOC matrix present smaller grains in the outer diameter, which indicates the inward-diffusion of SiO_2. Similar observations have also been made for Nextel 720 embedded in mullite matrices. For such cases, the excess of SiO_2 from the matrix reacts with the α-alumina grains from the fiber forming a mullite rich region near to the interface [133, 134]. On the other hand, diffusion of Si species from Nextel 720 fibers to the matrix has also been reported for composites with pure alumina matrices [135, 136].

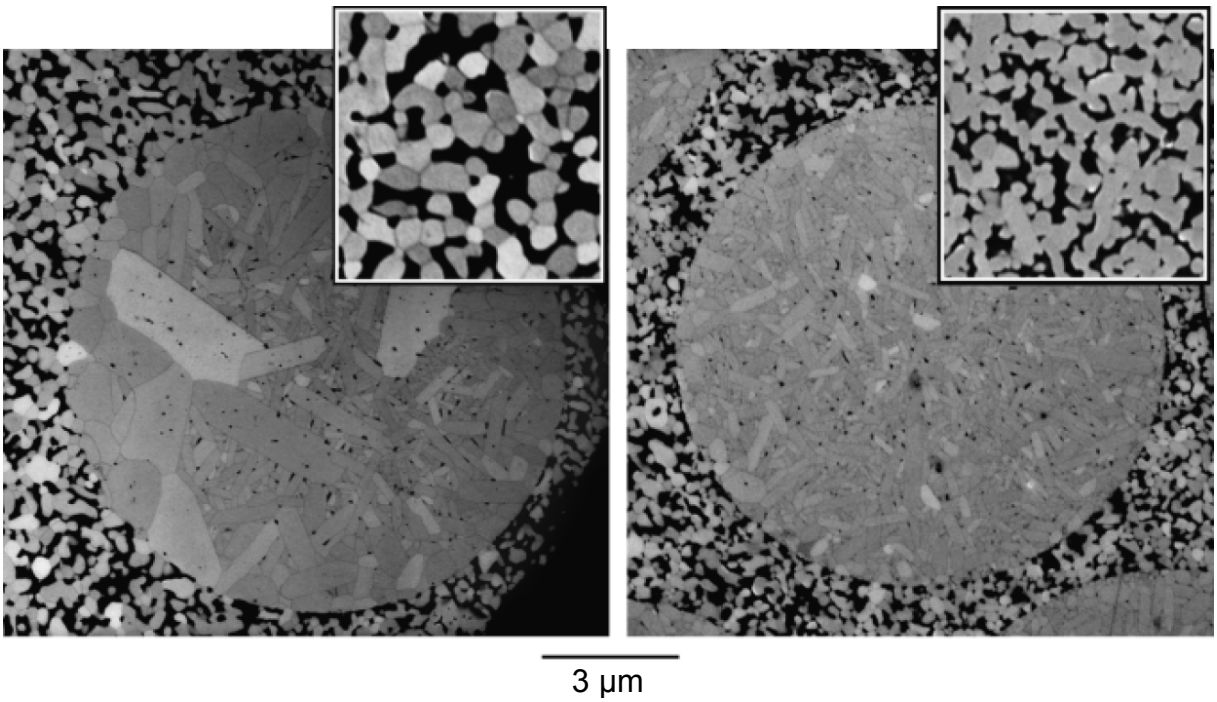

Figure 2.11: Microstructures of Nextel 610 fibers in porous matrices after firing at 1400°C for 2 h. Reference composite with pure alumina matrix (left), and composite with alumina matrix doped with silica (right). Adapted from [131].

2.5 References

[1] D. B. Miracle, D. B. Donaldson, G. F. Vander Voort. *ASM Handbook, Volume 21: Composites*. ASM International®, Materials Park, OH, USA, 2001.

[2] A. Kelly, C. Zweben. *Comprehensive Composite Materials*. Pergamon, Oxford, United Kingdom, 2000.

[3] R. Naslain. "Design, preparation and properties of non-oxide CMCs for application in engines and nuclear reactors: an overview". Composites Science and Technology, vol. 64 (2), pp. 155-170, 2004.

[4] A. G. Evans, F. W. Zok. "The physics and mechanics of fibre-reinforced brittle matrix composites". Journal of Materials Science, vol. 29 (15), pp. 3857-3896, 1994.

[5] W. Krenkel, F. Berndt. "C/C–SiC composites for space applications and advanced friction systems". Materials Science and Engineering: A, vol. 412 (1–2), pp. 177-181, 2005.

[6] W. Krenkel, J. Georges Thébault. "Ceramic matrix composites for friction applications", pp. 647-671 in *Ceramic Matrix Composites*, N. P. Bansal, J. Lamon (Eds.). John Wiley & Sons, Inc., 2014.

[7] J. A. DiCarlo. "Advances in SiC/SiC composites for aero-propulsion", pp. 217-235 in *Ceramic Matrix Composites*, N. P. Bansal, J. Lamon (Eds.). John Wiley & Sons, Inc., 2014.

[8] C. Sauder. "Ceramic matrix composites: Nuclear applications", pp. 609-646 in *Ceramic Matrix Composites*, N. P. Bansal, J. Lamon (Eds.). John Wiley & Sons, Inc., 2014.

[9] A. Noeth, A. Rüdinger, W. Pritzkow. "Oxide ceramic matrix composites – Manufacturing, machining, properties and industrial applications". Ceramic Applications, vol. 3, pp. 48-54, 2015.

[10] F. W. Zok. "Developments in oxide fiber composites". Journal of the American Ceramic Society, vol. 89 (11), pp. 3309-3324, 2006.

[11] R. Kerans, T. Parthasarathy. "Crack deflection in ceramic composites and fiber coating design criteria". Composites Part A: Applied Science and Manufacturing, vol. 30 (4), pp. 521-524, 1999.

[12] R. J. Kerans, R. S. Hay, N. J. Pagano, T. Parthasarathy. “The role of the fiber-matrix interface in ceramic composites”. American Ceramic Society Bulletin, vol. 68 (2), pp. 429-442, 1989.

[13] M.-Y. He, J. W. Hutchinson. “Kinking of a crack out of an interface”. Journal of Applied Mechanics, vol. 56 (2), pp. 270-278, 1989.

[14] D. Koch, K. Tushtev, G. Grathwohl. “Ceramic fiber composites: Experimental analysis and modeling of mechanical properties”. Composites Science and Technology, vol. 68 (5), pp. 1165-1172, 2008.

[15] C. Levi, F. Zok, J.-Y. Yang, M. Mattoni, J. Löfvander. “Microstructural design of stable porous matrices for all-oxide ceramic composites”. Zeitschrift für Metallkunde, vol. 90 (12), pp. 1037-1047, 1999.

[16] K. A. Keller, T.-I. Mah, T. A. Parthasarathy, C. M. Cooke. “Fugitive interfacial carbon coatings for oxide/oxide composites”. Journal of the American Ceramic Society, vol. 83 (2), pp. 329-336, 2000.

[17] K. Tushtev, R. S. M. Almeida. “Oxide/oxide CMCs – Porous matrix composite systems; Composites with interface coatings”, pp. 130-157 in *Comprehensive Composite Materials II*, P. W. R. Beaumont, C. H. Zweben (Eds.), vol. 5. Elsevier, 2017.

[18] N. S. Jacobson. “Corrosion of silicon-based ceramics in combustion environments”. Journal of the American Ceramic Society, vol. 76 (1), pp. 3-28, 1993.

[19] R. C. Robinson, J. L. Smialek. “SiC recession caused by SiO_2 scale volatility under combustion conditions: I, experimental results and empirical model”. Journal of the American Ceramic Society, vol. 82 (7), pp. 1817-1825, 1999.

[20] F. Lamouroux, S. Bertrand, R. Pailler, R. Naslain, M. Cataldi. “Oxidation-resistant carbon-fiber-reinforced ceramic-matrix composites”. Composites Science and Technology, vol. 59 (7), pp. 1073-1085, 1999.

[21] J. A. Heathcote, X. Y. Gong, J. Y. Yang, U. Ramamurty, F. W. Zok. “In-plane mechanical properties of an all-oxide ceramic composite”. Journal of the American Ceramic Society, vol. 82 (10), pp. 2721-2730, 1999.

[22] H. G. Halverson, W. A. Curtin. “Stress rupture in ceramic-matrix composites: Theory and experiment”. Journal of the American Ceramic Society, vol. 85 (6), pp. 1350-1365, 2002.

[23] F. F. Lange, W. C. Tu, A. G. Evans. “Processing of damage-tolerant, oxidation-resistant ceramic matrix composites by a precursor infiltration and pyrolysis method”. Materials Science and Engineering: A, vol. 195, pp. 145-150, 1995.

[24] W.-C. Tu, F. F. Lange, A. G. Evans. “Concept for a damage-tolerant ceramic composite with "strong" interfaces”. Journal of the American Ceramic Society, vol. 79 (2), pp. 417-424, 1996.

[25] C. G. Levi, J. Y. Yang, B. J. Dalgleish, F. W. Zok, A. G. Evans. “Processing and performance of an all-oxide ceramic composite”. Journal of the American Ceramic Society, vol. 81 (8), pp. 2077-2086, 1998.

[26] P. E. D. Morgan, D. B. Marshall. “Ceramic composites of monazite and alumina”. Journal of the American Ceramic Society, vol. 78 (6), pp. 1553-1563, 1995.

[27] E. Boakye, R. S. Hay, M. D. Petry. “Continuous coating of oxide fiber tows using liquid precursors: Monazite coatings on Nextel 720™”. Journal of the American Ceramic Society, vol. 82 (9), pp. 2321-2331, 1999.

[28] R. A. Jurf, S. C. Butner. “Advances in oxide-oxide CMC”. Journal of Engineering for Gas Turbines and Power, vol. 122 (2), pp. 202-205, 2000.

[29] E. Volkmann, K. Tushtev, D. Koch, C. Wilhelmi, J. Göring, K. Rezwan. “Assessment of three oxide/oxide ceramic matrix composites: Mechanical performance and effects of heat treatments”. Composites Part A: Applied Science and Manufacturing, vol. 68 (0), pp. 19-28, 2015.

[30] Walter E. C. Pritzkow Spezialkeramik. “Oxide/oxide ceramic matrix composite Keramikblech®”, datasheet. Filderstadt, Germany, 2012.

[31] M. B. Ruggles-Wrenn, S. Mall, C. A. Eber, L. B. Harlan. “Effects of steam environment on high-temperature mechanical behavior of Nextel™720/alumina (N720/A) continuous fiber ceramic composite”. Composites Part A: Applied Science and Manufacturing, vol. 37 (11), pp. 2029-2040, 2006.

[32] M. B. Ruggles-Wrenn, T. Kutsal. “Effects of steam environment on creep behavior of Nextel™720/alumina-mullite ceramic composite at elevated temperature”. Composites Part A: Applied Science and Manufacturing, vol. 41 (12), pp. 1807-1816, 2010.

[33] A. Evans, D. Marshall, F. Zok, C. Levi. “Recent advances in oxide-oxide composite technology”. Advanced Composite Materials, vol. 8 (1), pp. 17-23, 1999.

[34] M. C. Halbig, M. H. Jaskowiak, J. D. Kiser, D. Zhu. “Evaluation of ceramic matrix composite technology for aircraft turbine engine applications”, pp. 7-10 in *51st AIAA Aerospace Sciences Meeting including the New Horizons Forum and Aerospace Exposition*. American Institute of Aeronautics and Astronautics, 2013.

[35] J. A. DiCarlo, M. van Roode. “Ceramic composite development for gas turbine engine hot section components”, pp. 221-231 in *Proceedings of ASME Turbo Expo 2006: Power for Land, Sea, and Air*, vol. 2. American Society of Mechanical Engineers, 2006.

[36] K. L. More, L. R. Walker, Y. Wang, E. Lara-Curzio, T. M. Brummett, M. van Roode, J. R. Price, A. Szweda, G. Merrill. “Microstructural and mechanical characterization of a hybrid oxide CMC combustor liner after 25,000-hour engine test”, pp. 255-263 in *Proceedings of ASME Turbo Expo 2009: Power for Land, Sea, and Air*, vol. 1. American Society of Mechanical Engineers, 2009.

[37] J. A. Momson, K. M. Kauth. “Design and analysis of a CMC turbine blade tip seal for a land-based power turbine”, pp. 249-256 in *Proceedings of 22nd Annual Conference on Composites, Advanced Ceramics, Materials, and Structures*, D. E. Bray (Ed.). John Wiley & Sons, Inc., 2010.

[38] K. Wood. “Ceramic-matrix composites heat up”. *CompositesWorld – High-Performance Composites*, vol. 21. Cincinnati, USA: Gardner Business Media, Inc., pp. 38-45, 2013.

[39] G. Gardiner. “Aeroengine composites. Part 1: The CMC invasion”. *CompositesWorld*, vol. 1. Cincinnati, USA: Gardner Business Media, Inc., pp. 38-41, 2015

[40] J. Göring, S. Hackemann, B. Kanka. “WHIPOX®: Ein faserverstärkter oxidkeramischer Werkstoff für Hochtemperatur-langzeitanwendungen”. Materialwissenschaft und Werkstofftechnik, vol. 38 (9), pp. 766-772, 2007.

[41] N. Waibel. “In einem bett aus kleinen kissen”. *DLR Magazin*, vol. 147. Cologne, Germany: Deutsches Zentrum für Luft- und Raumfahrt e.V. (DLR), pp. 20-23, 2015.

[42] T. J. McMahon. “Advanced hot gas filter development”, pp. 47-56 in *Proceedings of 24th Annual Conference on Composites, Advanced Ceramics, Materials, and Structures*, T. Jessen, E. Ustundag (Eds.). John Wiley & Sons, Inc., 2008.

[43] A. Szweda, S. Butner, J. Ruffoni, C. Bacalski, J. Lane, J. Morrison, G. Merrill, M. van Roode, A. Fahme, N. Miriyala. “Development and evaluation of hybrid oxide/oxide ceramic matrix composite combustor liners”, pp. 315-321 in *Proceedings of ASME Turbo Expo 2005: Power for Land, Sea, and Air*, vol. 1. American Society of Mechanical Engineers, 2005.

[44] J. B. Davis, D. B. Marshall, K. S. Oka, R. M. Housley, P. E. D. Morgan. “Ceramic composites for thermal protection systems”. Composites Part A: Applied Science and Manufacturing, vol. 30 (4), pp. 483-488, 1999.

[45] A. E. Segall. “Failure of a continuous fiber ceramic composite after exposure to combustion ambients”. Engineering Failure Analysis, vol. 9 (4), pp. 469-479, 2002.

[46] K. A. Keller, G. Jefferson, R. J. Kerans. “Oxide-oxide composites”, pp. 236-272 in *Ceramic Matrix Composites*, N. P. Bansal, J. Lamon (Eds.). John Wiley & Sons, Inc., 2014.

[47] R. Dong, Y. Hirata, H. Sueyoshi, M. Higo, Y. Uemura. “Polymer impregnation and pyrolysis (PIP) method for the preparation of laminated woven fabric/mullite matrix composites with pseudoductility”. Journal of the European Ceramic Society, vol. 24 (1), pp. 53-64, 2004.

[48] M. Gerendás, Y. Cadoret, C. Wilhelmi, T. Machry, R. Knoche, T. Behrendt, T. Aumeier, S. Denis, J. r. Göring, D. Koch. “Improvement of oxide/oxide CMC and development of combustor and turbine components in the HIPOC program”, pp. 477-490 in *Proceedings of ASME Turbo Expo 2011: Turbine Technical Conference and Exposition*. American Society of Mechanical Engineers, 2011.

[49] F. F. Lange, C. G. Levi, F. W. Zok. “Processing fiber reinforced ceramics with porous matrices”, pp. 427-447 in *Comprehensive Composite Materials*, A. Kelly, C. Zweben (Eds.). Pergamon, 2000.

[50] H. T. Larker, R. Lundberg. “Near net shape production of monolithic and composite high temperature ceramics by hot isostatic pressing (HIP)”. Journal of the European Ceramic Society, vol. 19 (13–14), pp. 2367-2373, 1999.

[51] T. Radsick, B. Saruhan, H. Schneider. “Damage tolerant oxide/oxide fiber laminate composites”. Journal of the European Ceramic Society, vol. 20 (5), pp. 545-550, 2000.

[52] M. L. Antti, E. Lara-Curzio, R. Warren. “Thermal degradation of an oxide fibre (Nextel 720)/aluminosilicate composite”. Journal of the European Ceramic Society, vol. 24 (3), pp. 565-578, 2004.

[53] A. R. Bunsell, M. H. Berger. “Fine diameter ceramic fibres”. Journal of the European Ceramic Society, vol. 20 (13), pp. 2249-2260, 2000.

[54] A. K. Dhingra. “Metal matrix composites reinforced with Fibre FP (α-Al_2O_3)”. Philosophical Transactions of the Royal Society of London A: Mathematical, Physical and Engineering Sciences, vol. 294 (1411), pp. 559-564, 1980.

[55] A. K. Dhingra, N. Peacock, A. R. Ubbelohde, C. Manfre. “Alumina Fibre FP”. Philosophical Transactions of the Royal Society of London A: Mathematical, Physical and Engineering Sciences, vol. 294 (1411), pp. 411-417, 1980.

[56] J. C. Romine. “New high-temperature ceramic fiber”, pp. 755-765 in *Proceedings of 11th Annual Conference on Composites and Advanced Ceramic Materials*, W. Smothers (Ed.). John Wiley & Sons, Inc., 2008.

[57] Y. Abe, S. Horikiri, K. Fujimura, E. Ichiki. “High performance alumina fiber and alumina/aluminum composites”, pp. 1427-1434 in *Progress in Science and Engineering of Composites*, T. Hayashi, K. Kawata, S. Umekawa (Eds.). Japan Society of Composite Materials, 1982.

[58] D. D. Johnson. “Nextel 312 ceramic fiber from 3M”. Journal of Industrial Textiles, vol. 11 (4), pp. 282-296, 1982.

[59] M. Schmücker, F. Flucht, H. Schneider. “High temperature behaviour of polycrystalline aluminosilicate fibres with mullite bulk composition. I. Microstructure and strength properties”. Journal of the European Ceramic Society, vol. 16 (2), pp. 281-285, 1996.

[60] D. D. Johnson, A. R. Holtz, M. F. Grether. “Properties of Nextel 480 ceramic fibers”, pp. 744-754 in *Proceedings of 11th Annual Conference on Composites and Advanced Ceramic Materials: Ceramic Engineering and Science*, W. Smothers (Ed.). John Wiley & Sons, Inc., 2008.

[61] D. J. Pysher, K. C. Goretta, R. S. Hodder, R. E. Tressler. “Strengths of ceramic fibers at elevated temperatures”. Journal of the American Ceramic Society, vol. 72 (2), pp. 284-288, 1989.

[62] C. Lesniewski, C. Aubin, A. R. Bunsell. “Property-structure characterisation of a continuous fine alumina-silica fibre”. Composites Science and Technology, vol. 37 (1–3), pp. 63-78, 1990.

[63] K. Jakus, V. Tulluri. “Mechanical behavior of a Sumitomo alumina fiber at room and high temperature”, pp. 1338-1349 in *Proceedings of 13th Annual Conference on Composites and Advanced Ceramic Materials: Ceramic Engineering and Science*, J. B. Wachtman Jr. (Ed.). John Wiley & Sons, Inc., 2008.

[64] J. D. Birchall. “The preparation and properties of polycrystalline aluminium oxide fibres”. Transactions and journal of the British Ceramic Society, vol. 82 (4), pp. 143-145, 1983.

[65] J. T. A. Pollock. “Filamentary sapphire – Part 1. Growth and microstructural characterisation”. Journal of Materials Science, vol. 7 (6), pp. 631-648, 1972.

[66] M. H. Berger, A. R. Bunsell. “Oxide fibers”, pp. 147-173 in *Comprehensive Composite Materials*, K. Anthony, Z. Carl (Eds.). Pergamon, 2000.

[67] Y. Saitow, K. Iwanaga, S. Itou, T. Fukumoto, T. Utsunomiya. “Preparation of continuous high purity α-alumina fiber”, pp. 808-819 in *Proceedings of 37th International SAMPE Symposium and Exhibition*, G. C. Grimes (Ed.). Society for the Advancement of Material and Process Engineering, 1992.

[68] V. Lavaste, M. H. Berger, A. R. Bunsell, J. Besson. “Microstructure and mechanical characteristics of alpha-alumina-based fibres”. Journal of Materials Science, vol. 30 (17), pp. 4215-4225, 1995.

[69] D. M. Wilson, D. C. Lueneburg, S. L. Lieder. “High temperature properties of Nextel 610 and alumina-based nanocomposite fibers”, pp. 609-621 in *Proceedings of 17th Annual Conference on Composites and Advanced Ceramic Materials: Ceramic Engineering and Science*, J. B. Wachtman Jr. (Ed.). John Wiley & Sons, Inc., 2008.

[70] D. Wilson. “Statistical tensile strength of Nextel™ 610 and Nextel™ 720 fibres”. Journal of Materials Science, vol. 32 (10), pp. 2535-2542, 1997.

[71] D. M. Wilson, S. L. Lieder, D. C. Lueneburg. “Microstructure and high temperature properties of Nextel 720 fibers”, pp. 1005-1014 in *Proceedings of 19th Annual Conference on Composites, Advanced Ceramics, Materials, and Structures*, J. B. Wachtman Jr. (Ed.). John Wiley & Sons, Inc., 2008.

[72] F. Deléglise, M. H. Berger, D. Jeulin, A. R. Bunsell. “Microstructural stability and room temperature mechanical properties of the Nextel 720 fibre”. Journal of the European Ceramic Society, vol. 21 (5), pp. 569-580, 2001.

[73] F. Deléglise, M. H. Berger, A. R. Bunsell. “Microstructural evolution under load and high temperature deformation mechanisms of a mullite/alumina fibre”. Journal of the European Ceramic Society, vol. 22 (9–10), pp. 1501-1512, 2002.

[74] C. J. Armani, M. B. Ruggles-Wrenn, R. S. Hay, G. E. Fair. “Creep and microstructure of Nextel™ 720 fiber at elevated temperature in air and in steam”. Acta Materialia, vol. 61 (16), pp. 6114-6124, 2013.

[75] Y. Wang, H. Cheng, H. Liu, J. Wang. “Microstructure and room temperature mechanical properties of mullite fibers after heat-treatment at elevated temperatures”. Materials Science and Engineering: A, vol. 578 (0), pp. 287-293, 2013.

[76] D. M. Wilson, L. R. Visser. “Nextel™ 650 ceramic oxide fiber: New alumina-based fiber for high temperature composite reinforcement”, pp. 363-373 in *Proceedings of 24th Annual Conference on Composites, Advanced Ceramics, Materials, and Structures*, T. Jessen, E. Ustundag (Eds.), vol. 21. Wiley Online Library, 2000.

[77] M. Schmücker, H. Schneider, T. Mauer, B. Clauß. “Kinetics of mullite grain growth in alumino silicate fibers”. Journal of the American Ceramic Society, vol. 88 (2), pp. 488-490, 2005.

[78] W. Yoon, P. Sarin, W. M. Kriven. “Growth of textured mullite fibers using a quadrupole lamp furnace”. Journal of the European Ceramic Society, vol. 28 (2), pp. 455-463, 2008.

[79] C. Peng, P. Liu, J. Hu, T. Hua, Y. Shen, B. Zhao, G. Tang. “Preparation of uniaxially aligned mullite ceramic fibers by electrospinning”. Colloids and Surfaces A: Physicochemical and Engineering Aspects, vol. 457 (0), pp. 1-7, 2014.

[80] A. Poulon-Quintin, M. H. Berger, A. R. Bunsell. “Mechanical and microstructural characterisation of Nextel 650 alumina-zirconia fibres”. Journal of the European Ceramic Society, vol. 24 (9), pp. 2769-2783, 2004.

[81] B. Cheng, X. Tao, L. Shi, G. Yan, X. Zhuang. “Fabrication of ZrO_2 ceramic fiber mats by solution blowing process”. Ceramics International, vol. 40 (9, Part B), pp. 15013-15018, 2014.

[82] B. H. King, J. W. Halloran. “Polycrystalline yttrium aluminum garnet fibers from colloidal sols”. Journal of the American Ceramic Society, vol. 78 (8), pp. 2141-2148, 1995.

[83] T. Ishikawa. “Advances in inorganic fibers”, pp. 109-144 in *Polymeric and Inorganic Fibers*, vol. 178. Springer Berlin Heidelberg, 2005.

[84] B. Clauss, D. Schawaller. “Modern aspects of ceramic fiber development”. Advances in Science and Technology, vol. 50, pp. 1-8, 2006.

[85] 3M Co. “Nextel™ – Ceramic textiles technical notebook”, datasheet. St. Paul, Minesota, USA, 2010.

[86] Mitsui Mining Materials Co., Ltd. “Fine ceramic materials – General catalog”, datasheet. Tokyo, Japan, 2011.

[87] Nitivy Co., Ltd. “Nitivy ALF™”, datasheet. Tokyo, Japan, 2011.

[88] D. Schawaller, B. Clauß, M. R. Buchmeiser. “Ceramic filament fibers – A review”. Macromolecular Materials and Engineering, vol. 297 (6), pp. 502-522, 2012.

[89] D. M. Wilson. “Spun (slurry and sol-gel) ceramic fibers”, pp. 8779-8782 in *Reference Module in Materials Science and Materials Engineering*, S. Hashmi (Ed.). Elsevier, 2016.

[90] Y. Wang, H. Cheng, H. Liu, J. Wang. “Effects of sintering temperature on mechanical properties of 3D mullite fiber (ALF FB3) reinforced mullite composites”. Ceramics International, vol. 39 (8), pp. 9229-9235, 2013.

[91] S. Baskaran, S. D. Nunn, D. Popovic, J. W. Halloran. “Fibrous monolithic ceramics: I Fabrication, microstructure, and indentation behavior”. Journal of the American Ceramic Society, vol. 76 (9), pp. 2209-2216, 1993.

[92] B. Clauß. “Fibers for ceramic matrix composites”, pp. 1-20 in *Ceramic Matrix Composites*, W. Krenkel (Ed.). Wiley-VCH Verlag GmbH & Co. KGaA, 2008.

[93] P. Baldus, M. Jansen, D. Sporn. “Ceramic fibers for matrix composites in high-temperature engine applications”. Science, vol. 285 (5428), pp. 699-703, 1999.

[94] P. E. Cantonwine. “Strength of thermally exposed alumina fibers – Part I. Single filament behavior”. Journal of Materials Science, vol. 38 (3), pp. 461-470, 2003.

[95] J. J. Masson, E. Bourgain. “Some guidelines for a consistent use of the Weibull statistics with ceramic fibres”. International Journal of Fracture, vol. 55 (4), pp. 303-319, 1992.

[96] M. R'Mili, N. Godin, J. Lamon. “Flaw strength distributions and statistical parameters for ceramic fibers: The normal distribution”. Physical Review E, vol. 85 (5), pp. 1-6, 2012.

[97] W. Weibull. “A statistical distribution function of wide applicability”. Journal of Applied Mechanics, vol. 103, pp. 293-297, 1951.

[98] P. E. Cantonwine. “Strength of thermally exposed alumina fibers – Part II. Bundle behavior”. Journal of Materials Science, vol. 38 (3), pp. 471-480, 2003.

[99] R. S. Hay, G. E. Fair, T. Tidball. “Fiber strength after grain growth in Nextel 610 alumina fiber”. Journal of the American Ceramic Society, vol. 98 (6), pp. 1907-1914, 2015.

[100] H. D. Wagner, S. L. Phoenix, P. Schwartz. “A study of statistical variability in the strength of single aramid filaments”. Journal of Composite Materials, vol. 18 (4), pp. 312-338, 1984.

[101] H. D. Wagner. “Stochastic concepts in the study of size effects in the mechanical strength of highly oriented polymeric materials”. Journal of Polymer Science Part B: Polymer Physics, vol. 27 (1), pp. 115-149, 1989.

[102] R. W. Rice. “Ceramic tensile strength-grain size relations: grain sizes, slopes, and branch intersections”. Journal of Materials Science, vol. 32 (7), pp. 1673-1692, 1997.

[103] Z. R. Xu, K. K. Chawla, X. Li. “Effect of high temperature exposure on the tensile strength of alumina fiber Nextel 610”. Materials Science and Engineering: A, vol. 171 (1), pp. 249-256, 1993.

[104] G. Das. “Thermal stability of single crystal and polycrystalline alumina fibers and 85% Al_2O_3-15 % SiO_2 fibers”, pp. 977-986 in *19th Annual Conference on Composites, Advanced Ceramics, Materials, and Structures*, J. B. Wachtman Jr. (Ed.). John Wiley & Sons, Inc., 2008.

[105] J. He, D. R. Clarke. “Determination of fibre strength distributions from bundle tests using optical luminescence spectroscopy”. Proceedings of the Royal Society of London. Series A: Mathematical, Physical and Engineering Sciences, vol. 453 (1964), pp. 1881-1901, 1997.

[106] M. Schmücker, F. Flucht, P. Mechnich. “Degradation of oxide fibers by thermal overload and environmental effects”. Materials Science and Engineering: A, vol. 557 (0), pp. 10-16, 2012.

[107] J. Göring, H. Schneider. “Creep and subcritical crack growth of Nextel 720 alumino silicate fibers as received and after heat treatment at 1300°C”, pp. 95-102 in *21st Annual*

Conference on Composites, Advanced Ceramics, Materials, and Structures, J. P. Singh (Ed.). John Wiley & Sons, Inc., 2008.

[108] R. S. Hay, E. E. Boakye, M. D. Petry, Y. Berta, K. Von Lehmden, J. Welch. "Grain growth and tensile strength of 3M Nextel 720™ after thermal exposure", pp. 153-163 in *Proceedings of 23rd Annual Conference on Composites, Advanced Ceramics, Materials, and Structures*, E. Ustundag, G. Fischman (Eds.). John Wiley & Sons, Inc., 2008.

[109] C. Milz, J. Goering, H. Schneider. "Mechanical and microstructural properties of Nextel™ 720 relating to its suitability for high temperature application in CMCs", pp. 191-198 in *Proceedings of 23rd Annual Conference on Composites, Advanced Ceramics, Materials, and Structures*, E. Ustundag, G. Fischman (Eds.). John Wiley & Sons, Inc., 2008.

[110] M. D. Petry, T.-I. Mah. "Effect of thermal exposures on the strengths of Nextel™ 550 and 720 filaments". Journal of the American Ceramic Society, vol. 82 (10), pp. 2801-2807, 1999.

[111] D. M. Wilson, L. R. Visser. "High performance oxide fibers for metal and ceramic composites". Composites Part A: Applied Science and Manufacturing, vol. 32 (8), pp. 1143-1153, 2001.

[112] K. G. Dassios, M. Steen, C. Filiou. "Mechanical properties of alumina Nextel™ 720 fibres at room and elevated temperatures: Tensile bundle testing". Materials Science and Engineering: A, vol. 349 (1–2), pp. 63-72, 2003.

[113] D. M. Wilson. "New high temperature oxide fibers", pp. 1-12 in *High Temperature Ceramic Matrix Composites*, W. Krenkel, R. Naslain, H. Schneider (Eds.). Wiley-VCH Verlag GmbH & Co. KGaA, 2002.

[114] C. J. Armani, M. B. Ruggles-Wrenn, G. E. Fair, R. S. Hay. "Creep of Nextel™ 610 fiber at 1100°C in air and in steam". International Journal of Applied Ceramic Technology, vol. 10 (2), pp. 276-284, 2013.

[115] M. W. Barsoum. *Fundamentals of ceramics*. Taylor & Francis, 2002.

[116] V. H. Hammond, D. M. Elzey. "Comparing the creep response of alumina tows and single filaments". Scripta Materialia, vol. 46 (4), pp. 287-291, 2002.

[117] M. B. Ruggles-Wrenn, S. S. Musil, S. Mall, K. A. Keller. “Creep behavior of Nextel™610/Monazite/Alumina composite at elevated temperatures”. Composites Science and Technology, vol. 66 (13), pp. 2089-2099, 2006.

[118] S. Hackemann, F. Flucht, W. Braue. “Creep investigations of alumina-based all-oxide ceramic matrix composites”. Composites Part A: Applied Science and Manufacturing, vol. 41 (12), pp. 1768-1776, 2010.

[119] J. A. DiCarlo. “Creep limitations of current polycrystalline ceramic fibers”. Composites Science and Technology, vol. 51 (2), pp. 213-222, 1994.

[120] W. R. Cannon, T. G. Langdon. “Creep of ceramics – Part 1. Mechanical characteristics”. Journal of Materials Science, vol. 18 (1), pp. 1-50, 1983.

[121] D. J. Gooch, G. W. Groves. “The creep of sapphire filament with orientations close to the c-axis”. Journal of Materials Science, vol. 8 (9), pp. 1238-1246, 1973.

[122] H. M. Yun, J. C. Goldsby. “Tensile creep behavior of polycrystalline alumina fibers”: NASA Technical Memorandum 106269, pp. 1-9, 1993.

[123] D. J. Pysher, R. E. Tressler. “Tensile creep rupture behavior of alumina-based polycrystalline oxide fibers”, pp. 218-226 in *Proceedings of the 16th Annual Conference on Composites and Advanced Ceramic Materials: Ceramic Engineering and Science Proceedings*, J. B. Wachtman Jr. (Ed.). John Wiley & Sons, Inc., 2008.

[124] W. R. Cannon, T. G. Langdon. “Creep of ceramics – Part 2. An examination of flow mechanisms”. Journal of Materials Science, vol. 23 (1), pp. 1-20, 1988.

[125] R. S. Hay, C. J. Armani, M. B. Ruggles-Wrenn, G. E. Fair. “Creep mechanisms and microstructure evolution of Nextel™ 610 fiber in air and steam”. Journal of the European Ceramic Society, vol. 34 (0), pp. 2413-2426, 2014.

[126] M. Schmücker, H. Schneider, T. Mauer, B. Clauβ. “Temperature-dependent evolution of grain growth in mullite fibres”. Journal of the European Ceramic Society, vol. 25 (14), pp. 3249-3256, 2005.

[127] R. S. Hay, G. E. Fair, K. A. Keller, T. Tidball. “Determination of 3-D alumina grain orientation, size, shape, and growth kinetics from 2-D data in Nextel™610 fibers”. Journal of the American Ceramic Society, vol. 98 (7), pp. 2295-2306, 2015.

[128] Y. Xu, L. Cheng, L. Zhang, H. Yin, X. Yin. “Mechanical properties of 3D fiber reinforced C/SiC composites”. Materials Science and Engineering A, vol. 300 (1-2), pp. 196-202, 2001.

[129] J. C. Goldsby, H. M. Yun, G. N. Morscher, J. A. DiCarlo. “Annealing effects on creep of polycrystalline alumina-based fibers”. Materials Science and Engineering: A, vol. 242 (1-2), pp. 278-283, 1998.

[130] M. Schmücker, P. Mechnich. “Microstructural coarsening of Nextel™ 610 fibers embedded in alumina-based matrices”. Journal of the American Ceramic Society, vol. 91 (4), pp. 1306-1308, 2008.

[131] M. Schmücker, P. Mechnich. “Improving the microstructural stability of Nextel™ 610 alumina fibers embedded in a porous alumina matrix”. Journal of the American Ceramic Society, vol. 93 (7), pp. 1888-1890, 2010.

[132] E. Volkmann, M. D. Barros, K. Tushtev, W. E. C. Pritzkow, D. Koch, J. Göring, C. Wilhelmi, G. Grathwohl, K. Rezwan. “Influence of the matrix composition and the processing conditions on the grain size evolution of Nextel 610 fibers in ceramic matrix composites after heat treatment”. Advanced Engineering Materials, vol. 17 (5), pp. 610-614, 2015.

[133] M. Schmücker, B. Kanka, H. Schneider. “Temperature-induced fibre/matrix interactions in porous alumino silicate ceramic matrix composites”. Journal of the European Ceramic Society, vol. 20 (14–15), pp. 2491-2497, 2000.

[134] M. Schmücker, F. Flucht, H. Schneider. “Temperature stability of 3M Nextel™ 610, 650, and 720 fibers – A microstructural study”, pp. 73-78 in *High Temperature Ceramic Matrix Composites*, W. Krenkel, R. Naslain, H. Schneider (Eds.). Wiley-VCH Verlag GmbH & Co. KGaA, 2006.

[135] S. Wannaparhun, S. Seal. “Combined spectroscopic and thermodynamic investigation of Nextel-720 fiber/alumina ceramic-matrix composite in air and water vapor at 1100°C”. Journal of the American Ceramic Society, vol. 86 (9), pp. 1628-1630, 2003.

[136] J. M. Mehrman, M. B. Ruggles-Wrenn, S. S. Baek. “Influence of hold times on the elevated-temperature fatigue behavior of an oxide-oxide ceramic composite in air and in steam environment”. Composites Science and Technology, vol. 67 (7–8), pp. 1425-1438, 2007.

3 Materials and methods

Within this chapter, a detailed description of the fibers and characterization methods employed is given. Along with the explanation of each method, a brief elucidation on their objectives is also presented, so the reader can have a better understanding of each method applicability. In summary, two mullite fibers were analyzed before and after different thermal exposures. The analysis was divided in two parts. At first, a deep investigation on the microstructure of the fibers through different characterization methods was carried out. Then, these microstructural observations were related to the fibers mechanical responses. Mechanical characterization included bundle tensile tests, and single filament tensile and creep tests at various temperatures. In addition, the methodology here described was also used to evaluate two alumina-based fibers.

3.1 Polycrystalline oxide fibers

As it was constantly evidenced in Chapter 2, the further development of Ox-CMCs depends on the production of oxide fibers with higher thermal stability. Therefore, the main objective of this work is the study of the performance of high-temperature oxide fibers. In this sense, the main investigations here performed were conducted with the mullite fibers Nextel 720 (Lot. 10015) and CeraFib 75. Detailed information about Nextel 720 was given in Section 2.3.2, and the main data given by its manufacturer are displayed in Table 3.1. CeraFib 75 is a relatively new oxide fiber, which was supplied as a laboratory batch from DITF and CeraFib GmbH. This almost fully crystalline mullite fiber was developed to operate at higher temperatures than the commercially available oxide fibers [1]. The production of the fiber is based on the dry-spinning process using a solution with a composition near to the stoichiometric 3/2 mullite, 72 wt.% alumina – 28 wt.% silica. Due to the volatilization of Si species however, the chemical composition of the fiber after pyrolysis is of about 75–25 wt.%, respectively. This results in a 10 μm fiber containing mullite grains with traces of alumina. Further information of the tested fibers is also given in Table 3.1. As shown in the table, the fibers have a different chemical composition. Still, a direct comparison between

them is justified since they are the only fully crystalline mullite fibers available. Additionally, these fibers have the same fields of application related to high-temperature conditions.

Table 3.1: General information of the studied fibers according to their manufacturer [2-4].

Fiber	Manufacturer	Composition (wt.%)	Diameter (μm)	Denier (den)	Strength (MPa)
CeraFib 75	DITF	75 Al_2O_3 25 SiO_2	10	1050	2200
CeraFib 99	DITF	99 Al_2O_3 1 Oxides	10	1265	2900
Nextel 720	3M	85 Al_2O_3 15 SiO_2	10-12	3000	2100
Nextel 610	3M	>99 Al_2O_3	10-12	3000	3100

Most of the methods described below were also used to characterize alumina fibers. The fiber Nextel 610 (Lot. 12647) and the laboratory fiber CeraFib 99 were used for this comparison. Nextel 610 is considered to be the strongest oxide fiber at room temperature, but its alumina microstructure is rather susceptible to thermal degradation, cf. Section 2.4.3. On the other side, CeraFib 99 is an alumina-based fiber with the addition of oxide dopants to inhibit fiber grain growth. This new fiber is also produced by the dry-spinning technique, and was supplied by DITF and CeraFib GmbH.

3.2 Heat treatment

To analyze the thermal stability, the studied fibers were subjected to thermal exposures. In this sense, the analyses listed below were performed with fibers in the as-received state (AR) and after different heat treatments, unless specified. The heat treatments consisted of 25 h exposure to the temperatures of 1000°C (HT 1000), 1200°C (HT 1200), 1300°C (HT 1300) and 1400°C (HT 1400). These temperatures were selected to represent possible temperatures that can be achieved during the lifetime of the fibers. The exposure time of 25 h was chosen in order to ensure that the fibers would present significant property changes based on previous

works, cf. Section 2.4.3. The heat treatments were done in a high-temperature chamber furnace LHT 04/17 (Nabertherm GmbH, Lilienthal, Germany), using a heating rate of 100 °C/h and a cooling rate of 300 °C/h. For that, fiber bundles were sectioned in specific lengths, according to the respective experiment. These fiber bundles were placed on an alumina plate that was positioned in the middle of the furnace. After the heat treatment, the fiber bundles were stored in closed recipients until the subsequent sample preparation. For the experiments on AR fibers, the polymeric coating, in which the fibers are supplied, was thermally removed in the same chamber furnace at 600°C for 2 h. The handling and preparation of all fiber samples were done using surgical gloves to avoid contaminations.

3.3 Characterization methods

3.3.1 Scanning electron microscopy

The high performance of polycrystalline oxide fibers is mainly related to their fine grain arrangement. Hence, it is of extreme importance the monitoring of these nano-sized microstructures to ensure the mechanical properties of the fiber. Microstructural observations could be perceived by scanning electron microscopy (SEM). In order to reveal the grain arrangements, an extent specimen preparation method was conceptualized in this work. The main problem of revealing the grain boundaries is that conventional chemical etching techniques are not easily applied to oxide materials, because of their high chemical resistance. Therefore, a thermal etching was performed for this matter. The author acknowledges that the temperatures used for the thermal etching can also impair the microstructure of the fibers. However, since the microstructural analyses were done on fibers thermally etched under the same conditions, the comparison of results is still valid in a qualitative way.

In order to perform the thermal etching, sample surface preparation was carried out. Since the handling of the fibers is difficult, fiber bundle samples were first inserted in a shrinkage tube for their correct alignment. The tube was shrieked at 200°C using a hot air gun PHG 630 DCE (Robert Bosch GmbH, Stuttgart, Germany). Subsequently, the shrieked tube containing the fibers was embedded in slow-curing transparent epoxy EpoFix (Struers ApS, Ballerup, Denmark) using a vacuum impregnation unit CitoVac 05926119 (Struers ApS, Ballerup, Denmark). Surface preparation was done using an automatic polishing machine Mecatech 234 (PRESI, Eybens, France) in several steps, see Table 3.2. At first, samples were grinded to

obtain a plane surface using resin bonded diamond discs MD-Piano (Struers ApS, Ballerup, Denmark) with grit sizes of 80, 220, 500 and 1200. Afterwards, samples were polished using woven acetate polishing cloths MD-Dac (Struers ApS, Ballerup, Denmark) and two different diamond suspensions DiaPro (Struers ApS, Ballerup, Denmark) with particle sizes of 9 and 3 μm. After surface preparation, samples were cleaned in a Bransonic® ultrasonic cleaner 1510E-MT (Branson Ultrasonics Corporation, Connecticut, USA).

Table 3.2: Parameters used for the sample surface preparation.

Step	Time (s)	Base speed (rpm)	Head speed (rpm)	Head direction	Force (N)
Grinding, 80	-	250	120	same	25
Grinding, 220	120	250	120	same	25
Grinding, 500	130	250	120	same	20
Grinding, 1200	120	250	120	contra	20
Polishing, 9 μm	105	250	120	contra	20
Polishing, 3 μm	80	250	120	contra	25

Before the thermal etching, the embedding resin used for surface preparation was thermally extracted. This was done in the chamber furnace LHT 04/17 at 800°C for 2 h. The prepared surface could be then etched using a customized tube furnace (Vecstar Ltd., Chesterfield, United Kingdom). The procedure consisted of pushing the samples to the middle of the tube furnace, region at the etching temperature, and then slowly pushing the sample back. Thermal etching was done at 1300°C and 1200°C, both lasting 30 min, for mullite and alumina fibers, respectively. Etching parameters were chosen in accordance to procedures found in the literature [5-7] and pre-tests. Attention was given to use the lowest etching temperature possible to avoid possible grain growth. Therefore, the same etching temperature was used for all fibers before and after the heat treatments.

The cross-sections of the etched fibers were observed using a ZEISS Supra 40 SEM (ZEISS, Oberkochen, Germany). The micrographs were obtained using low acceleration voltage of 0.5-1.0 kV on samples without sputtering. For each fiber condition, pictures were taken from the middle of five different fibers. For the quantification of the results, the grain size was

determined using the intercept-line method [8] on all pictures with the software Lince (TU Darmstadt, Germany). The method consists of tracing lines in different directions, and manually marking the grain intersections, as exemplified in Figure 3.1. For statistical purposes, more than 200 grains were analyzed this way for each fiber condition.

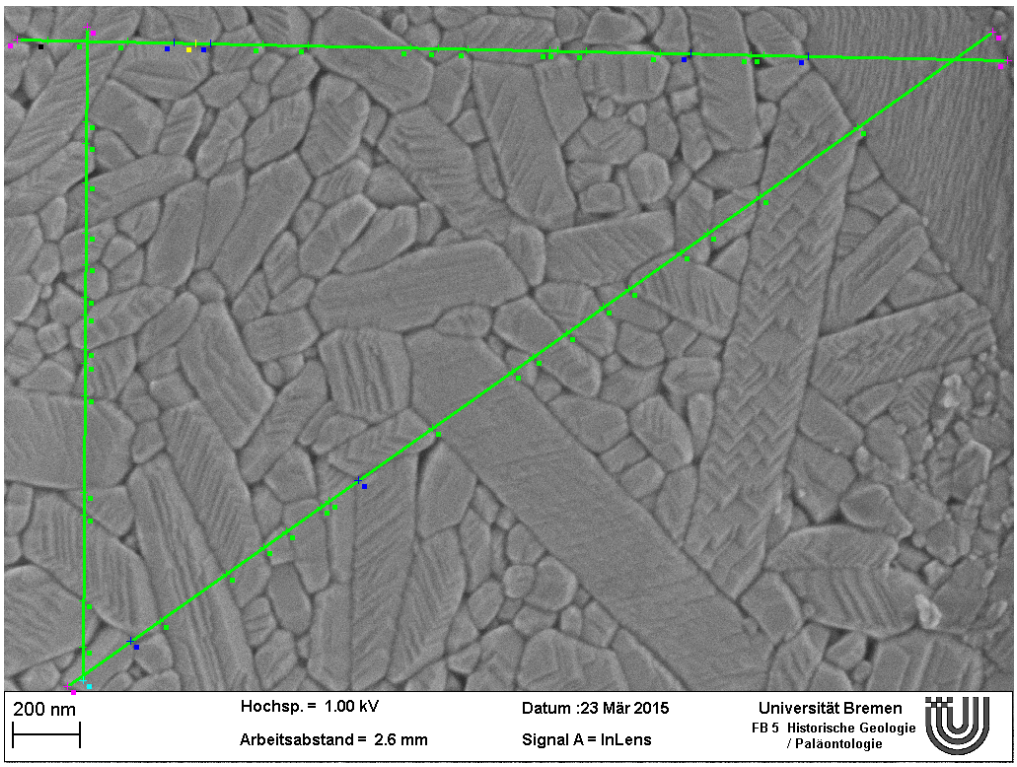

Figure 3.1: Example of analysis by the intercept-line method.

3.3.2 Energy dispersive X-ray

Together with the SEM, energy dispersive X-ray analysis (EDX) was also carried out. The measurements were done on as-received samples to verify their chemical composition, since it might differ from the information given by the manufacturers due to variations on the fiber processing. For that, data were collected with a XFlash® 6T|30 detector (Bruker Nano GmbH, Berlin, Germany) attached to the SEM. Sample preparation was much easier than the procedure described above. Fibers were glued to the sample holder using carbon tape, and subsequently sputtered with carbon. For the EDX, an acceleration voltage of 15 kV was used on the fibers surface. Chemical elements were quantified using the software ESPRIT 1.9 (Bruker Nano GmbH, Berlin, Germany).

3.3.3 X-ray diffraction

To better understand the microstructure of the polycrystalline fibers, the present crystal phases were analyzed. X-ray diffraction (XRD) was used to identify and quantify the phases along with other useful information about them. The preparation of the specimens was done by crushing the fiber bundles into a fine powder using a porcelain mortar 55/3 and pestle 56/00 (Haldenwanger Technische Keramik GmbH, Waldkraiburg, Germany). Samples were crushed this way for about 10 min in order to obtain a homogeneous powder that could be later compared to standards during data compilation. X-ray diffraction data were collected at room temperature on a Bragg-Brentano PANalytical X'Pert MPD PRO diffraction system (PANalytical GmbH, Kassel-Waldau, Germany), equipped with Cu-Kα radiation (λ = 1.5418 Å), ¼° fixed divergence, primary and secondary Soller slits with 0.04 rad aperture, secondary Ni-filter and X'Celerator detector system with 127 channels. Samples were prepared with the standardized PANalytical loading system using circular sample holders with 16 mm of diameter. Scans were performed in the range from 5° to 120° 2θ, step width of 0.0167°2θ; total measuring time of about 68 min.

After the measurements, the line profiles were corrected with the Rietveld procedure using the least square approach [9]. Rietveld refinements were done with the software Diffracplus Topas 4.2 (Bruker AXS GmbH, Karlsruhe, Germany). With the refinements, the crystalline phases could be identified and quantified. In addition, the lattice constants *a*, *b* and *c* were calculated with the refined profiles. For the mullite fibers, the lattice parameter *a* could also be related to the composition of the mullite phase. Using the equation proposed by Fischer [10], the mol content of alumina in the mullite phase was calculated as:

$$\text{Alumina content} \equiv 144.5\, a - 1029.5 \qquad (4)$$

Another important parameter obtained with the XRD analysis was the determination of the crystallite size. Even though they are different parameters, the crystallite size can be related to the grain size in the case of the polycrystalline fibers. The determination of the crystallite size was done by analyzing the height of the peaks [11], considering the Lorentz components [12]. With this study, it was possible to analyze separately the crystallite size of the mullite and alumina phases, in the case of mullite fibers, which was not possible through the micrographs.

Still, both values, crystallite and grain size, were compared for all fibers to see if they are in accordance.

3.3.4 High-temperature XRD

In situ high-temperature XRD measurements were also performed on the mullite fibers. Due to their more complex microstructure, it is expected that mullite fibers will undergo crystal phase transformations at elevated temperatures. Therefore, several XRD scans were performed over time at 1200°C. Measurements were performed in the same diffractometer described above, and equipped with a high-temperature chamber HTK1200N (Anton Paar, Vienna, Austria). Data acquisition parameters were different than the room-temperature measurements in order to reduce the measuring time. Data were collected from 5 to 120° 2θ, step width of 0.017°, resulting in a measuring time of 46 minutes for each scan. For control, measurements were also done during the heating of the sample by holding the temperature constant at room temperature, 200, 400, 600, 800 and 1000°C. At 1200°C, the temperature was kept constant, and scans were done continuously for approximately 8 h. In total, 11 diffraction patterns were measured at 1200°C. The main analysis performed in this experiment was in relation to the quantification of the crystalline phases, performed with the Rietveld refinements.

3.3.5 Density measurement

Another physical property measured for the oxide fibers was the density. This parameter was used to evaluate the as-received fibers. Given the fine microstructure of the fibers, the detection of defects is rather difficult. Therefore, the measurement of the density can be used as an indication of possible micro porosity in the fibers [13]. Density measurements were done based on the principle of Archimedes, following the norm ASTM D 3800 [14]. The equipment used was a laboratory balance BP210S (Sartorius AG, Göttingen, Germany) with resolution of 0.1 mg, and adapted for suspension weighing as shown in Figure 3.2. For the measurement, AR fiber bundles with 5 m of length were used.

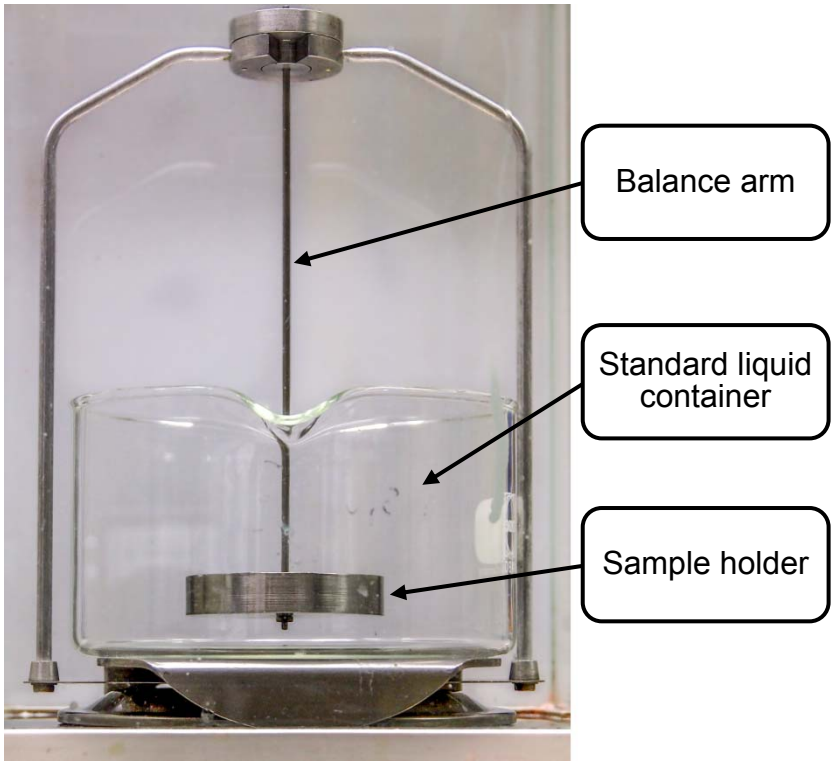

Figure 3.2: Adapted Archimedes balance for fiber density measurement.

The density of the sample was calculated by the relation of the dry and submersed weight of the specimens. First, the fiber bundle was weighted in air. Then, the fibers were submersed in absolute ethanol. This was done inside a vacuum chamber to avoid accumulation of air between the fibers. The immersed fiber bundle was weighed, and the density could be measured with Equation 5.

$$\rho = \frac{W}{W - W_l}\,\rho_l \tag{5}$$

where ρ is the material density, W is the sample weight in air, W_l is the apparent immersed weight of the sample, and ρ_l is the standard liquid density, 0.789 g/cm^3 for absolute ethanol. The calculated fiber density was later used to determine the area of the fiber bundle, as it will be described in Section 3.4.3.

3.4 Mechanical tests

3.4.1 Single-filament tensile test

Since the fibers studied in this project are used as reinforcements for composites, the tensile strength was the main parameter used to compare the specimens. Fibers can be tested in two ways: extracting and testing each single filament, or testing the whole bundle of fibers. The most traditional way of evaluating reinforcement fibers is by single filament tests, because it measures directly the strength of each fiber. However, this procedure can be tedious considering the small size and difficult handling of the samples. In this work, the fibers were tested as single filaments, described below, and also as fiber bundles, described in Section 3.4.3.

Single-filament tensile tests were performed in accordance to the standard DIN EN 1007-4 [15]. Tests were conducted in a servo-motor testing machine designed at the institute, depicted in Figure 3.3. This testing machine was equipped with a load cell ULC-1N (Interface Inc., Arizona, USA) for the measurement of the applied load, and a linear variable differential transducer LVDT AX/1/S (Solartron Metrology, Bognor Regis, United Kingdom) for the measurement of the specimen displacement. Since the single filaments are rather difficult to handle, samples were first glued to a paper frame using a two-component epoxy glue UHU Plus Schnellfest (UHU GmbH & Co., Bühl, Germany). The paper frame was designed for the correct positioning and alignment of the fiber with the testing machine, as well as for defining the gauge length of the specimens. Two gauge lengths were used: 25 mm, according to the standard, and 70 mm, to be compared with the samples of the creep tests described in Section 3.4.4. After the correct positioning of the sample, the sides of the paper frame were cut so only the fiber was tensioned. Samples were tested until failure with a traveling speed of 1 mm/min. In total, 30 samples were tested for each fiber condition.

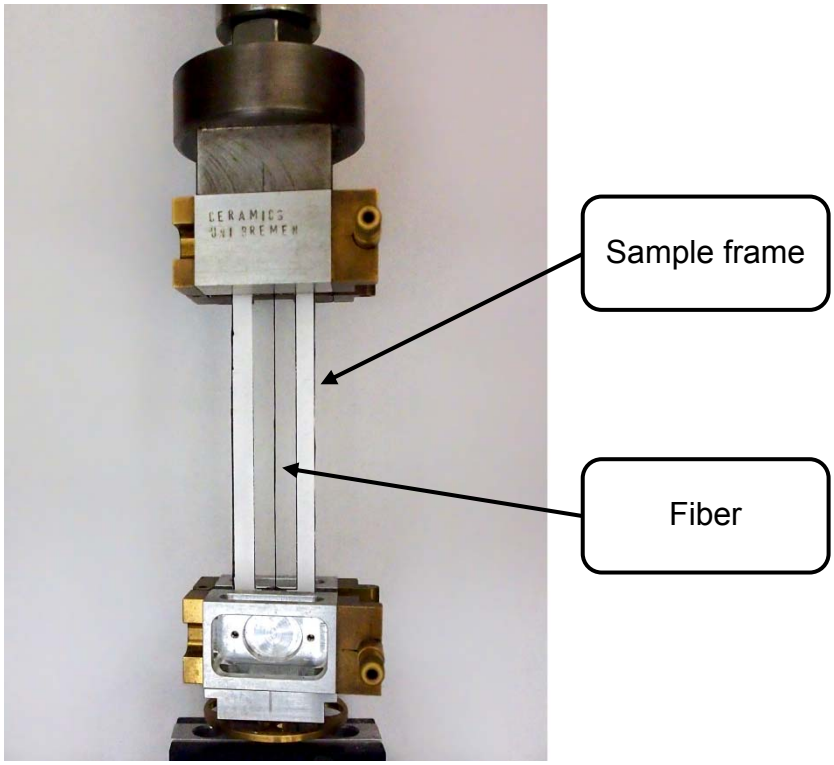

Figure 3.3: Test set-up for single filament tensile test.

After the tests, the strength of each filament was calculated with Equation 6:

$$\sigma = \frac{F_{MAX}}{A_0} \tag{6}$$

where σ is the strength, F_{MAX} is the maximum force measured during the tensile test, and A_0 is the sample initial area. The cross-section area of each filament was determined after the test by analyzing the fracture surface using an optical microscope SENSOFAR PLμ 2300 (Sensofar Group, Terassa, Spain). Weibull distribution was used to describe the strength of the tested filaments. In this matter, the characteristic strength and the Weibull modulus were determined with the maximum likelihood estimation [16, 17].

With this testing set-up, the deformation of the fiber could not be directly calculated since the displacement measured was due to the deformation of the fiber and the deformation of the testing rig. Consequently, the system compliance was determined prior to testing. For that, specimens were tested with the gauge lengths of 25 mm, 40 mm and 70 mm, as exemplified in

Figure 3.4a, and the total compliance C_i was determined for each sample length. Note that C_i is the inverse of the inclination of the load *vs.* displacement curve. Five samples were tested for each length, and the total compliance was then plotted against the samples initial length, Figure 3.4b. By performing a linear regression, the system compliance with a fiber length of zero can be estimated. In other words, this is the system compliance without a fiber being tested, which is the compliance of the testing machine C_p. Values of C_p were determined for each fiber in the as-received state, and are displayed in Table 3.3.

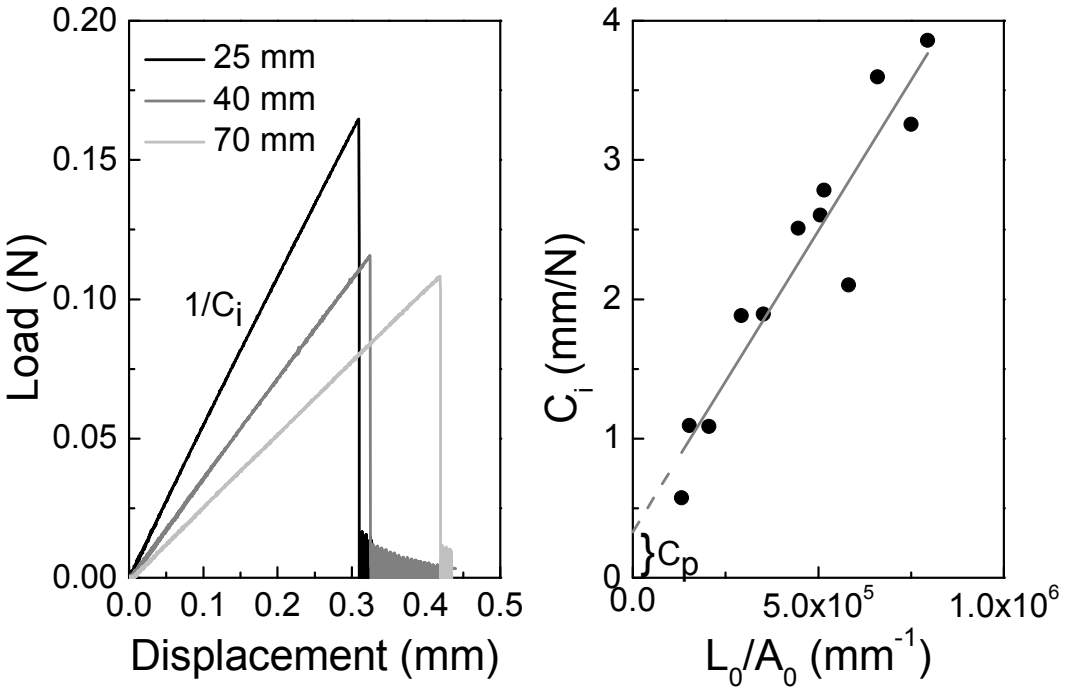

Figure 3.4: Example of system compliance correction performed for room-temperature tests: samples tested with different gauge length resulting in different system rigidity (left), linear regression of the system rigidity in relation to the tested fiber length (right).

With the system compliance, the deformation and the elastic modulus of the tested filaments were determined with Equation 7 and Equation 8, respectively.

$$\varepsilon = \frac{F\ (C_i - C_p)}{L_0} \times 100\% \qquad (7)$$

$$E = \frac{L_0}{A_0\,(C_i - C_p)} \tag{8}$$

where ε is the strain, F is the applied force, L_0 is the initial sample length, and E is the elastic modulus of the fiber. The strain to failure of the fibers was also described with the Weibull statistics, while the elastic modulus was characterized by the normal distribution.

Table 3.3: Testing machine compliance for single filament tensile tests at room temperature (C_p) and heated length compliance (C_h) for the tests at 1000, 1100, 1200 and 1400°C.

Fiber	C_p (mm/N)	C_h 1000°C (mm/N)	C_h 1100°C (mm/N)	C_h 1200°C (mm/N)	C_h 1400°C (mm/N)
CeraFib 75	0.330	0.437	0.483	0.559	0.761
CeraFib 99	0.799	0.372	0.421	0.512	-
Nextel 720	0.289	0.244	0.262	0.289	0.395
Nextel 610	0.409	-	-	-	-

3.4.2 High-temperature tensile test

The mechanical behavior of the fibers at high temperature is of great concern. In this matter, single filament tensile tests at elevated temperatures were also conducted. The tests were done in accordance the standard DIN EN 1007-6 [18], following the cold-end method. The testing machine was the same described above. To achieve the testing temperature, a two heating element oven was designed, see Figure 3.5. The oven consists of two SiC heating element igniters 210 N (Norton Ignitor Co., Massachusetts, USA) and isolation walls of 10 mm each. A thermocouple type-R was also positioned in the middle of the oven to control the testing temperature. The total length of the oven was of 40 mm. Therefore, 70 mm samples were used for this test. Sample preparation was the same as described in Section 3.4.1. After the correct positioning and alignment, the frame was cut out and the fiber heated to the testing temperature with a rate of 1 °C/s. Before starting the test, the target temperature was held for 5 min. Specimens were then tested until failure with a traveling speed of 1 mm/min at the temperatures of 900-1400°C. Only AR fibers were tested this way, and a sample size of 30 fibers was used for each temperature.

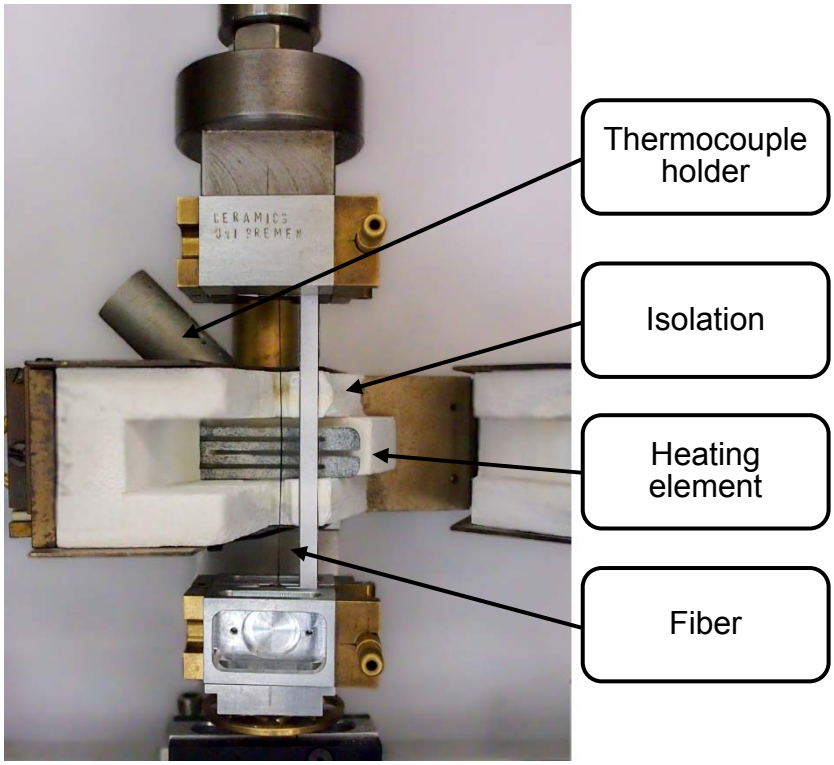

Figure 3.5: Test set-up for single filament tensile test with oven.

Since the temperature inside the oven is not constant, temperature profiles were measured for each testing temperature used. The profiles were done by measuring the temperature along the vertical axis of the oven with a thermocouple type-S traveling with a speed of 1 mm/min. Figure 3.6 shows an example of a measured temperature profile, in which different regions can be identified in relation to the temperatures along the vertical axis. The initial length of the fiber L_0 is divided into three regions. L_h is the portion of the fiber that is at the testing temperature considering a ΔT of 25°C, which is of about 9 mm. L_{d1} and L_{d2} are the remaining lengths of the oven that are at temperatures below the testing temperature, while L_{c1} and L_{c2} are the lengths of the sample outside of the oven, where the temperature tends to 25°C, room temperature. The actual temperature profiles of every temperature used can be seen in Appendix A.3. Given that the control thermocouple, used during the tensile tests, was positioned in the middle of the oven, at a temperature below the maximum temperature, the temperature profiles were also used to correlate the control temperature with the actual testing temperature.

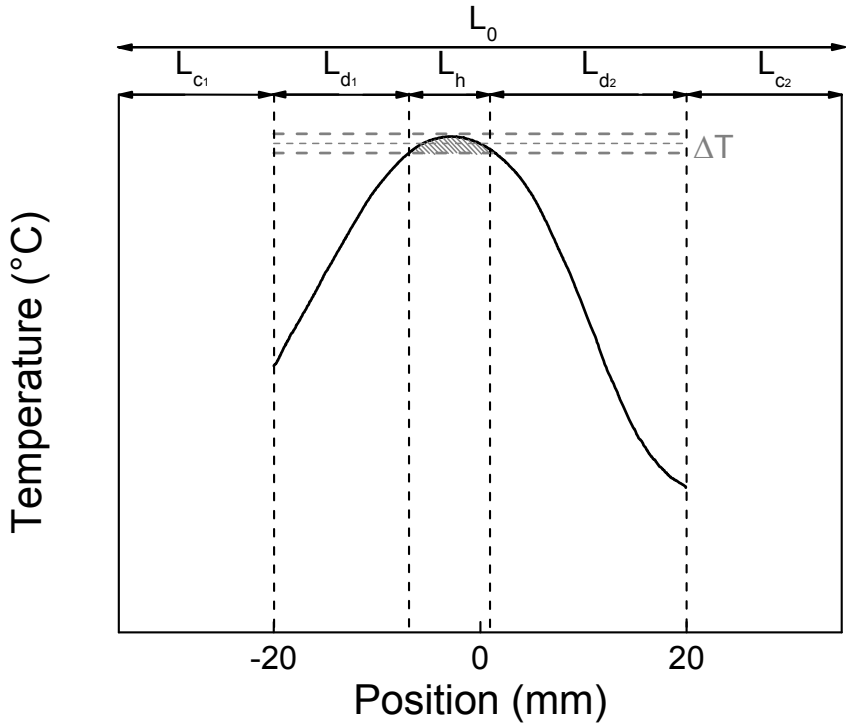

Figure 3.6: Example of temperature profile of the oven used for single filament tensile tests at elevated temperatures.

For the calculation of the strain of the fiber at the testing temperature (ε_h), system compliance was determined prior to the high-temperature tests. In this case, it was necessary to determine the compliance of the heated length L_h, since the displacement measured during test was due to the deformation of the testing machine, previously determined as C_p, and of the whole length of the fiber, divided into L_h, L_d, L_c. For that, fibers were tested with different initial lengths of 70 mm, 80 mm and 100 mm, in other words, varying L_c. Subsequently, the total compliance C_i was plotted against the initial fiber length. By performing a linear regression until the length of the oven ($L_h + L_d$), the compliance of the oven ($C_h + C_d$) can be determined. Then, the variation of the compliance inside the oven was interpolated considering the compliance of the testing machine C_p, as exemplified in Figure 3.7. The compliance of the heated length C_h was then equal to the variation of the compliance along L_h. C_h was determined for all fibers at the testing temperatures used, and the values can be seen in Table 3.3.

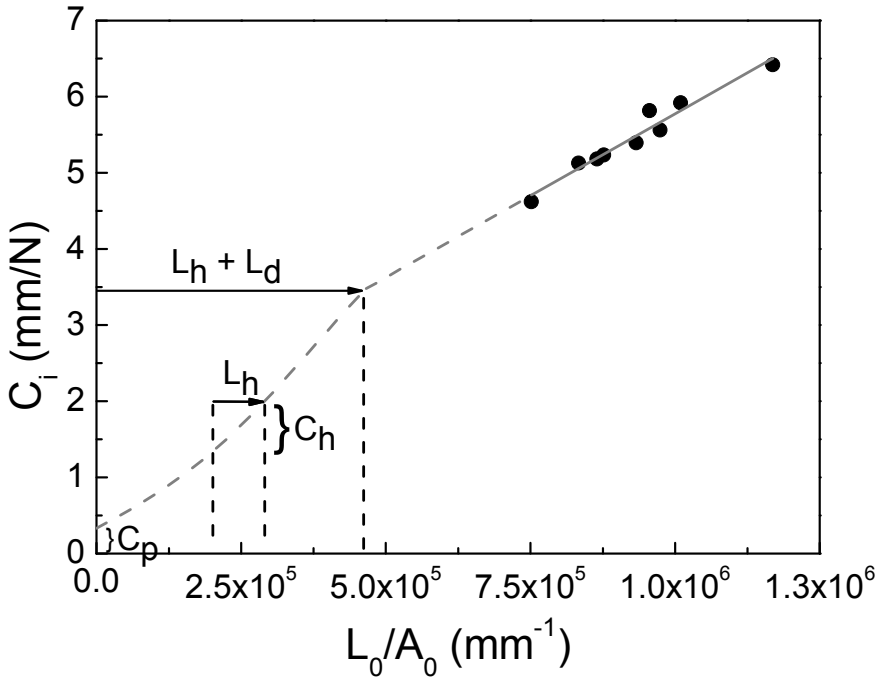

Figure 3.7: Example of system compliance correction performed for high-temperature tests.

The deformation ε_h and the elastic modulus E_h of the fiber at the heated region was then determined with the equations below:

$$\varepsilon_h = \frac{F\ C_h}{L_h} \times 100\% \tag{9}$$

$$E_h = \frac{L_h}{A_0\ C_h} \tag{10}$$

3.4.3 Fiber bundle tensile test

The second method used to characterize the strength of the fibers was the fiber bundle test. In this test, the whole bundle of fibers is stressed at the same time. Several authors defend the use of this test over experiments on single filament. The main advantage of this test is the considerable easier sample preparation. Due to the small size of the fibers, the separation and handling of single filaments is rather tiresome. Not to mention that this extensive handling can already damage the fibers. According to the literature, it is even suggested that the weaker fibers of the bundle break during the separation, therefore altering the measured strength

distribution [19]. In the case of fiber bundle tests, the whole bundle is tested, which avoids the damage during sample preparation. The sample size of this test is also considerably higher, given that one fiber bundle can contain more than 400 fibers. In addition, results from fiber bundle tests are somewhat more representative considering that fibers are normally used as bundles in composites [20]. Nevertheless, the main drawback of this testing technique is that the results are rather dependent on the alignment and interaction of the fibers in the bundle. Hence, only the strength of the whole bundle can be directly measured. In order to evaluate the strength of the fibers in the bundle, a more extensive data treatment must be performed, as it will be shown later in this section

Fiber bundle tensile tests were done in accordance to the standard DIN EN 1007-5 [21], but with a gauge length of 25 mm. The reason for this smaller specimen length is due to the acquisition of acoustic emission signals, which will be explained later in this section. All experiments were performed on an universal testing machine Zwick/Roell Z005 (Zwick GmbH, Ulm, Germany) equipped with a U2B / 5kN load cell (HBM Inc., Massachusetts, USA). A photo of the testing set-up can be seen in Figure 3.8. Sample preparation method was similar to the one used for single-filament tests, but it proved to be a lot easier. Fiber bundles were aligned in alcohol and glued in between two paper board frames using a stronger two-component epoxy glue UHU Plus Endfest 300 (UHU GmbH & Co., Bühl, Germany). The specimens were attached to the testing machine using metallic plates. Then, the frames were cut and the bundle tested with a traveling speed of 0.01 mm/min. Samples were tested until all fibers of the bundle were apparently broken, *i.e.*, measured force tending to zero. Three fiber bundles were tested this way for each fiber condition.

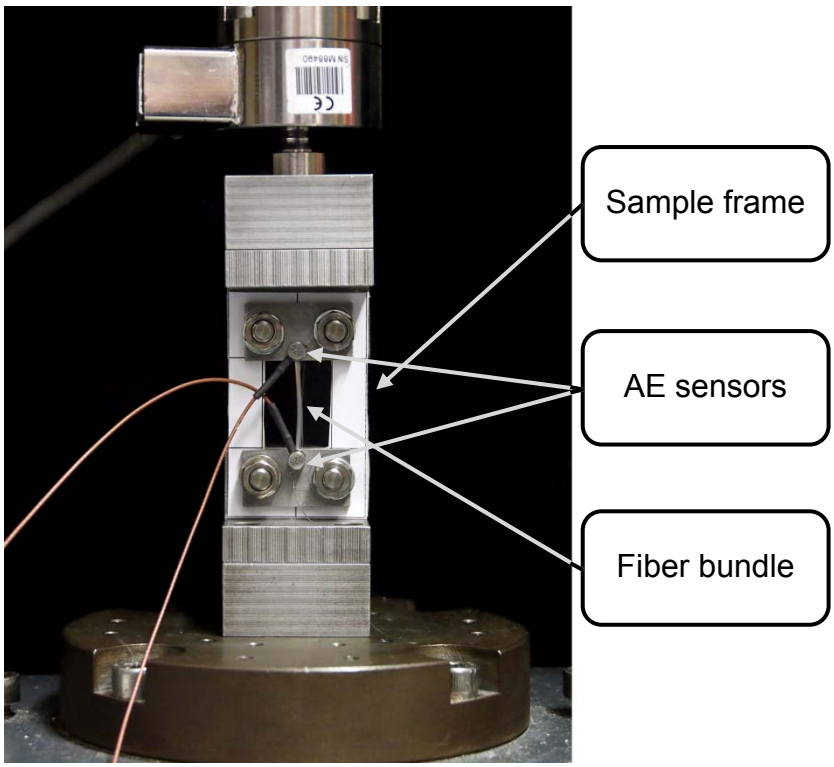

Figure 3.8: Test set-up for fiber bundle tensile test with acoustic emission sensors.

The strength of the bundle was calculated using Equation 6, but considering the initial fiber bundle area. It should be noted that since the weaker fibers in the bundle fail before the maximum load is achieved, the calculated stress does not account for the instant area of the bundle, and therefore, the term apparent stress/strength is used. The estimation of the initial bundle area was done prior to testing. For that, three AR bundles with a length L_0 of 100 mm were weighed. Considering that the area of the bundle is constant along its length, the initial bundle area was calculated with the average values of the three bundles using Equation 11.

$$A_B = \frac{W}{\rho\, L_0} \tag{11}$$

where A_B is the fiber bundle initial area, W is the weight of a fiber bundle with length L_0, and ρ is the density of the fibers calculated according to Section 3.3.5.

The drawback of measuring the apparent strength of the fiber bundles is that this parameter is rather dependent on how the fibers are arranged. After the fibers start to fail, the load is

redistributed to the other load-carrying fibers. If the surrounding fibers fail to sustain this load redistribution, an avalanche failure effect will take place [22, 23]. For this reason, the apparent strength of the bundle is much smaller than the single-filament strength, and depends on the interaction of the fibers. Some authors even suggest that the use of lubricants can increase the apparent bundle strength [24, 25]. Given these facts, the correct way to analyze the results of fiber bundle tests is by estimating the failure distribution of the fibers in the bundle. For this purpose, several authors have used the acoustic emission (AE) approach [24-26]. The idea of this technique is to monitor the acoustic waves that the sample emits. Perturbations, *e.g.*, a fiber failing, alter this acoustic wave. By applying predefined parameters, these perturbations (hits) are detected and recorded, which can be later associated to a specific event.

The AE detection device used was an AMSY4-MC2 (Vallen Systeme GmbH, Icking, Germany) with two VS 600-Z2 piezoelectric AE sensors (Vallen Systeme GmbH, Icking, Germany). Since the sensors could not be attached to the fiber bundle directly, they were glued to the metallic plates of the upper and lower fixtures using EVA-based hot glue, Pattex Hot Sticks (Henkel AG & Co., Düsseldorf, Germany), cf. Figure 3.8. As mentioned before, the gauge length used, 25 mm, was smaller than the one described in the standard DIN EN 1007-5 [21]. This reduced length was used for better acquisition of the acoustic emission signals, *i.e.*, to avoid the attenuation of the signals before they reached the sensors. Here the author acknowledges that other authors also used different gauge lengths than the one described by the standard when measuring acoustic emission signals, *e.g.*, Pappas et al. [26] tested samples with 30 mm gauge length. During the tensile tests, the device pre-amplified the signals measured by both sensors, and recorded the wave information whenever a hit was identified. The parameters used to identify a hit were threshold, duration discrimination time (DDT) and rearm time (RT). Whenever the amplitude of the measured acoustic wave surpasses the threshold, the device starts to record a hit. To define the duration of the hit, DDT was measured every time the wave amplitude "crossed" the threshold. If no threshold crossing happens between the DDT interval, the device considers the whole event as one hit. Afterwards, RT was measured, and if no threshold crossing happens, the device can then start recording a new event. If there is a threshold crossing during the RT interval, the device associates this second event with the previous hit and the event is recorded as a cascaded hit. To help the reader to understand how a hit is identified, Figure 3.9 presents a schematic of an

acoustic wave during an event. The parameters used for the acquisition and filtering of the data were defined experimentally, and are shown in Table 3.4.

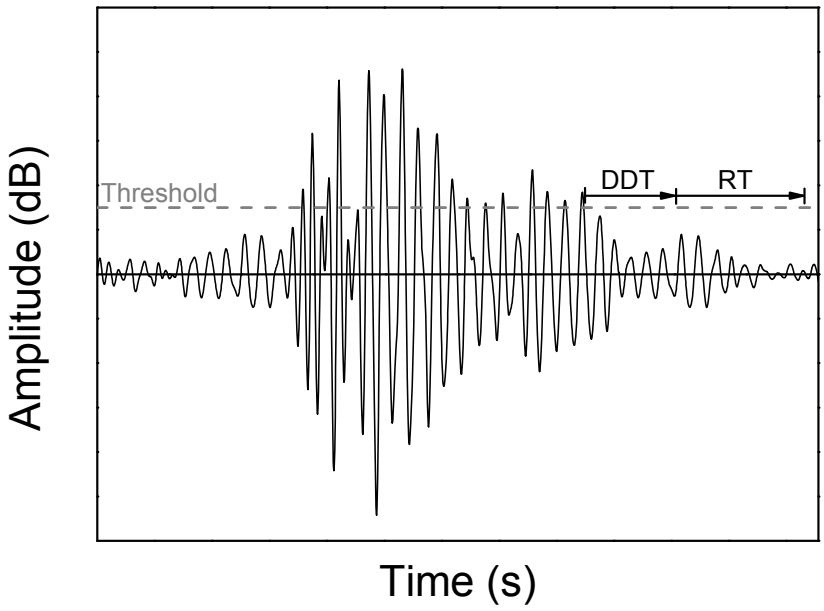

Figure 3.9: Schematic of an acoustic emission wave showing the hit detection parameters: threshold, duration discrimination time (DDT) and rearm time (RT).

Table 3.4: Parameters used for acoustic emission acquisition.

Coupling	EVA
Preamplifier gain	34 dB
Acquisition filter	95-850 kHz
Threshold	40 dB
Duration discrimination time (DDT)	50 μs
Rearm time (RT)	100 μs
Threshold crossing filter	>35

Considering that the fibers only deform elastically before failing, each hit was associated with a fiber failure. With this set-up, the fiber failures could be identified as long as they were 50 μs apart. To avoid noise, only hits with more than 40 threshold crossings were used in this

analysis. This filter was defined by measuring the acoustic wave of twenty different single filaments breaking. The filtered hits were synchronized with the data from the testing machine, and it was then possible to identify the moment, *i.e.*, apparent stress and deformation, that each fiber in the bundle failed. With these results, the failure distribution of the fibers in the bundle could be estimated. The distribution was done in relation to the strain values since it does not depend on the number of load-carrying fibers in the bundle, which varies during the test when the fibers start to fail [20]. It is suggested in the literature that different distributions can fit the results of bundle tensile tests, depending on the fiber bundle [27, 28]. Therefore, results were fitted using Weibull, normal, log-normal and gamma distributions. Since the Weibull statistics was the best fit for most results, this distribution was used for the comparison of the different fiber conditions. In this sense, the characteristic strength of the fibers was calculated as follows:

$$\sigma_0 = E_B\, \varepsilon_0 \tag{12}$$

where σ_0 is the characteristic strength, E_B is the initial fiber bundle elastic modulus, before fiber failure takes place, and ε_0 is the characteristic strain to failure estimated with the AE results. For the calculation of the strain, the system compliance was measured prior to testing with the procedure explained in Section 3.4.1 using bundle lengths of 25, 70 and 100 mm.

3.4.4 Creep test

The long-term mechanical performance of the fibers was accessed through tensile creep tests on single filaments. This test can be considered the most representative of possible Ox-CMCs applications, in which the components are mechanically loaded at elevated temperatures for several times. Different creep loads and temperatures were used to characterize AR fibers. In addition, heat treated mullite fibers were also tested under the same conditions to evaluate the influence of a previous thermal exposure on the long-term performance of these fibers.

Creep tests performed followed the standard DIN EN 15365 [29]. Figure 3.10 shows the testing rig that was constructed at the institute for the creep tests, based on previous works [30, 31]. Basically, the upper end of the single filament was attached to the upper fixture of the equipment, while the lower end was attached to a weight. To apply the creep stress, a dead load system was chosen with the intention of obtaining a precise and constant load. An oven,

similar to the one described in Section 3.4.2, was placed in the center to heat the middle of the sample to the testing temperature. The displacement of the specimen was recorded by a capacitive non-contact displacement transducer Capa NCDT 600 (Micro-Epsilon Messtechnik GmbH, Ortenburg, Germany) placed in a platform below the dead weight, measuring the distance between the platform and the end of the sample. The temperature of the displacement sensor was also recorded during the test to account for the dilatation of the testing rig.

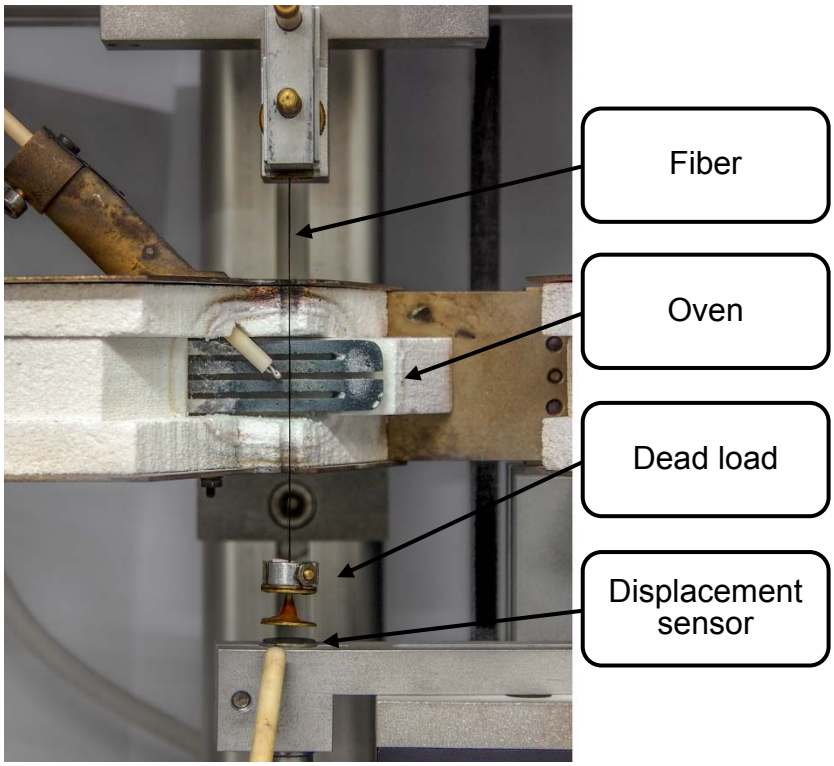

Figure 3.10: Test set-up for single filament creep tensile test.

The testing procedure was as follows. First, the fiber was clamped to the fixture device and the dead load outside of testing rig. The distance between the fixture and the load was set as 70 mm, *i.e.*, the initial length of the sample L_0. Then, both devices were attached to the testing rig. Before heating the specimen, the platform of the displacement sensor was moved up until it touched the dead weight, and therefore, the load applied to the fiber was null. Afterwards, the sample was heated at a rate of 1 °C/s, and the target temperature was held for 15 min before starting the test. Subsequently, the load was slowly released by moving the platform 1 mm down using a micrometer screw. The specimens were tested until failure, or until the run-out time of 50 h was achieved. Three different loads were used on the tests: 1.60, 2.12 and

2.63 g for CeraFib fibers; and 2.63, 3.62 and 4.22 g for Nextel fibers. Heavier loads were used for Nextel fibers because of their bigger diameter, cf. Table 3.1. Nonetheless, the actual applied stress was later calculated by measuring the cross-section area of the samples on the SENSOFAR optical microscope. The experiments were conducted at the temperatures of 1100, 1200 and 1300°C. In general, two samples were tested for each condition presented above.

As already discussed for the high-temperature tensile tests, the drawback of using the cold-end method is that the measured displacement is due to not only the deformation of the fiber at the testing temperature, but also due to the deformation of the fiber sections at lower temperatures. For this reason, an effective length L_{eff} was determined, which relates the measured displacement with the creep strain of the specimen at the heated region. The method used was based on the work of Morrell [32], which considers that the total creep strain, due to the fiber at different temperatures, and the total strain rate are given as:

$$\varepsilon_T = \frac{\Delta l}{L_0} \quad ; \quad \dot{\varepsilon}_T = \frac{\dot{\Delta} l}{L_0} = \frac{1}{L_0} \int_0^{L_0} \dot{\varepsilon}\, dl \qquad (13)$$

where ε_T is the total creep strain, Δl is the variation of length, *i.e.*, total displacement measured, and L_0 is the initial length.

By definition, the creep strain of the specimen at the heated region is given by the total displacement measured and the effective length L_{eff}. Therefore, the creep strain and strain rate at the testing temperatures are:

$$\varepsilon_h = \frac{\Delta l}{L_{eff}} \quad ; \quad \dot{\varepsilon}_h = \frac{\dot{\Delta} l}{L_{eff}} = \frac{1}{L_{eff}} \int_0^{L_0} \dot{\varepsilon}\, dl \qquad (14)$$

where ε_h is the creep strain at the testing temperature.

By dividing Equation 13 with Equation 14, the relation between the total strain rate and the strain rate at the heated region can be expressed as:

$$\frac{\dot{\varepsilon}_T}{\dot{\varepsilon}_h} = \frac{L_{eff}}{L_0} \tag{15}$$

Now considering that the creep rate follows the power rule, Equation 3, and that the different regions of the sample are all subjected to the same creep stress, but different temperatures, the creep rate can be expressed as:

$$\dot{\varepsilon} = \frac{A\sigma^n}{L_0} \int_0^{L_0} \exp\left(\frac{-Q}{R\,T(l)}\right) dl \tag{16}$$

where *T(l)* is the temperature profile, cf. Figure 3.6, and T_h is the temperature of the heated region considering a ΔT of 25°C.

Combining both equations, the relation between the creep rates can be rewritten as:

$$\frac{\dot{\varepsilon}_T}{\dot{\varepsilon}_h} = \frac{L_{eff}}{L_0} = \frac{1}{L_0} \int_0^{L_0} \exp\left[\frac{-Q}{R}\left(\frac{1}{T(l)} - \frac{1}{T_h}\right)\right] dl \tag{17}$$

Since the temperature profile was obtained through a discrete method acquisition, it is then pertinent to discretize Equation 17. Utilizing a numerical summation of increments of length *b*, the effective length can be estimated as:

$$L_{eff} = \frac{L_0}{k} \sum_{i=0}^{k} \exp\left[\frac{-Q}{R}\left(\frac{1}{T_i} - \frac{1}{T_h}\right)\right] \quad ; \qquad L_0 = k\,b \tag{18}$$

From Equation 18, it is possible to see that L_{eff} is a function of the temperature profile and the activation energy of the tested fiber Q. However, Q can only be defined experimentally by fitting the strain rate of fibers tested at different temperatures. The problem is that to calculate the strain rate, L_{eff} is needed, which in turn depends on Q. To solve this mathematical problem, the iteration method was applied. For that, creep tests under the same stress of 150 MPa were performed at the temperatures of 1100-1300°C. First, the strain rate $\dot{\varepsilon}_h$ was calculated by Equation 14, but using the length of the heated region L_h, refer to Section 3.4.2. Secondly, the results were fitted by Equation 3, and the approximate activation energy Q_1 was estimated. The third step was to estimate an approximation of the effective length $L_{eff,1}$ using Equation 18 and the value of Q_1. With $L_{eff,1}$, these three steps were repeated and a new approximation of the effective length $L_{eff,2}$ was determined. This procedure was repeated until the new calculated effective length $L_{eff,i+1}$ was equal to the one estimated in the previous steps $L_{eff,i}$. Thus, the effective length of each testing temperature, and the activation energy, were determined for each fiber as shown in Table 3.5.

Table 3.5: Calculated activation energy (Q) and effective length (L_{eff}) for single filament creep tests at 1100-1300°C.

Fiber	Q (kJ/mol)	L_{eff} 1100°C (mm)	L_{eff} 1200°C (mm)	L_{eff} 1300°C (mm)
CeraFib 75	785	10.58	11.00	11.42
CeraFib 99	637	11.46	11.95	-
Nextel 720	746	10.72	11.17	11.62
Nextel 610	611	11.70	12.19	-

3.5 References

[1] S. Petzold, M. Morche, J. Taesler. “Oxide-ceramic continuous fibres and ceramic fibre reinforced composites – Innovative materials for the firing process”. ZI International, vol. 64, pp. 24-31, 2011.

[2] 3M Co. “Nextel™ – Ceramic textiles technical notebook”, datasheet. St. Paul, Minesota, USA, 2010.

[3] CeraFib GmbH. “Produktdatenblatt – CeraFib 75 Mullit-Faser”, datasheet. Meißen, Germany, 2013.

[4] CeraFib GmbH. “Produktdatenblatt – CeraFib 99 Korund-Faser”, datasheet. Meißen, Germany, 2013.

[5] R. Ruh, K. S. Mazdiyasni, M. Mendiratta. “Mechanical and microstructural characterization of mullite and mullite-SiC-Whisker and ZrO_2-Toughened-Mullite-SiC-Whisker Composites”. Journal of the American Ceramic Society, vol. 71 (6), pp. 503-512, 1988.

[6] D.-Y. Jeng, M. Rahaman. “Sintering and crystallization of mullite powder prepared by sol-gel processing”. Journal of Materials Science, vol. 28 (18), pp. 4904-4909, 1993.

[7] U. Taffner, V. Carle, U. Schafer. “Preparation and microstructural analysis of high-performance ceramics”, pp. 1057-1066 in *ASM Handbook, Volume 09 - Metallography and Microstructures*, G. F. Vander Voort (Ed.). ASM International, 2004.

[8] DIN. “Hochleistungskeramik – Monolithische Keramik; Allgemeine und strukturelle Eigenschaften Teil 3: Bestimmung der Korngröße und der Korngrößenverteilung (Linienschnittverfahren)”. *DIN EN 623-3*, 2003.

[9] H. M. Rietveld. “A profile refinement method for nuclear and magnetic structures”. Journal of Applied Crystallography, vol. 2 (2), pp. 65-71, 1969.

[10] R. X. Fischer, H. Schneider, D. Voll. “Formation of aluminum rich 9: 1 mullite and its transformation to low alumina mullite upon heating”. Journal of the European Ceramic Society, vol. 16 (2), pp. 109-113, 1996.

[11] J. I. Langford, A. J. C. Wilson. “Scherrer after sixty years: A survey and some new results in the determination of crystallite size”. Journal of Applied Crystallography, vol. 11 (2), pp. 102-113, 1978.

[12] R. Delhez, T. H. de Keijser, E. J. Mittemeijer. “Determination of crystallite size and lattice distortions through X-ray diffraction line profile analysis”. Fresenius' Zeitschrift für analytische Chemie, vol. 312 (1), pp. 1-16, 1982.

[13] F. Deléglise, M. H. Berger, D. Jeulin, A. R. Bunsell. “Microstructural stability and room temperature mechanical properties of the Nextel 720 fibre”. Journal of the European Ceramic Society, vol. 21 (5), pp. 569-580, 2001.

[14] ASTM. “Standard Test Method for Density of High-Modulus Fibers”. *ASTM D 3800*, 1985.

[15] DIN. “Hochleistungskeramik – Keramische Verbundwerkstoffe – Verfahren zur Prüfung der Faserverstärkungen Teil 4: Bestimmung der Zugeigenschaften von Fasern bei Raumtemperatur”. *DIN EN 1007-4*, 2004.

[16] A. C. Cohen. “Maximum likelihood estimation in the Weibull distribution based on complete and on censored samples”. Technometrics, vol. 7 (4), pp. 579-588, 1965.

[17] H. Rockette, C. Antle, L. A. Klimko. “Maximum likelihood estimation with the Weibull model”. Journal of the American Statistical Association, vol. 69 (345), pp. 246-249, 1974.

[18] DIN. “Hochleistungskeramik – Keramische Verbundwerkstoffe – Verfahren zur Prüfung der Faserverstärkungen Teil 6: Bestimmung der Zugeigenschaften von Fasern bei hoher Temperatur”. *DIN EN 1007-6*, 2008.

[19] Z. Chi, T.-W. Chou, G. Shen. “Determination of single fibre strength distribution from fibre bundle testings”. Journal of Materials Science, vol. 19 (10), pp. 3319-3324, 1984.

[20] K. G. Dassios, M. Steen, C. Filiou. “Mechanical properties of alumina Nextel™ 720 fibres at room and elevated temperatures: Tensile bundle testing”. Materials Science and Engineering: A, vol. 349 (1–2), pp. 63-72, 2003.

[21] DIN. “Hochleistungskeramik – Keramische Verbundwerkstoffe – Verfahren zur Prüfung der Faserverstärkungen Teil 5: Bestimmung der Verteilung von Zugfestigkeit und Zugdehnung von Fasern im Faserbündel bei Raumtemperatur”. *DIN EN 1007-5*, 2003.

[22] V. Calard, J. Lamon. “Failure of fiber bundles”. Composites Science and Technology, vol. 64 (5), pp. 701-710, 2004.

[23] L. Neckel, J. G. Pereira da Silva, P. Guglielmi, D. Hotza, H. A. Al-Qureshi, O. R. K. Montedo, C. P. Bergmann, R. Janssen. “Mechanical tests and simulation on load sharing in alumina fiber bundles”. Ceramics International, vol. 41 (10, Part A), pp. 13257-13263, 2015.

[24] R. Hill, E. U. Okoroafor. “Weibull statistics of fibre bundle failure using mechanical and acoustic emission testing: The influence of interfibre friction”. Composites, vol. 26 (10), pp. 699-705, 1995.

[25] M. R’Mili, M. Moevus, N. Godin. “Statistical fracture of E-glass fibres using a bundle tensile test and acoustic emission monitoring”. Composites Science and Technology, vol. 68 (7), pp. 1800-1808, 2008.

[26] Y. Z. Pappas, A. Kontsos, T. H. Loutas, V. Kostopoulos. “On the characterization of continuous fibres fracture by quantifying acoustic emission and acousto-ultrasonics waveforms”. NDT & E International, vol. 37 (5), pp. 389-401, 2004.

[27] M. R'Mili, N. Godin, J. Lamon. “Flaw strength distributions and statistical parameters for ceramic fibers: The normal distribution”. Physical Review E, vol. 85 (5), pp. 1-6, 2012.

[28] J. Lamon, M. R’Mili, H. Reveron. “Investigation of statistical distributions of fracture strengths for flax fibre using the tow-based approach”. Journal of Materials Science, vol. 51 (18), pp. 8687-8698, 2016.

[29] DIN. “Advanced technical ceramics - Mechanical properties of ceramic fibres at high temperature in a non-reactive environment - Determination of creep behaviour by the cold end method”. *FprEN 15365 (E)*, 2009.

[30] J. A. DiCarlo. “Property goals and test methods for high temperature ceramic fibre reinforcement”. Ceramics International, vol. 23 (4), pp. 283-289, 1997.

[31] O. Lesemann. “Untersuchungen zum Hochtemperaturverhalten keramischer Verstärkungsfasern”, PhD thesis. Universität Bremen, Bremen, Germany, 2005.

[32] R. Morrell. “A tensile creep-testing apparatus for ceramic materials using simple knife-edge universal joints”. Journal of Physics E: Scientific Instruments, vol. 5 (5), pp. 465, 1972.

BLANK PAGE

4 Tensile and creep performance of a novel mullite fiber at high temperatures

The novel fiber CeraFib 75 with a composition near to pure mullite was analyzed with respect to its potential for high-temperature applications. This mullite fiber free of glass phase was aimed to overcome the strength of commercial oxide fibers at high temperatures. Tensile tests at room and high temperatures ranging from 900 to 1400°C and creep tests were performed. Nextel™ 720, another crystalline mullite–alumina fiber, was tested as a reference. Microstructure and crystal phase analysis of the new fiber revealed mullite grains with traces of γ- and α-alumina in-between; it contains occasionally defects causing a reduced strength at room temperature. Remarkably, at temperatures beyond 1200°C, CeraFib 75 presented higher tensile strength than Nextel™ 720. During tensile tests at 1400°C, an extended region of inelastic deformation was observed for CeraFib fibers only, which was related to a grain boundary sliding mechanism. Creep rates were of the same order of magnitude for both fibers.

4.1 Introduction

Advances in the aerospace field promoted a development of structural materials capable of withstanding mechanical loads at aggressive environments. Ceramic matrix composites (CMC) proved to be good candidates for this field mainly because of their high strength, thermal and chemical stability, and considerable toughness [1]. Due to their thermo-mechanical resistance, early developments were initiated on systems based on either carbon or silicon carbide [2]. However, a crescent demand for applications at corrosive environments made these types of materials less suitable due to oxidation and consequent loss of mechanical properties [3]. More attention was then given to CMCs based on oxide ceramics [4], which are commonly categorized as all-oxide CMCs.

Being stable oxides by nature, this class of material is resistant against oxidation induced degradation even at high temperatures. Therefore, they gained space on applications such as gas turbine combustors, heat shields and heat exchangers [5, 6]. Nevertheless, the lower

strength of oxide fibers, in comparison to non-oxide materials, limited their relevance in the past. The first attempt on producing oxide fibers is dated in the 70s with the production of fibers based on alumina–silica [7]. At that stage, oxide fibers presented two main problems related to low mechanical resistance at room temperature and low thermal stability. The development of all-oxide CMCs was strongly driven in the 90s by the commercialization of fully crystalline oxide fibers [8]. Nowadays, the usage of oxide fibers is mainly related to the ones developed by the American company Minnesota Mining and Manufacturing (3M). With the trademark of Nextel 610, this 99% alumina fiber presents the highest tensile strength of available oxide fibers of around 3 GPa [9]. The high strength of this fiber is achieved by its fine microstructure of sub-micrometer α-alumina grains and the addition of dopants to reduce grain growth effects. In the further course, several other fibers were produced with the addition of mullite or zirconia phases to increase the thermal stability. Another fiber which is widely commercially used is the Nextel 720, which is an alumina–mullite fiber presenting higher tensile strength and creep resistance than Nextel 610 at temperatures above 1100°C. This better performance is credited to the morphology and size of the mullite grains [9], and makes Nextel 720 currently to be estimated as the preferred fiber for long-term applications.

Nonetheless, temperature is still a limiting factor for the appliance of oxide CMCs. They are prone to degradation of their strength and embrittlement when subjected to high thermal loads, which is normally associated with the degradation of the fibers [10-12]. Early studies by Wilson [13] showed that the aforementioned fibers present strength loss when tested at temperatures above 1000°C. The strength retention of the fibers has also been studied by other authors, and the results obtained are somewhat conflicting. Deléglise [14] reported that Nextel 720 fibers tested at 1200°C retained only 20% of its room-temperature strength while Wilson [13] stated a strength retention of 80% at the same temperature. It is also possible to find creep studies in the literature showing that these fibers are also susceptible to creep at those temperatures [14-16]. Additionally, Schmücker [17, 18] noticed in his works that the sub-micrometer fiber grains are prone to coarsening at high temperatures, and the phenomenon can be aggravated when the fibers are embedded in a matrix [19]. At this point, it is important to highlight that such temperatures can occur during the processing and application of oxide composites.

Hence, there is a need of development of oxide fibers capable of maintaining their mechanical strength at high temperatures. In this matter, the German company CeraFib GmbH, based on

research of the Institute of Textile Chemistry and Chemical Fibers (ITCF Denkendorf), is developing oxide fibers which are able to operate at higher temperatures [20]. This work aims to analyze the performance of the recently developed CeraFib 75 fiber when subjected to tensile loads at critical temperatures. This fiber presents a composition similar to pure mullite and aims applications at high temperatures. For that, several tensile tests at different temperatures were performed. The authors also take into account that the results found in the literature for Nextel 720 can be rather different depending on the source, and therefore, the same characterization methodology was applied to test this commercial fiber for comparison. Additional tests were conducted at the temperature of 1400°C, at which the fibers started presenting an unexpected non-linear deformation. Creep properties were also analyzed and the deformation phenomena were interpreted with respect to the results obtained from the analysis of microstructure and phase content.

4.2 Experimental

4.2.1 Materials

The main object of the studies in this work is the mullite fiber CeraFib 75. This small diameter fiber (10-12 μm) produced by dry-spinning has an initial composition close to stoichiometric 3/2 mullite (72 wt.% alumina – 28 wt.% silica). During processing, the silica content is decreased due to the formation of volatile Si species, which leads to an end composition of 75–25 wt.%. The final microstructure is expected to be of mullite grains with traces of smaller alumina grains dispersed. This represents a great advance since the Si is stable in the alumina-rich mullite phase and not free as a glass phase. For comparison, another commercial fiber was tested. Nextel 720 is an 85–15 wt.% alumina–silica fiber produced by a sol-gel route. Its microstructure is known to be of a mosaic of mullite grains with elongated alumina grains [14]. It is important to highlight that the fibers do not present the same chemical composition, but the comparison is justified since both are the only fully crystalline mullite fibers available. Table 4.1 summarizes the main information regarding the fibers, and presents the density measurement here performed according to norm ASTM D 3800.

Table 4.1: Summary of tested fibers.

Fiber	Manufacturer	Composition (wt %) #	Density (g/cm^3)
Nextel 720	3M Co.	85 Al_2O_3 – 15 SiO_2	3.17 ± 0.09
CeraFib 75	CeraFib GmbH	75 Al_2O_3 – 25 SiO_2	3.26 ± 0.19

Information by manufacturer

4.2.2 Characterization methods

Before the mechanical tests, other characterization methods were performed in regard to microstructure and phase investigation. X-ray diffraction (XRD) analysis was conducted to identify and quantify the phases present on each fiber. For that, fibers were crushed into a powder and then analyzed using a SEIFFERT XRD 3003 research edition XRD.

Grain size measurement was realized by the analysis of the microstructure using the line-intercept method with the help of the image analysis software Lince (TU Darmstadt, Germany). To do so, fibers were embedded in epoxy resin, and then ground, polished, and followed by thermal extraction of the resin at 800°C. The microstructure was revealed by a thermal etching process at 1300°C for 40 min. Finally, pictures of the microstructure were taken from five different fibers using a scanning electron microscope (SEM), Zeiss SUPRA 40, with an acceleration voltage of 0.5 kV.

4.2.3 Mechanical tests

Single filament tensile tests were performed according to norms DIN EN 1007-4 and 1007-6. Sample preparation was done with surgical gloves to avoid contaminations. Various testing temperatures were used starting at room temperature and then ranging from 900 to 1400°C. The fibers were tested in a tensile testing machine equipped with a 1 N load cell, model Interface ULC-1N-535, and a linear variable differential transformer (LVDT) sensor of ±1 mm. A two SiC heating element oven was used for the tests at high temperature. System compliance was measured prior to testing. 30 samples were tested with a traveling speed of 1 mm/min until failure for statistical meaning. The cross-section area of every fiber tested was determined after testing with an optical microscope, SENSOFAR PLμ 2300. Thus, the stress–strain relation of each individual fiber could be determined taking into account the gauge length of 25 mm.

Creep tests were also carried out to determine the creep parameters at the mentioned temperatures. The stress and temperature effects on creep were assumed to be described by

the standard power law creep equation, Equation 3. The stress exponent was determined from tests done at 1200°C with three different loads applied. The determination of the apparent activation energy for creep was performed at temperatures of 1100-1300°C and a constant stress of 150 MPa. For the later test, the diameter measurement was carried out before the test in order to assure the applied stress. A total of two specimens were tested for each testing condition. Tests were conducted until the fiber failure or until the run-out time of 100 h was achieved. A dead load system was used to achieve better control of the applied load, and the same oven used for tensile tests was applied for the creep tests. The effective gauge length was calculated based on the relation reported earlier [21], Equation 18, and determined as 11.0 and 11.17 mm for CeraFib 75 and Nextel 720, respectively.

4.3 Results

4.3.1 Fiber overview

The thermal etch procedure was proved to be efficient to reveal the microstructure of CeraFib 75 fibers. SEM pictures of the thermally etched cross-sections of as-received fibers can be seen in Figure 4.1. On the pictures, mullite grains are identified as the main phase. Since the alumina grains are less resistant to thermal etching, they could not be differentiated. Grain size measurement by line-intercept method was performed on five different fibers of each type, and only mullite grains were taken into consideration. The results pointed that CeraFib presents grains of 195±39 nm, some being spherical, and some others more elongated. In addition, experiments were performed on Nextel 720 fiber using the same parameters for thermal etching. The microstructure revealed is of small faceted mullite grains of about 160±31 nm, while the alumina grains were over-etched. In the literature, the microstructure of Nextel 720 is described as a mosaic structure of 500 nm aggregate mullite grains. These aggregates consist of slightly misoriented 100 nm grains, which are separated by low angle boundaries with elongated alumina grains embedded on them [22]. Since only one phase could be identified with the thermal etching performed in this study, only the 160 nm mullite grains could be observed in the microstructure here reported for Nextel 720.

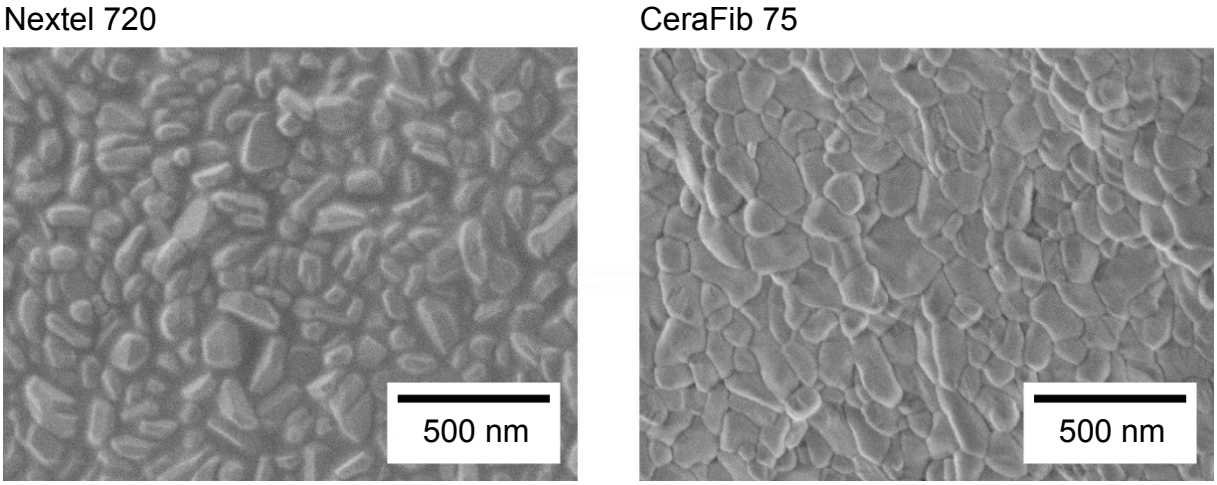

Figure 4.1: SEM micrographs showing the arrangement of the main phase (mullite grains) of CeraFib 75 and Nextel 720.

More differences could be perceived by the XRD analysis, which is represented in Figure 4.2. Mullite and alumina phases were confirmed for both fibers, but with different intensities. Quantification of the phase contents is presented in Table 4.2. Again, a higher content of alumina was identified for Nextel 720 because of its initial composition. Nonetheless, the crystal phase of present alumina differs on the fibers. As seen on Table 4.2, CeraFib 75 has alumina in form of γ-Al_2O_3 and α-Al_2O_3, corundum, in small contents. These phases differ in structure, and corundum is known for being the most stable between them. The small amount of α-alumina present on CeraFib was measured on the quantitative phase analyses determined from Rietveld refinements, and is not labeled in Figure 4.2 because of its low content. Nextel 720 presented only corundum phase as second phase in accordance to its composition.

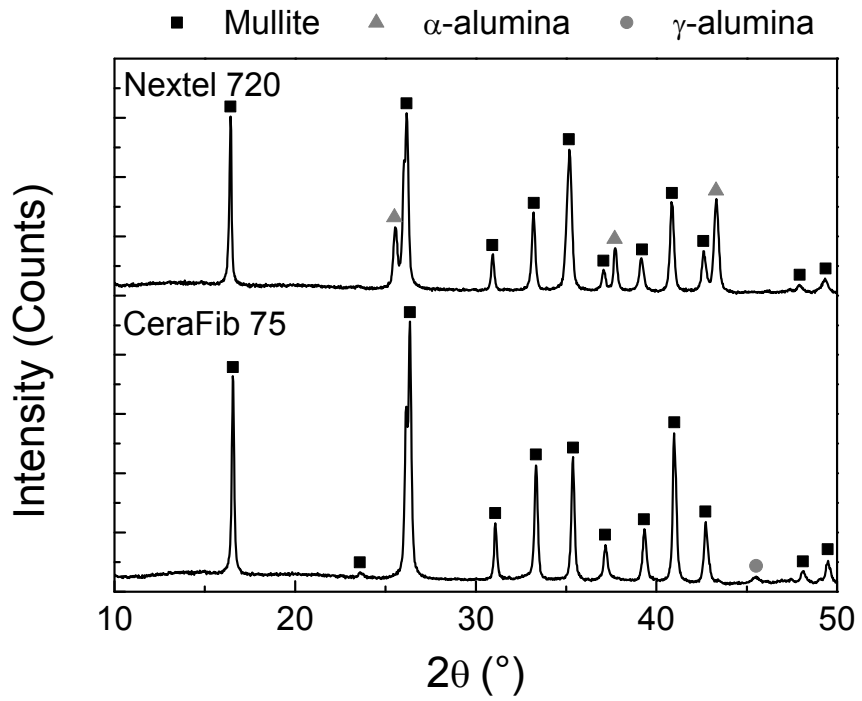

Figure 4.2: X-ray analysis of tested fibers.

Table 4.2: Phase contents of the fibers by XRD analysis.

Phase	Nextel 720 (wt.%)	CeraFib 75 (wt.%)
Mullite	58.7	96.5
α-alumina	41.3	0.5
γ-alumina	-	3.0

4.3.2 Tensile tests

The first mechanical characterization performed was the single filament tensile tests. During the preparation of specimens, it was noticed that the handling of CeraFib fibers was particularly difficult. Nextel fibers are supplied with a polymeric sizing, which is normally removed before usage, while the new fiber had no sizing. This coating is done for a better handling and transportation of the bundle and, therefore, the procedure of separating single filaments from the supplied bundle was easier for Nextel. As for the test at room temperature, the observed stress–strain curve was linear-elastic up to fracture. Additionally, both fibers presented a similar elastic modulus, 225±25 GPa for CeraFib and 221±16 GPa for Nextel. Figure 4.3 (left) shows the strength of the fibers by means of a Weibull distribution.

Differences can be seen on both Weibull parameters that describe the failure distribution. Nextel 720 achieved higher results for characteristic strength (σ_0) at room temperature reaching 1650 MPa, whereas CeraFib 75 presented a lower value of 1420 MPa. The Weibull modulus *m* was also higher for Nextel. The fracture surface found for most fibers is exemplified in Figure 4.3(a) showing a rather plain surface. However, three out of the 30 CeraFib fiber lot presented larger volumetric defects, as shown in Figure 4.3(b). These fibers correspond to the lower values seen in the distribution; strength lower than 950 MPa.

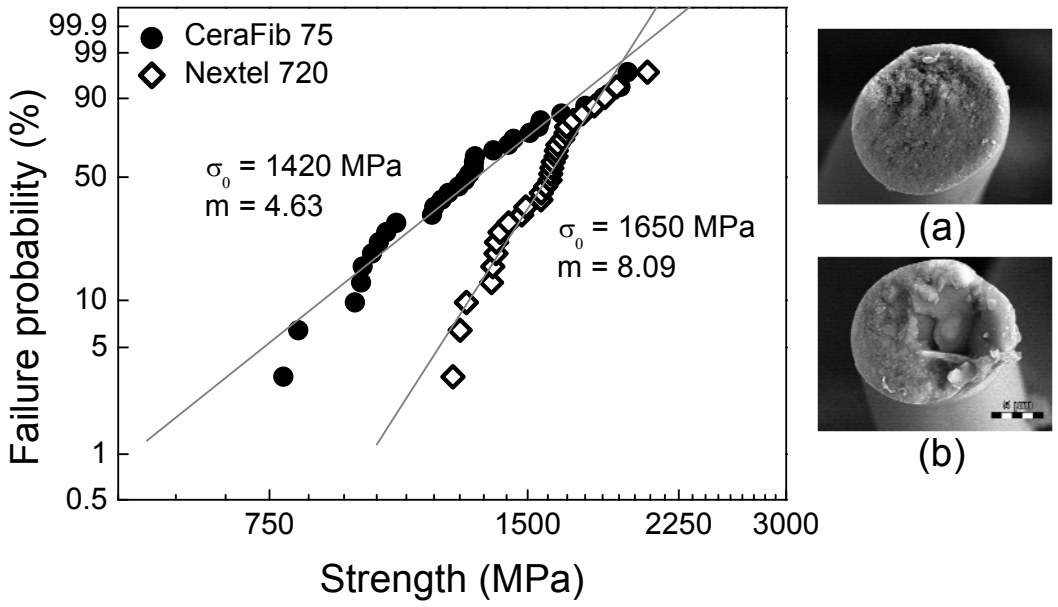

Figure 4.3: Weibull failure distribution of tensile strength at room temperature (left). Typical fracture surface of CeraFib fibers showing high strength (a), while 10% of the lot with low strength contain larger defects (b).

Contrary to the results at room temperature, CeraFib had better strength retention at higher temperatures as illustrated in Figure 4.4. In the graph, each dot represents the characteristic strength determined from 30 fibers at the related test temperature and normalized by the strength at room temperature. The absolute values of the Weibull parameters and the calculated E-modulus are reported in Table 4.3. The strength of the fibers starts to decrease at 1000°C, and CeraFib 75 retains more of its original strength. Beyond 1200°C, the new fiber achieved higher values of strength than Nextel, reaching a difference of 50% at 1400°C. The Weibull modulus also decreases with the increasing temperature, which is observed at

temperatures higher than 1000°C for Nextel. The relatively modest decrease of *m* for CeraFib is only realized at temperatures higher than 1200°C, where both fibers reach the same low level of *m*. The relatively large scatter of strength for CeraFib is kept at all temperatures as being caused by the occasional presence of large defects, while additional degradation effects become active at increasing temperatures in the Nextel fibers.

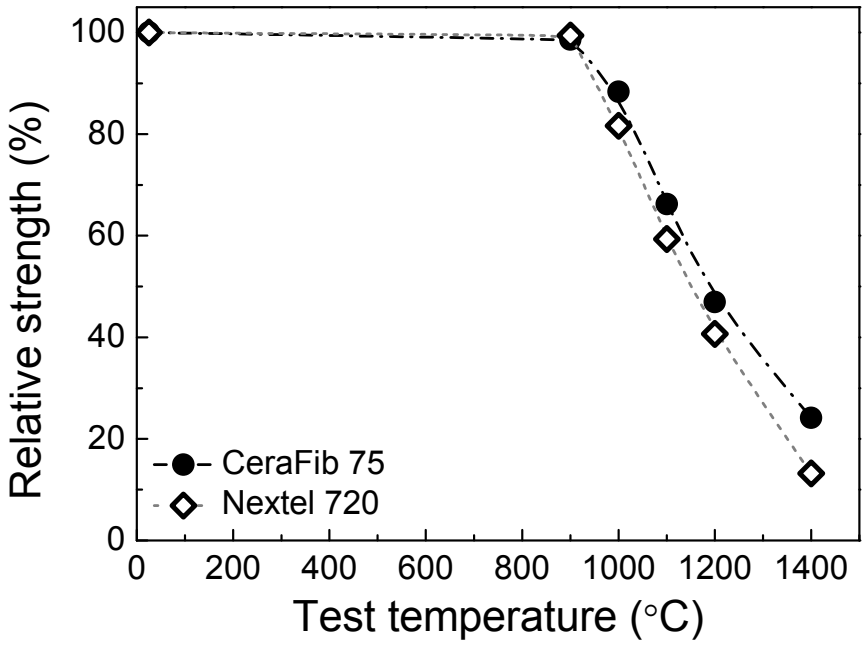

Figure 4.4: Strength retention of fibers tested at different temperatures.

Table 4.3: Measured Weibull parameters of the strength distribution and elastic modulus for the fibers tested at different temperatures.

Testing temperature	σ_0 (MPa)		m		E-modulus (GPa)	
	Nextel	CeraFib	Nextel	CeraFib	Nextel	CeraFib
Room temperature	1650	1420	8.1	4.6	221 ± 17	225 ± 25
900 °C	1640	1398	7.6	4.5	213 ± 16	204 ± 19
1000 °C	1349	1255	5.4	5.1	205 ± 17	193 ± 14
1100 °C	1000	940	5.8	4.9	190 ± 14	180 ± 18
1200 °C	671	667	3.4	3.5	185 ± 12	176 ± 16
1400 °C	197	303	3.0	3.0	175 ± 16	163 ± 21

Investigations were also done on the mechanical behavior of the fibers during loading. Figure 4.5 shows the stress *vs*. strain plots of fibers tested at different temperatures. Values of elastic modulus slightly decreased at higher test temperatures as seen in Table 4.3. Nevertheless, up to 1200°C the samples presented a similar behavior to the experiments at room temperature, which is characterized as a linear deformation followed by a sudden failure. When tested at 1400°C, however, the fibers started to exhibit some non-linear behavior. A particularly small inelastic deformation was detected for Nextel at the end of the tests followed by the brittle failure. This small non-linear region at high temperature is normally associated with creep deformation for this type of fiber [13]. On the other hand, CeraFib 75 presented an extended region of non-linear deformation, which arises mainly as the test proceeds without a further increase of stress. Thus, the specimen can withstand this applied stress at a considerably high level for such temperature.

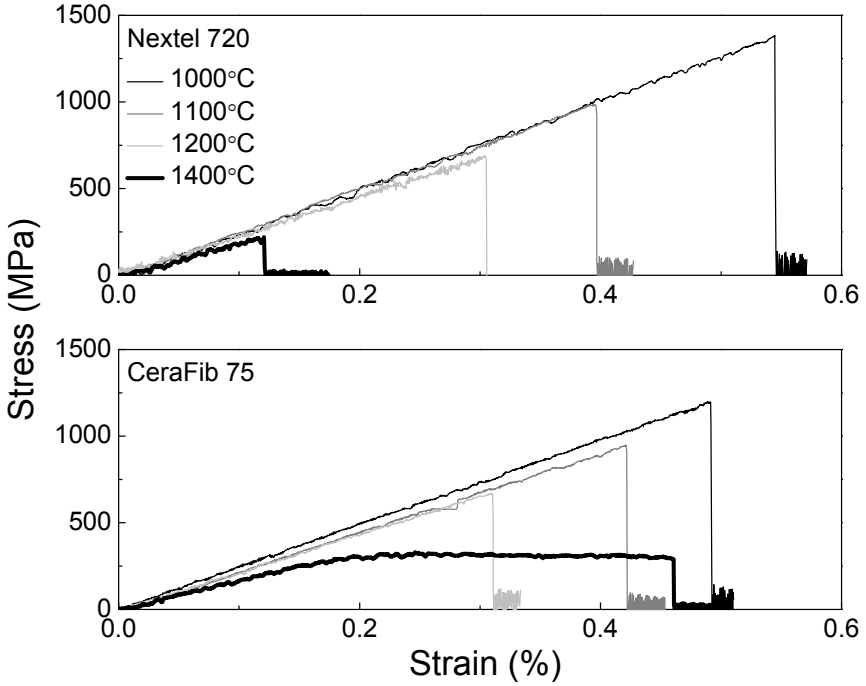

Figure 4.5: Stress–strain relationship from tensile tests of both fibers at different testing temperatures.

Further experiments were performed at 1400°C to analyze this phenomenon. Tensile tests with different traveling speeds, ranging from 0.5 to 5.0 mm/min, were conducted; however, a speed-related effect could not be observed for CeraFib fibers. The results of all tests performed at 1400°C are shown in Figure 4.6. The measured strength is plotted against the inelastic deformation at failure for each filament tested. As mentioned before, Nextel 720 presents only small inelastic deformation, preferentially for fibers with higher strength. A large scattering is observed for the novel fiber. Approximately one third of the fiber lot is comparable with respect to strength and inelastic deformation with the total collective of the Nextel fibers. However, the majority of fibers (2/3) can be characterized by higher strength and the increased tendency for extended inelastic deformation. Here, the total deformation prior failure ranges from 0.2% to 1.0% for the novel fiber. Once more, fibers with big defects, Figure 4.3(b), were seen on four CeraFib fibers tested.

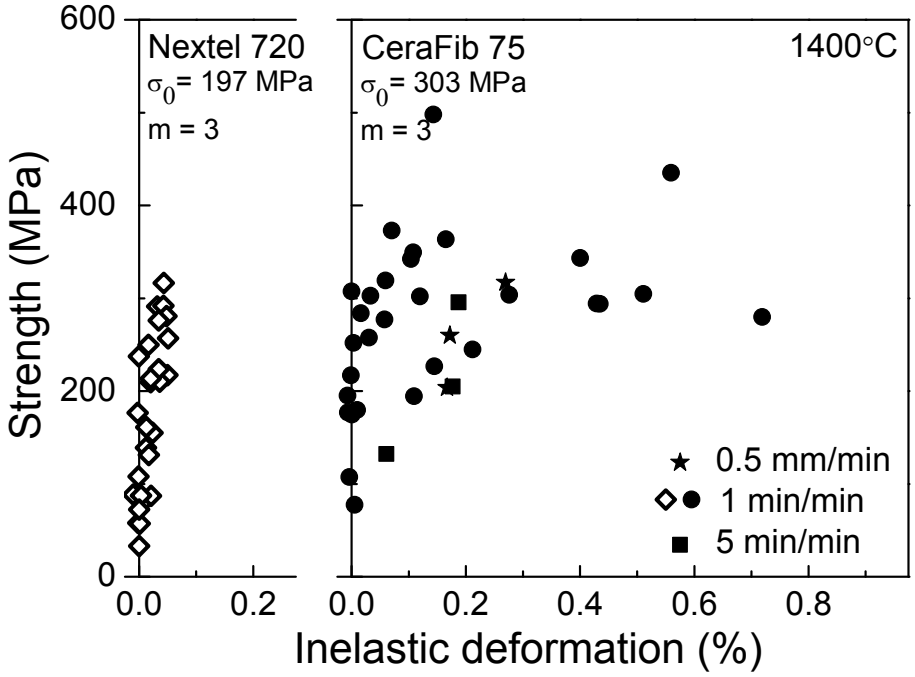

Figure 4.6: Strength *vs*. inelastic deformation for fibers tested at 1400°C with different loading rates. Fibers with high strength show some tendency for inelastic deformation, which can be rather extended for individual CeraFib fibers.

4.3.3 Creep tests

Based on the results obtained from tensile tests at 1400°C, creep tests were performed to investigate the creep characteristics and their possible contribution to the fiber behavior during quasi-static tests. The main objective of this test was to analyze the creep rate of the materials under various conditions. Thus, tests with different loads and temperatures of 1100-1300°C were performed. Tests at 1000°C were also done, but no creep deformation was observed for both fibers. Examples of creep curves under different stresses at 1200°C for CeraFib fibers can be seen in Figure 4.7. During test, only primary and secondary creep stages could be observed. During the first hour of the test, the creep rate decreased considerably, while in the later stages, the creep rate tended to a constant value. Thus, the steady-state creep rate was determined and used to evaluate the effects of stress and temperature on creep. For tests in which the steady-state region was not clear, *i.e.*, specimens that failed within a few hours of test, the minimum creep rate was used for the analysis. The specimens loaded by high stresses failed in absence of the third creep stage, which characterizes the brittle behavior seen for most ceramics. Additionally, a relation between the total time to rupture and the applied stress was also observed, in which the fibers tested with stresses lower than 200 MPa

did not fail after the run-out time of 100 h was achieved. The results of creep tests with Nextel fibers presented the similar creep characteristics as described above and time to rupture was measured with no significant difference between the fibers.

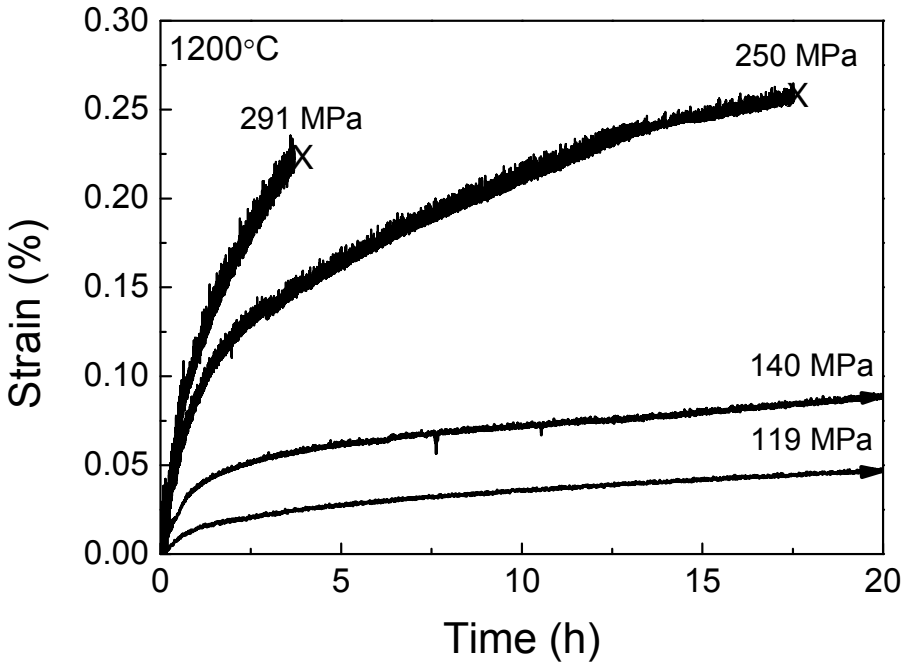

Figure 4.7: Creep deformation *vs*. time for CeraFib 75 tested at 1200°C under different applied stresses. Arrows indicate that samples did not fail in the given time. Values of strain were corrected.

Figure 4.8 summarizes the creep performance of the fibers for various test conditions. Only small differences can be seen by comparing both fibers, in which CeraFib 75 presented slightly higher creep rates. This difference is more pronounced when low stresses are applied. At higher stresses/temperatures, this difference is not seen. From the tests at constant temperature, Figure 4.8 (left), a stress exponent of 2.8 and 3.9 was measured for CeraFib 75 and Nextel 720, respectively. The findings for Nextel were similar to the results measured by Armani [15]. On his studies, Armani presented values of n for Nextel 720 of about 3 when the fibers were tested under stresses lower than 300 MPa, and values of 5 when tested with loads higher than 300 MPa. The value here reported, 3.9, is in between. Apparent creep activation energies were determined with the results obtained at different testing temperatures, Figure 4.8 (right). Q was calculated for CeraFib fibers with 785 kJ/mol and for Nextel with

746 kJ/mol. These results are also similar to the ones published by Deléglise [14] for Nextel 720, 702 kJ/mol.

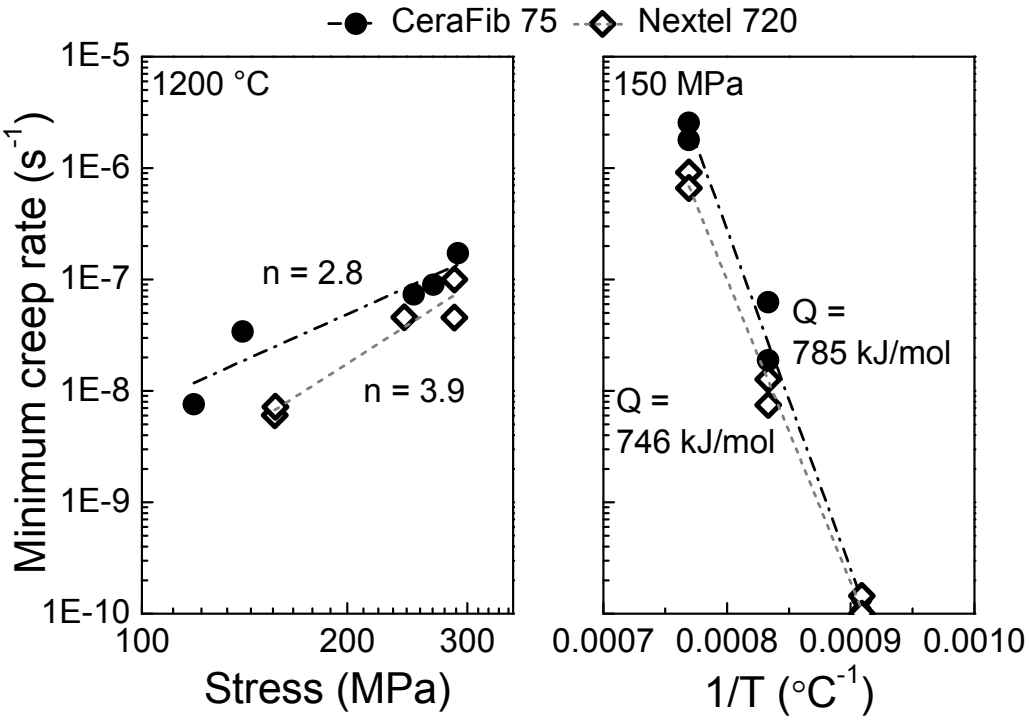

Figure 4.8: Stress (left) and temperature (right) effects on creep of both fibers for the determination of *n* and *Q*.

4.4 Discussion

4.4.1 Room-temperature properties

The tensile tests performed in this work give a sufficient statistical analysis of the mechanical properties of the new fiber. CeraFib 75 ended up with a somewhat lower strength than Nextel 720 at room temperature. Three factors can be discussed in order to explain this result. The first is related to the chemical composition and resulting microstructure of the fibers. As seen on the XRD analysis, Nextel 720 presents a higher content of alumina phase, which is dispersed along the microstructure in small α-alumina grains. It is already known that those fine elongated grains of alumina in the mosaic structure of mullite confer the high strength of this fiber at room temperature [22]. A second reason is related to the rather large difference between the Weibull modulus *m* for both fibers, *i.e.*, the broader strength distribution of CeraFib. As demonstrated in Figure 4.3, the larger part of the lot of 30 new fibers being tested

overlap in their strength with the total distribution of Nextel, while about 1/3 of this fiber lot is restricted in their strength to rather low values. In contrast to the high strength fibers, these low strength fibers contain large microstructural defects. As illustrated in Figure 4.3(b), these defects can be rather big, which explain the lower strength of the fiber. This may be due to the early stage of development of the new fiber and should be avoided during the next development steps. It can be expected that the eradication of these processing-derived defects would lift the strength level of the new fiber to the level of Nextel 720. The potential to reach this target has been proved by the results manifested in Figure 4.3. A third factor for the difference between Nextel and the new fiber may be caused by the difficulties of handling and separation of CeraFib fibers during sample preparation. Some authors [23, 24] state that the sample preparation can already infer damage to the fibers and alter the distribution of results. Since CeraFib had a more complicated handling, it may be conjectured that more damage could be generated during sample preparation.

Additionally, similar values of E-modulus were measured with no large differences between both fibers, although the new fiber shows a tendency for slightly higher values. With respect to the relatively large alumina content in Nextel, one would expect the reversed tendency. This result may be used for the indication of some micro-porosity in Nextel. Table 4.1 presents the results obtained by density measurements, where Nextel presented lower density. Although no direct relation could be made in this work, calculated density is in accordance to the work of Deléglise [25], where micro-porosity of 5.8% was measured for as-received Nextel 720 fibers.

4.4.2 Strength retention and creep at high temperatures

In contrast to the tests at room temperature, the new fiber presented better performance than Nextel at higher temperatures. The better strength retention of CeraFib 75 can be credited to the higher content of mullite, which is more stable at these elevated temperatures. In addition, the slightly larger grains may also be favorable to confer higher stability. Nevertheless, both fibers started presenting strength reduction at 1000°C, and Nextel with a slightly stronger decrease. A reduction of the Weibull modulus m was observed for the fibers as well. This decrease is more pronounced for Nextel leading to the same low level of $m = 3$ at 1400°C for both fibers. While the broad strength distribution of the new fiber reflects the occasional presence of large microstructural defects as discussed before, Nextel shows a continuous drop of m with increasing temperature. This effect may be due to local changes of the

microstructure leading to fiber degradation and the growth of local defects. Changes of the mullite composition and structure [11], recrystallization and grain growth [14] and thermal grooving [26] may be participating on this degradation process. In the case of CeraFib 75, γ-alumina can transform into α-alumina starting at 900°C [27]. However, no grain growth is expected during test because of the short duration that the fiber is at the testing temperature and since the kinetics at these temperatures is too slow [28].

Creep tests revealed a different tendency from the tensile tests at high temperature, however. Even though presenting better strength retention, CeraFib fibers showed slightly higher creep rates at lower stresses applied. A higher resistance to creep at lower loads of Nextel 720 can be associated with its microstructure. The aggregate mosaic morphology reduces the grains motion, and therefore diminishes creep strain. Another fact of relevance seen on the tests was the measured stress exponent and its relation to the dominant creep mechanisms. Previous works relate interface-reaction controlled creep, $n \approx 3$, for Nextel 720 tested with stresses lower than 300 MPa and dislocation creep or void growth, $n \approx 5$, for higher loads [15]. The results here reported are in the middle of the aforementioned for the commercial fiber. As for CeraFib 75, the calculated value of 2.8 can be related to grain boundary sliding according to literature [29].

The biggest difference between the fibers was observed during tensile testing at 1400°C, when inelastic deformation events were considered. Such inelastic processes are hardly noticed for Nextel 720, and the same is true for a part of the CeraFib fiber lot. Although being subjected to a strong drop of strength, these fibers can fairly withstand inelastic deformation. This may be credited to the particular microstructure, in which the absence of glassy phases plays the most dominant role. However, in the larger part of the CeraFib fiber lot, inelastic deformation takes place to a great deal during the tensile test. It is remarkable that this deformation increases during the longest part of the test duration where the applicable stress remains fairly constant in spite of the continuously progressing fiber elongation. This behavior resembles the classic creep performance with increasing time-dependent creep strain under constant stress. As discussed before, the observed creep phenomena are to be attributed to a grain boundary sliding mechanism. Besides, the same mechanism was already seen for polycrystalline mullite materials creep tested at 1400°C [30]. Therefore, this phenomenon can also be related to the higher deformation achieved by this fiber on the tensile tests. Even at high temperature, the mullite grains are still stable and their motion is reduced. However, their

surroundings composed of grain boundaries and alumina grains are more prone to deformation. Since these mullite grains cannot have much movement, when a certain amount of energy is achieved, they simply slip through their borders, which are not stable. In the end, the mullite grains experience little deformation, but this motion promotes the higher deformation seen for CeraFib tests.

The differences in the lot of tested CeraFib fibers, in which some present inelastic deformation and others not, shall once more be emphasized. This difference indicates that microstructural species which allow the non-linear deformation are not uniformly distributed in all fibers. Some fibers seem to be free of any phases which enable inelasticity. Others may contain chemical heterogeneities which can be connected with intergranular glass phases. It is well known that these glass phases can be avoided only with extreme difficulties in single-phase mullite structures [31]. If present in the grain boundaries, these glassy phases allow much easier inelastic deformation. In addition, the presence of alkali contaminants can promote the dissolution of mullite into liquid phases [14], which would contribute even more for the non-linear deformation. It can then be concluded that the difficulties to produce single-phase mullite fibers without a glass phase were only partially overcome in the current production process. On the other side, this process brought about new fibers as well, which proved their excellent potential beyond the currently available fibers. It is then the task for further development efforts to secure the high standard for the whole production process.

This behavior of CeraFib at higher temperatures can be very interesting for composites applications, not to mention its higher strength under such conditions. Non-linear deformation can enhance the pseudo-plasticity, leading to higher damage tolerance of the composite and promoting a higher reliability of the in-field component. Besides other applications, oxide–oxide CMCs are normally developed for thermal shielding of hot gas filters and combustors. On such applications, a thermal load applied for long-term duration is often expected, but also higher thermal peak loads for a short period of time can happen. If the material in this case can sustain sufficient compliance by deformation without failure, the survival probability of the component will be improved. Thus, the novel fiber is suggested for applications that require resistance to oxidation and high temperatures for which the commercially available fibers offer only a limited suitability.

4.5 Conclusion

In this work, the new mullite fiber CeraFib 75 has been characterized with respect to the application in high-temperature resistant components. The Nextel 720 fiber is known to offer currently the highest creep resistance and high-temperature stability of all commercially available oxide fibers. Both fibers were therefore included in this analysis to enable their direct comparison.

The microstructure of CeraFib consists of mullite grains with traces of smaller α- and γ-alumina grains, while the Nextel fiber contains a higher amount of fine alumina grains distributed among larger mullite grains. Both fibers showed broad strength distributions with the strongest fibers of both types reaching the same strength level. However, relatively large defects were identified in few CeraFib fibers; the characteristic strength and the Weibull modulus *m* are thus lower compared with Nextel 720 at room temperature. Considering the strength retention at high temperatures CeraFib shows better performance with its characteristic strength starting at 1200°C. Creep tests revealed lower resistance at lower applied loads, but considering higher stresses, *i.e.*, 250 MPa, the overall performance of the two fibers was similar. Thus, taking into account the power law creep equation and the lower stress exponent measured for CeraFib 75, it is expected that the novel fiber will have better performance at 1200°C and higher stresses applied.

As mentioned above, the new fiber was designed for applications at high temperature and it proved to have promising properties for this purpose. An unexpected behavior was observed for the new fiber at 1400°C, in which most of the tested fibers reacted with an elastic–pseudo-plastic behavior. This non-linearity was associated with the creep mechanism grain boundary sliding, which was also identified during creep tests. At such conditions, it is suggested that two main aspects are determinant for the mechanical behavior of the new fiber: density of defects for the strength, and microstructure heterogeneity for the total deformation. Nextel fibers did not present such feature as the fibers failed before this mechanism could take place. As a conclusion it can be stated that the new fiber has proved to offer at room temperature the excellent potential demonstrated so far by Nextel 720 and to surpass it at high temperatures.

4.6 Acknowledgements

The authors would like to thank the Brazilian Ministry of Science and Technology (CNPq) for the financial support through the program Science without Borders and the company CeraFib GmbH for the supply of testing materials. We also thank H. Lührs and T. Schumacher from University of Bremen for the XRD analysis. Helpful discussions with E. Volkmann are also gratefully acknowledged.

4.7 References

This chapter was adapted, license no. 4183081295036, from:

R. S. M. Almeida, K. Tushtev, B. Clauß, G. Grathwohl, K. Rezwan. “Tensile and creep performance of a novel mullite fiber at high temperatures”. Composites Part A: Applied Science and Manufacturing, vol. 76 (0), pp. 37-43, 2015.

The article is mainly based on the work of the first author and author of this thesis Renato S. M. Almeida. The precise contributions of each author are listed below.

Table 4.4: Authors contributions for Chapter 4.

Author	Contribution
Almeida, R. S. M.	Conceptualized the work, performed and analyzed the experiments, wrote the manuscript
Tushtev, K.	Gave conceptual and scientific advices, helped in the scientific evaluation and editing of the manuscript
Clauß, B.	Gave materials specific input and helped to evaluate and edit manuscript
Grathwohl, G.	Gave conceptual and scientific advices, helped in the scientific evaluation and editing of the manuscript
Rezwan, K.	Gave conceptual advices, helped in the scientific evaluation and editing of the manuscript

[1] D. Koch, K. Tushtev, G. Grathwohl. “Ceramic fiber composites: Experimental analysis and modeling of mechanical properties”. Composites Science and Technology, vol. 68 (5), pp. 1165-1172, 2008.

[2] S. Schmidt, S. Beyer, H. Knabe, H. Immich, R. Meistring, A. Gessler. “Advanced ceramic matrix composite materials for current and future propulsion technology applications”. Acta Astronautica, vol. 55 (3), pp. 409-420, 2004.

[3] R. C. Robinson, J. L. Smialek. “SiC recession caused by SiO_2 scale volatility under combustion conditions: I, experimental results and empirical model”. Journal of the American Ceramic Society, vol. 82 (7), pp. 1817-1825, 1999.

[4] F. W. Zok. “Developments in oxide fiber composites”. Journal of the American Ceramic Society, vol. 89 (11), pp. 3309-3324, 2006.

[5] R. A. Jurf, S. C. Butner. “Advances in oxide-oxide CMC”. Journal of Engineering for Gas Turbines and Power, vol. 122 (2), pp. 202-205, 2000.

[6] U. Trabandt, B. Esser, D. Koch, R. Knoche, G. Tumino. “Ceramic matrix composites life cycle testing under reusable launcher environmental conditions”. International Journal of Applied Ceramic Technology, vol. 2 (2), pp. 150-161, 2005.

[7] A. R. Bunsell, M. H. Berger. “Fine diameter ceramic fibres”. Journal of the European Ceramic Society, vol. 20 (13), pp. 2249-2260, 2000.

[8] H. E. Deve, C. McCullough. “Continuous-fiber reinforced composites: A new generation”. Journal of the Minerals Metals & Materials Society, vol. 47 (7), pp. 33-37, 1995.

[9] D. Wilson. “Statistical tensile strength of Nextel™ 610 and Nextel™ 720 fibres”. Journal of Materials Science, vol. 32 (10), pp. 2535-2542, 1997.

[10] E. Volkmann, K. Tushtev, D. Koch, C. Wilhelmi, J. Göring, K. Rezwan. “Assessment of three oxide/oxide ceramic matrix composites: Mechanical performance and effects of heat treatments”. Composites Part A: Applied Science and Manufacturing, vol. 68 (0), pp. 19-28, 2015.

[11] M. L. Antti, E. Lara-Curzio, R. Warren. “Thermal degradation of an oxide fibre (Nextel 720)/aluminosilicate composite”. Journal of the European Ceramic Society, vol. 24 (3), pp. 565-578, 2004.

[12] D. Schawaller, B. Clauß, M. R. Buchmeiser. “Ceramic filament fibers – A review”. Macromolecular Materials and Engineering, vol. 297 (6), pp. 502-522, 2012.

[13] D. M. Wilson, L. R. Visser. “High performance oxide fibers for metal and ceramic composites”. Composites Part A: Applied Science and Manufacturing, vol. 32 (8), pp. 1143-1153, 2001.

[14] F. Deléglise, M. H. Berger, A. R. Bunsell. “Microstructural evolution under load and high temperature deformation mechanisms of a mullite/alumina fibre”. Journal of the European Ceramic Society, vol. 22 (9–10), pp. 1501-1512, 2002.

[15] C. J. Armani, M. B. Ruggles-Wrenn, R. S. Hay, G. E. Fair. “Creep and microstructure of Nextel™ 720 fiber at elevated temperature in air and in steam”. Acta Materialia, vol. 61 (16), pp. 6114-6124, 2013.

[16] C. J. Armani, M. B. Ruggles-Wrenn, G. E. Fair, R. S. Hay. “Creep of Nextel™ 610 fiber at 1100°C in air and in steam”. International Journal of Applied Ceramic Technology, vol. 10 (2), pp. 276-284, 2013.

[17] M. Schmücker, F. Flucht, P. Mechnich. “Degradation of oxide fibers by thermal overload and environmental effects”. Materials Science and Engineering: A, vol. 557 (0), pp. 10-16, 2012.

[18] M. Schmücker, H. Schneider, T. Mauer, B. Clauβ. “Temperature-dependent evolution of grain growth in mullite fibres”. Journal of the European Ceramic Society, vol. 25 (14), pp. 3249-3256, 2005.

[19] M. Schmücker, P. Mechnich. “Microstructural coarsening of Nextel™ 610 fibers embedded in alumina-based matrices”. Journal of the American Ceramic Society, vol. 91 (4), pp. 1306-1308, 2008.

[20] S. Petzold, M. Morche, J. Taesler. “Oxide-ceramic continuous fibres and ceramic fibre reinforced composites – Innovative materials for the firing process”. ZI International, vol. 64, pp. 24-31, 2011.

[21] R. Morrell. “A tensile creep-testing apparatus for ceramic materials using simple knife-edge universal joints”. Journal of Physics E: Scientific Instruments, vol. 5 (5), pp. 465, 1972.

[22] D. M. Wilson, S. L. Lieder, D. C. Lueneburg. “Microstructure and high temperature properties of Nextel 720 fibers”, pp. 1005-1014 in *Proceedings of 19th Annual Conference on Composites, Advanced Ceramics, Materials, and Structures*, J. B. Wachtman Jr. (Ed.). John Wiley & Sons, Inc., 2008.

[23] K. G. Dassios, M. Steen, C. Filiou. “Mechanical properties of alumina Nextel™ 720 fibres at room and elevated temperatures: Tensile bundle testing”. Materials Science and Engineering: A, vol. 349 (1–2), pp. 63-72, 2003.

[24] V. Calard, J. Lamon. “Failure of fiber bundles”. Composites Science and Technology, vol. 64 (5), pp. 701-710, 2004.

[25] F. Deléglise, M. H. Berger, D. Jeulin, A. R. Bunsell. “Microstructural stability and room temperature mechanical properties of the Nextel 720 fibre”. Journal of the European Ceramic Society, vol. 21 (5), pp. 569-580, 2001.

[26] M. D. Petry, T.-I. Mah. “Effect of thermal exposures on the strengths of Nextel™ 550 and 720 filaments”. Journal of the American Ceramic Society, vol. 82 (10), pp. 2801-2807, 1999.

[27] H. Schaper, L. Van Reijen. “A quantitative investigation of the phase transformation of gamma to alpha alumina with high temperature DTA”. Thermochimica Acta, vol. 77 (1), pp. 383-393, 1984.

[28] M. Schmücker, H. Schneider, T. Mauer, B. Clauß. “Kinetics of mullite grain growth in alumino silicate fibers”. Journal of the American Ceramic Society, vol. 88 (2), pp. 488-490, 2005.

[29] G. Bernard-Granger, C. Guizard, R. Duclos. “Compressive creep behavior in air of a slightly porous as-sintered polycrystalline α-alumina material”. Journal Of Materials Science, vol. 42 (8), pp. 2807-2819, 2007.

[30] S. Gustafsson, L. K. L. Falk, J. E. Pitchford, W. J. Clegg, E. Lidén, E. Carlström. “Development of microstructure during creep of polycrystalline mullite and a nanocomposite mullite/5 vol.% SiC”. Journal of the European Ceramic Society, vol. 29 (4), pp. 539-550, 2009.

[31] T. P. Herbell, D. R. Hull, A. Garg. “Hot hydrogen exposure degradation of the strength of mullite”. Journal of the American Ceramic Society, vol. 81 (4), pp. 910-916, 1998.

5 Thermal exposure effects on the strength and microstructure of a novel mullite fiber

The mechanical behavior of the novel fiber CeraFib 75 after various thermal exposures is examined. This fully crystalline mullite fiber was developed to exceed the thermal stability of commercially available oxide fibers. Therefore, heat treatments at temperatures ranging from 1000 to 1400°C for 25 h were performed and results compared to the well-established Nextel™ 720 fibers. Mechanical characterization was realized with bundle tensile tests using acoustic emission sensors to determinate the fiber failure distributions. Investigations showed that the initial fiber microstructure of mullite grains with traces of alumina transforms starting at 1200°C. Changes include dissociation of the alumina-rich mullite phase and grain growth. Thus, strength reduction is measured as a result of these microstructure transformations. Remarkably, at 1400°C, fibers become more fragile and Weibull statistics can no longer describe the failure distribution. A relation between the distribution shape and the load redistribution capability of fibers is suggested. This is more pronounced for Nextel™ 720 fibers, which present much bigger grains and retain only 10% of their original strength. However, CeraFib 75 fibers are more stable and exhibit a strength retention of 50% at the same conditions, which is attributed to the higher amount of mullite phase.

5.1 Introduction

Ceramic matrix composites (CMC) represent a progress on thermostructural materials because they combine considerable toughness aligned with the high strength of ceramic materials. Therefore, they gained importance on aerospace application and on different industrial fields like in the motorsport industry. However, it is still a great challenge on the field of CMCs to develop composites that are inert at oxidizing atmospheres and, at the same time, retain their mechanical properties at temperatures above 1000°C. Conventional SiC-based composites exhibit great mechanical performance at high temperature, but are still susceptible to degradation due to oxidation [1]. Thus, CMC based on all-oxide materials can be a viable option, given that they are resistant against oxidation by nature. Considering this main property, applications of oxide–oxide CMCs can be exemplified as components in gas

turbine combustors, heat shields, and heat exchangers [2, 3]. In such applications, it is expected that the component will undergo several thermal loads during its life time. Therefore, the reinforcements used must be stable to such harsh conditions. In this matter, most developments have been achieved on fibers based on alumina or alumina–silica compounds. One can say that, nowadays, the most used oxide fibers are the Nextel™ line, commercialized by the American company Minnesota Mining and Manufacturing (3M). Among this series of fibers, Nextel 720 is worth mentioning. This alumina–mullite fiber presents a filament tensile strength of about 2.1 GPa and the highest creep resistance and strength retention among the current oxide fibers. This better stability at high temperatures can be related to the morphology and size of the mullite grains, and therefore, Nextel 720 is considered to be the most suitable fiber for long-term applications [4].

As stated before, temperature can still be a limiting factor for the appliance of all-oxide CMCs, since they are prone to strength loss and embrittlement when exposed to temperatures above 1000°C. According to the literature, this loss is normally associated with the degradation of the fibers [5, 6]. It should be highlighted that these temperatures can be achieved on the aforementioned applications and even during the processing of the composites. Consequently, works studying the strength retention of oxide fibers can be found in the literature, but they are rather conflicting. The first work published on this topic is credited to Wilson [7]. In his studies, Nextel 720 and other alumina-based fibers were tested at room temperature before and after heat treatments for 100 h at temperatures ranging from 1000 to 1400°C. While Nextel 720 retained 85% of its strength up to 1300°C, the other oxide fibers showed a significant strength loss after the heat treatment at 1000°C. Petry and Mah [8], on the other hand, measured a strength retention of 90% and 75% for Nextel 720 after only 2 h exposure to 1100°C and 1300°C, respectively. Milz et al. [9] reported even lower stability at comparable conditions by describing a catastrophic degradation of the fiber, which was caused by local impurities. Still, Deléglise et al. [10] measured no significant strength loss for Nextel 720 after 5 h exposure up to 1400°C, but a major degradation after 24 h exposure. Nevertheless, the authors tend to agree that the strength decrease is caused by grain growth [8, 10] and grain-boundary grooving [11], even though these works lack on deep microstructure investigations. Grain growth kinetics for Nextel 720 was studied in more detail by Schmücker et al. [12, 13]. Grain size and morphology changes were reported after thermal exposure at temperatures above 1200°C for 2 h. However, further analysis pointed out that grain growth shows little time dependency at temperatures below 1600°C.

Considering the situation stated above, the importance of developing oxide fibers that are more stable at high temperatures is evident. In this matter, the Institute of Textile Chemistry and Chemical Fibers (ITCF, Denkendorf, Germany), together with the German company CeraFib GmbH (Olbersdorf, Germany), has developed oxide fibers, which are able to operate at higher temperatures [14] and shall be commercialized in the near future. Hence, the objective of this work is to study the mechanical behavior of the new fiber, CeraFib 75, after exposures to different critical temperatures. This novel fiber presents a nearly pure mullite structure and therefore, better performance at high temperatures, which was proven in previous works [15]. For comparison, the same treatments were conducted with Nextel 720 fibers. In addition, the authors acknowledge that little attention is given in the literature to the relation between changes in mechanical behavior and microstructure evolution after heat treatments, and these two topics are normally reported separately in more detail. Therefore, this paper presents several microstructure and crystal phase analysis which are quantified and related to the different aspects seen on the tensile tests of the fibers after the thermal exposure.

5.2 Experimental Procedure

5.2.1 Materials and Heat Treatment

Main investigations here reported are for the novel mullite fiber with the trademark of CeraFib 75. This fiber is produced by dry-spinning of a solution with composition near to stoichiometric mullite ($3Al_2O_3$–$2SiO_2$). During processing, the formation of volatile Si species reduces the overall silica content, which leads to a final composition of 75 wt.% of alumina and 25 wt.% of silica, and a microstructure of mullite grains with traces of alumina. On the other hand, Nextel 720 is an alumina–silica fiber (85–15 wt.%) produced via sol-gel route. Its microstructure is known to be of a mosaic of mullite grains with smaller and elongated alumina grains [16]. Table 5.1 summarizes relevant information of both fibers given by their respective manufacturers. It can be seen that Nextel 720 presents a different content of alumina in its composition, but this fiber was used for comparison since both are the only fully crystalline mullite fibers available and present the same field of interest, high-temperature applications.

Table 5.1: Summary of tested fibers. #

Fiber	Manufacturer	Composition (wt.%)	Diameter (μm)	No. of filaments per bundle
Nextel 720	3M	85 Al_2O_3 – 15 SiO_2	3.17 ± 0.09	800
CeraFib 75	CeraFib	75 Al_2O_3 – 25 SiO_2	3.26 ± 0.19	400

Information by manufacturer

The analyses were done on the fibers before (as-received) and after different heat treatments in air at temperatures of 1000°C and 1200-1400°C for 25 h. An exposure time of 25 h was chosen to ensure that changes would occur to the fibers, based on investigations found in the literature. Treatments were performed in a high-temperature chamber furnace (Nabertherm LHT 04/17, Lilienthal, Germany). Initial tensile tests on specimen thermally treated at 1000°C showed no differences to the results of as-received fibers, and therefore, no further investigations were done at that temperature.

5.2.2 Microstructure and Crystal Phases Analysis

Changes in the microstructure were perceived through scanning electron microscopy (SEM). Therefore, fibers were embedded in epoxy resin for surface preparation (grinding and polishing). Then, the epoxy resin was thermally extracted at 800°C for the subsequent thermal etching at 1300°C for 30 min to reveal the microstructure of the fibers. Finally, images of the microstructure were taken from five different fibers using a SEM (Zeiss SUPRA 40, Oberkochen, Germany) with an acceleration voltage of 0.5 kV. Moreover, energy-dispersive X-ray analysis (EDX) was conducted to measure the actual composition of the fiber in the as-received state.

Additional information on the crystal phase composition of the fibers was obtained by X-ray diffraction (XRD) technique. To do so, fibers were crushed into a powder and then analyzed at room temperature on a diffraction system (Bragg-Brentano PANalytical X'Pert MPD PRO, PANalytical GmbH, Kassel-Waldau, Germany), equipped with CuKα radiation (λ = 1.5418 Å) and X'Celerator detector system. Scans were performed in the range from 5 to 120°. Phase quantification and crystallite size were obtained by Rietveld refinements using the software Diffracplus Topas 4.2 (Bruker AXS GmbH, Karlsruhe, Germany).

5.2.3 Mechanical Tests

Tensile tests on fiber bundles were chosen for the mechanical characterization of the fibers. According to the literature, this type of test is more suitable for characterizing the strength of reinforcements because fibers are normally applied as tows. In addition, some authors agree that the preparation of fiber bundle specimens is easier and implies less damage to the fibers, therefore, it has lower influences on the results [17, 18]. For the experiments, fiber bundles were aligned in alcohol and specimens were prepared according to the norm DIN EN 1007-5, but with a gauge length of 25 mm. Tests were then performed at room temperature using an universal testing machine (Zwick/Roell Z005, Ulm, Germany) with a testing speed of 0.01 mm/min until total failure of the bundle. A total of three samples were tested for each fiber condition. Before testing, system compliance and the initial cross-section area of the bundles were measured according to the standards DIN EN 1007-5 and 1007-2, respectively.

For the determination of the fiber failure distribution within the bundle, an acoustic emission (AE) detection device (Vallen AMSY4-PC, Icking, Germany) was used during tensile bundle tests. The use of AE on bundle tests has already been discussed and proved by other authors [19, 20]. In this sense, the procedure here used was based on the technique reported earlier [20]. Two sensors were positioned in the upper and lower fixtures connecting the testing machine to the samples. Settings used for the AE system are listed in Table 5.2 and were determined experimentally and also based on the literature. With the given set up, each fiber failure (hit) could be detected during the test and a failure distribution could be traced using the correspondent fiber failure strain. A distribution based on strain values was used since it does not depend on the number of load-carrying fibers in the bundle which varies during the test [17]. Nevertheless, strength of the fibers can be determined by multiplying the measured strain by the initial modulus of the bundle, Equation 12, and this parameter was used in order to compare the fibers before and after the treatments. Moreover, statistical analysis were performed with the software Minitab® 17 (Minitab Inc., State College, PA) to test and identify which distribution (normal, Weibull, or log-normal) better fit the AE results using Anderson–Darling (A–D) statistic. This test measures how much the data points deviate from the fitted model with a higher weight in the beginning and end of the distribution. The A–D test is considered one of the most powerful statistical tool to decide whether a set of data follows a specific distribution [21].

Table 5.2: Parameters for acoustic emission acquisition.

Parameter	Value
Pre-amplifier gain	40 dB
Threshold	30 dB
Duration discrimination time (DDT)	50 μs
Rearm time (RT)	100 μs

In addition to investigations on bundles, filament tensile tests were performed in accordance to the norm DIN EN 1007-4. These tests were done to measure the elastic modulus (E-modulus) of the filaments. Fibers were tested in a tensile testing machine using an 1 N load cell and a linear variable differential transformer sensor of ±1 mm. Thirty samples were tested with a traveling speed of 1 mm/min until failure. The cross-section area of each fiber tested was determined after the test by measuring the fracture surface with an optical microscope (SENSOFAR PLμ 2300, Terrassa, Spain).

5.3 Results

5.3.1 Microstructure evolution

Thermal etching process was successfully done to reveal the microstructure of the fibers. Nextel 720 seemed to be more susceptible to the etching as its grain boundaries were better defined and the resultant image had a better contrast. Nonetheless, grains could be identified for both fibers after increasing the images contrast. Figure 5.1 shows images of the fibers before and after the heat treatments at 1200-1400°C, and changes in size and morphology of grains are noticeable. In the as-received state, CeraFib 75 fibers presented 200 nm mullite grains, some being spherical, and some others more elongated. As for Nextel, 150 nm faceted mullite grains could be perceived, which are slightly misoriented and form the mosaic-like structure described in the literature [22]. After the heat treatment at 1200°C, small grain growth could already be noticed, but the grains retained their shape. At the temperature of 1300°C and above, more elongated grains were seen and a progressive grain growth was observed. Most significant differences were seen at 1400°C, at which Nextel fibers started to present a bimodal distribution of elongated grains, most having approximately 400 nm and a

small amount of larger 1500 nm grains. In contrast, CeraFib 75 still demonstrated more uniform and more spherical 400 nm grains.

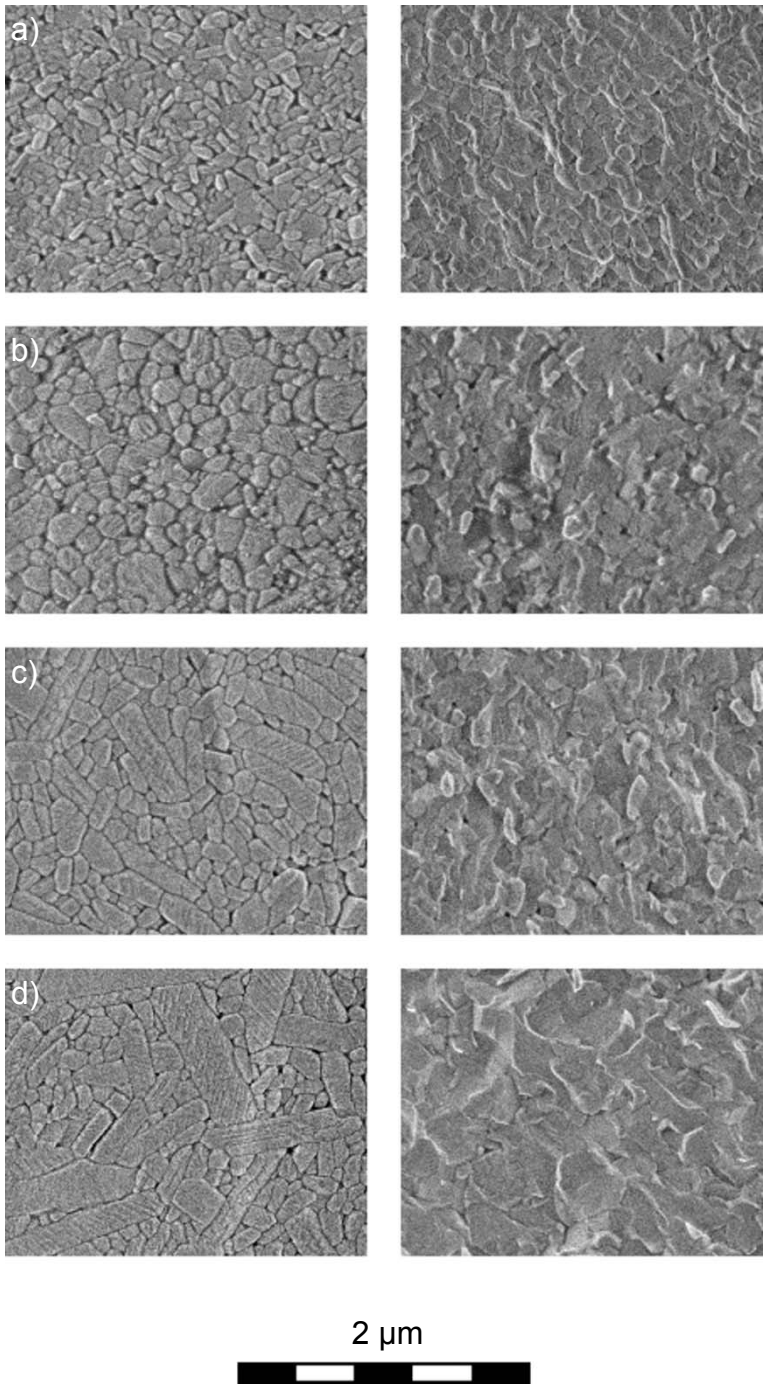

Figure 5.1: Microstructure evolution of Nextel 720 (left) and CeraFib 75 (right). Fibers as-received (a) and after heat treatments for 25 h at temperatures of 1200°C (b), 1300°C (c) and 1400°C (d).

Energy-dispersive X-ray analysis measurements, cf. Appendix A.4, showed small discrepancies to the chemical composition data given by the manufacturers, *e.g.*, an equivalent content of silica was measured as 24.25 and 13.99 wt.% for CeraFib 75 and Nextel 720, respectively. These differences are somewhat expected, given that the silica content might be reduced during fiber processing. From the X-ray diffraction patterns (Figure 5.2), mullite was identified as the main phase for both fibers and is not labeled in the graph. Significantly different amounts of corundum (α-alumina) were also detected, depending on the type of fiber and the thermal treatment. Additionally, as-received CeraFib 75 fibers contain minor amounts of γ-alumina. The quantitative phase content as a result of Rietveld refinements helped in the evaluation of the impact of heat treatment on the material composition. Results are displayed in Figure 5.3 for each fiber condition. A progressive increase in alumina phase content is seen after the thermal exposure. For CeraFib 75, the treatment at 1200°C promoted the transformation of γ- into α-alumina, and the increase in overall alumina phase content was seen only at temperatures above 1300°C. Significant changes in width and height of the diffraction peaks were also observed. With increasing temperature, diffraction peaks got higher and narrower, which can be attributed to an increase in crystallite size; the respective refinement results are discussed below in combination with the tensile tests results.

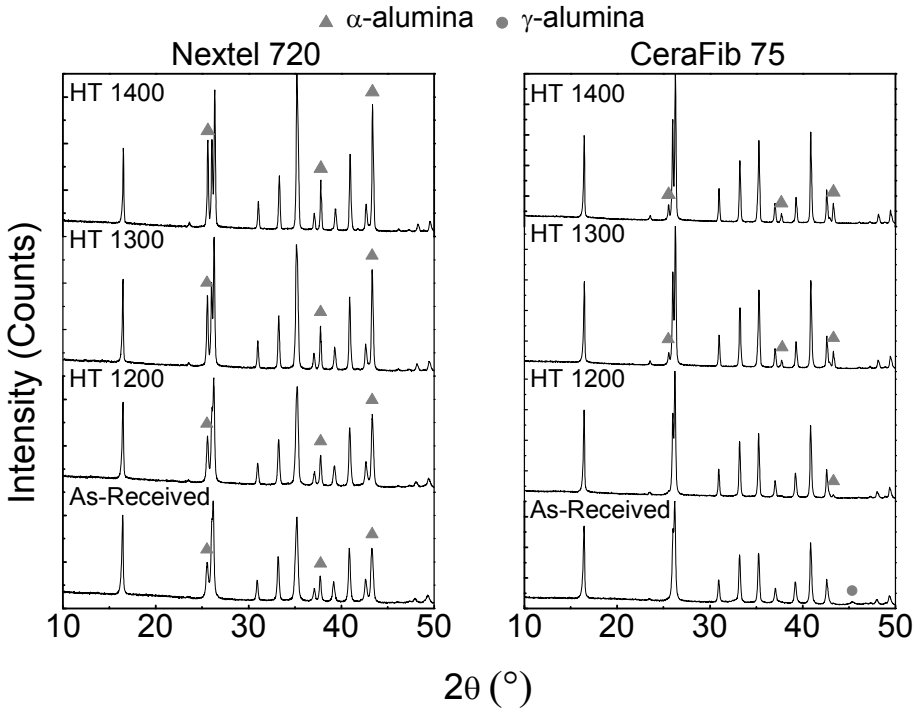

Figure 5.2: Sections of X-ray diffraction patterns of tested fibers as-received and after heat treatments for 25 h at temperatures of 1200-1400°C. Mullite was identified as the main phase (not labeled); two different alumina phases were also detected.

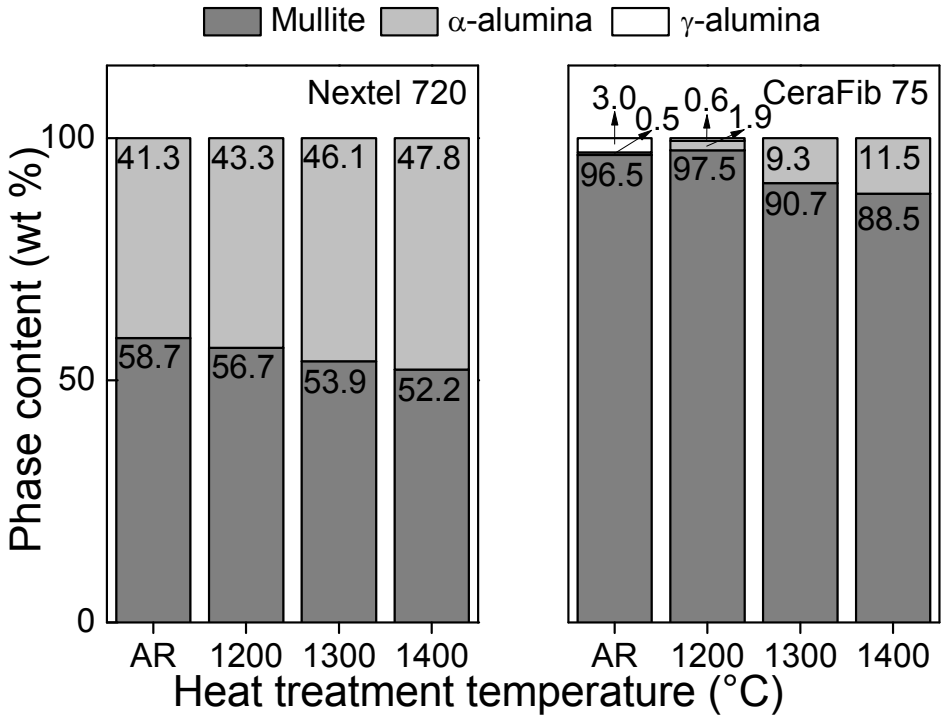

Figure 5.3: Crystal phase content of the fibers by Rietveld refinement of XRD results.

5.3.2 Mechanical Behavior

Investigations on the mechanical behavior were done with tensile tests on single filaments and bundles before and after the heat treatments. During preparation and handling of the fibers, the effect of the thermal exposure was already noticeable as the fibers became more fragile, *i.e.*, easily breakable. Even so, specimen preparation was successfully performed with the exception of Nextel 720 after the exposure to 1400°C. Those samples were extremely fragile and the fibers of the bundle were partially sintered together. Similar observations were already noticed by other authors during thermal aging of oxide fibers [7, 10]. Therefore, the fibers could not be separated and only bundle specimens were prepared. Filament tests of the other specimen showed a brittle behavior with only linear deformation until failure. Results of E-modulus from single filament tests are plotted as a function of heat-treatment temperature in Figure 5.4. As-received results were already discussed elsewhere [15], and CeraFib and Nextel fibers had similar elastic modulus of 225±25 GPa and 221±16 GPa, respectively. An increasing tendency on the E-modulus was observed for the fibers starting at the temperatures of 1200°C and 1300°C for Nextel 720 and CeraFib 75, respectively.

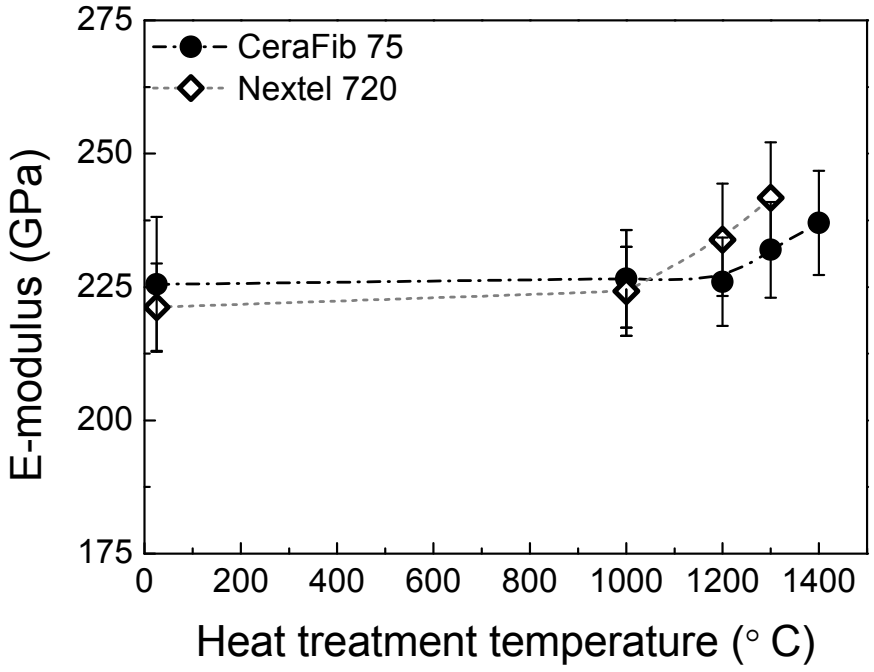

Figure 5.4: Measured E-modulus of single filament fibers as-received and after heat treatments for 25 h at temperatures of 1000-1400°C.

Strength of the fibers was analyzed by bundle tests with the assistance of an AE device. Figure 5.5 and Figure 5.6 present example curves of the bundle tests (left) for CeraFib and Nextel on each condition and the associated linearized Weibull distribution obtained by AE (right) for samples as-received and after the treatment at 1400°C. Since CeraFib and Nextel bundles have a different number of filaments and total cross-section area, the graphs plotted are in relation to the apparent stress, *i.e.*, the applied force divided by the initial bundle area. During test (cf. Figure 5.5 and Figure 5.6 left), different stages could be seen in the test curves. At first, the fibers in the bundle are tensioned and there is an increase in the slope until reaching a constant value, which shows that all the fibers are aligned. This constant value can be referred to the bundle modulus, and followed a similar tendency to the results of E-modulus shown in Figure 5.4. The inclination of the curve remains constant until the first fiber failure is detected. As the fibers start to fail, the number of load-carrying fibers decreases and so does the inclination of the curve until the maximum load is achieved. From this point on, the bundle has no longer enough load-carrying fibers and a smooth load drop is observed until the load tends to zero. AE hits were in accordance with the decrease on inclination and small load drops observed during test. However, small deviations on the total number of hits and the number of filaments per bundle given by the manufacturer were noticed, in which around 370 and 750 hits were measured for CeraFib 75 and Nextel 720 bundles, respectively. Samples heat treated until 1300°C followed a similar pattern as the one described for as-received, but exhibited lower bundle strength. Differences in the test curve were seen only at 1400°C; several steep load drops were observed after the maximum load. Additionally, a lower amount of AE hits was measured for those samples, 220 for CeraFib and 280 for Nextel, indicating multiple fiber failures.

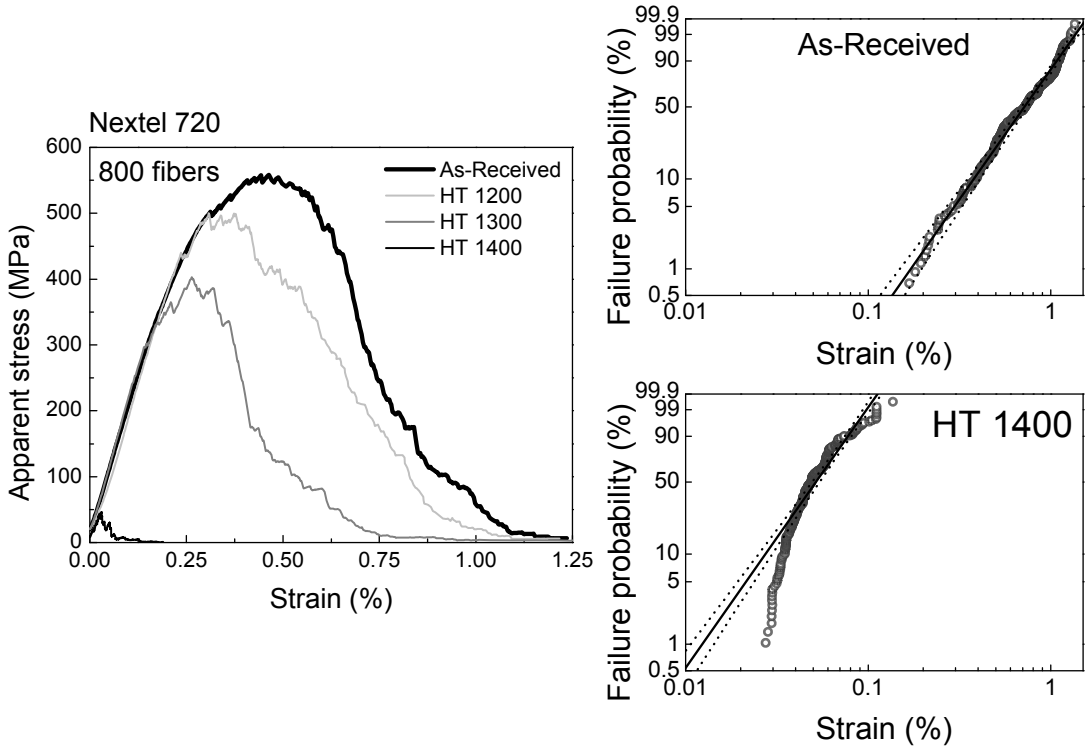

Figure 5.5: Bundle tensile test (left) for Nextel 720 fibers. Resultant strain failure distribution (right) for fibers as-received and heat treated at 1400°C.

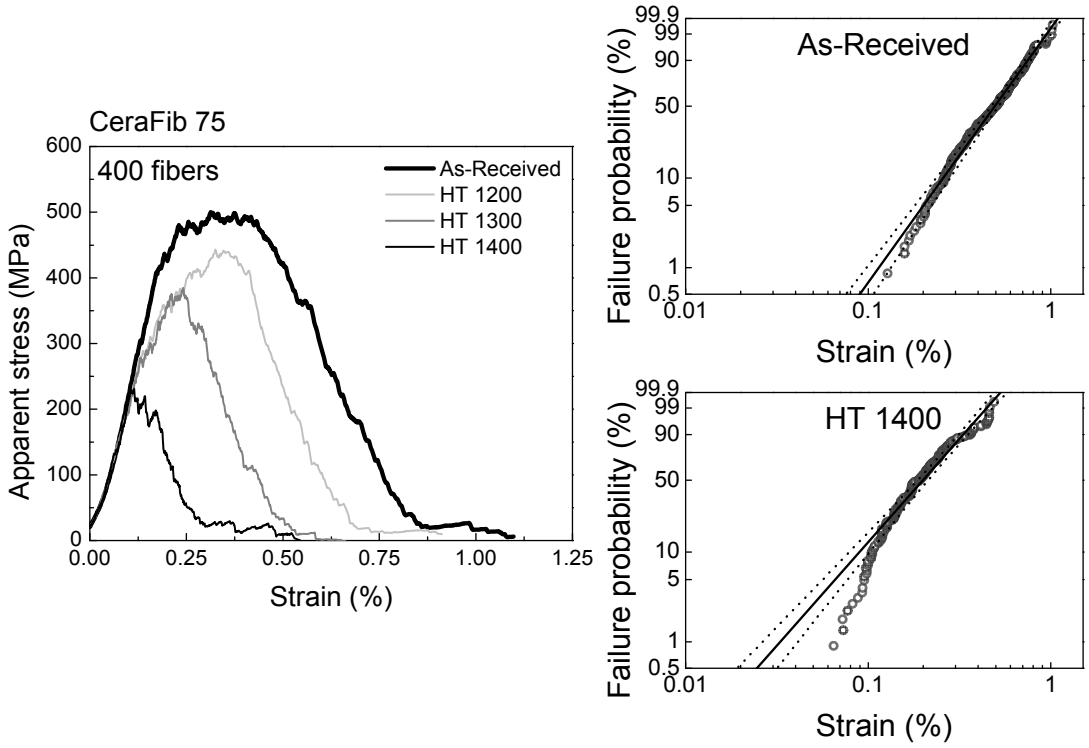

Figure 5.6: Bundle tensile test (left) for CeraFib 75 fibers. Resultant strain failure distribution (right) for fibers as-received and heat treated at 1400°C.

With the data acquired from the AE device, failure distributions could be traced with more than 200 data values for each specimen. Therefore, determination of the best fitting distribution could be done, given that a minimum of 150 samples is suggested for such analysis [23]. The A–D test was used for the determination, whereas a lower value indicates a better fit for the given distribution. Weibull was pointed out as the best fit for as-received fibers as exemplified in Figure 5.5 and Figure 5.6 (right), in which the data points followed the distribution line well. The same aspect was seen for the fibers heat treated with the exception of the exposure to 1400°C. For those specimens, the shape of the distribution had drastically changed and Weibull could no longer describe it with precision. Nevertheless, Weibull parameters were also calculated for those bundles for a comparison matter. A–D statistic for the fit of Weibull distribution is displayed in Table 5.3 along with the Weibull modulus (m) and characteristic strength (σ_0) of each specimen. Values of σ_0 displayed in the table were obtained by multiplying the characteristic strain (ε_0) of the measured distributions by the initial modulus of the bundle.

Table 5.3: Results of bundle tensile tests of heat treated fibers.

Heat	Nextel 720			CeraFib 75		
treatment	σ_0 (MPa)	m	A–D test	σ_0 (MPa)	m	A–D test
As-received	1427	3.8	1.09	1250	3.1	0.60
HT 1000	1459	4.2	0.96	1238	3.5	0.50
HT 1200	1332	4.1	1.24	1109	2.9	0.56
HT 1300	1049	3.9	3.09	835	3.3	1.94
HT 1400	118	4.3	5.53	623	3.4	3.42

Figure 5.7 summarizes the relation between strength retention and crystallite size, measured by bundle tests with AE and XRD refinements, respectively. Both fibers demonstrated similar behavior with treatments up to 1300°C and retained about 70% of their as-received strength. A similar tendency was also observed on single filament tests. Hence, Nextel 720 presented higher characteristic strength at such conditions. However, high degradation was seen for Nextel 720 after the heat treatment at 1400°C, *i.e.*, the bundle showed a strength retention of only 10%. Conversely, CeraFib bundles remained stable and presented a strength retention of 50% for the same condition. A comparable tendency was observed on the crystallite size of the fibers. At 1400°C, alumina grains of Nextel started experiencing a higher grain growth.

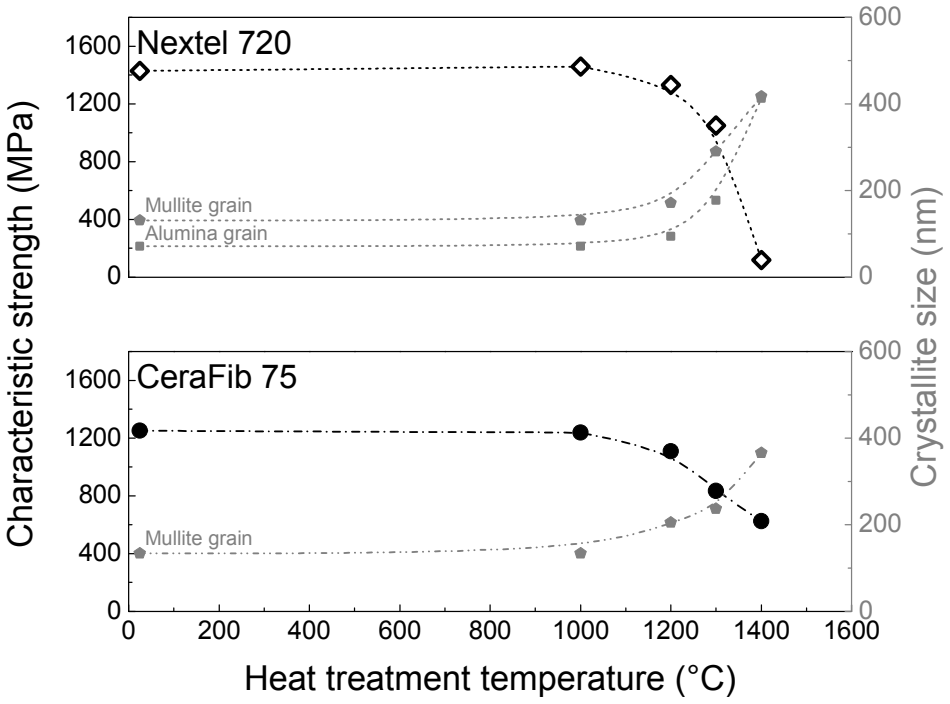

Figure 5.7: Strength retention of mullite fibers as-received and after heat treatments for 25 h at temperatures of 1000-1400°C, and its relation to fiber crystallite growth measured by Rietveld refinements.

5.4 Discussion

Microstructural changes could be perceived on the fibers after the 25 h treatments at different temperatures. These changes caused a reduction in the mechanical performance, and potential explanations for our observations will be presented as follows. CeraFib 75 is produced by a dry-spinning process followed by a pyrolysis treatment at temperatures between 1350°C and 1400°C. Due to the short period at the pyrolysis temperature, the fiber microstructure developed consists of metastable alumina-rich mullite and a few γ-alumina grains. The alumina content of the mullite phase could be determined from the refined lattice parameter using the equation proposed by Fischer [24], Equation 4, according to which the as-received mullite structure of CeraFib fibers contains 65 mol% Al_2O_3. In a similar matter, the mullite phase in Nextel 720 contains about 67.5 mol% Al_2O_3. The remaining alumina in the fibers is then crystallized as smaller corundum grains, or γ-alumina for CeraFib 75. Due to the metastability of the mullite phase, thermally activated transformations start at temperatures beyond 1000°C [24]. Thus, after a longer exposure to high temperatures, *e.g.*, treatments higher than 1200°C, the overall α-alumina content of both fibers increased, as seen in Figure 5.3. This increase is caused by the dissociation of the metastable (alumina-rich) mullite phase

into mullite with higher silica content and additional corundum grains. For Nextel 720, a steady increase in the α-alumina content was found with an elevation of the treatment temperature. CeraFib 75 on the other hand showed these transformations at temperatures higher than 1200°C due to the presence of the γ-alumina phase. With the treatment at 1200°C, only recystallization of γ- to α-alumina occurred, since the latter is the most stable phase [25]. In the end, both fibers showed an alumina content in mullite of 62 mol% after treatment at 1400°C. Figure 5.8 shows the alumina content inside the mullite phase for the tested fiber as a function of the heat treatment temperature. At this point, it is also important to highlight that the increasing tendency measured for the E-modulus of the filaments follows the increase in alumina phase detected. In other words, from 1200°C and 1300°C for Nextel 720 and CeraFib 75, respectively. This can be then associated with the higher stiffness of the alumina phase. Another observation that can be raised with XRD analysis is regarding the content of silica. For instance, considering Figure 5.3 and Figure 5.8, a silica content of 23.33 wt.% can be calculated for as-received CeraFib 75 fibers, which is lower than the value measured by EDX, 24.25 wt.%. Since the XRD analysis considers only crystalline phases, and the EDX measures the overall element content, it can be presumed that this difference might be due to the presence of an amorphous silica phase in low amounts of around 1 wt.%. In addition, a very small “bump” was observed in the diffraction pattern (Figure 5.2) between 15 and 30°, which also indicates the presence of an amorphous silica phase. After the heat treatments, however, no significant difference was seen. Therefore, it can be concluded that such amorphous phase is not present anymore and the total silica content is in the mullite crystal phase. A similar tendency was also observed for Nextel 720 fibers.

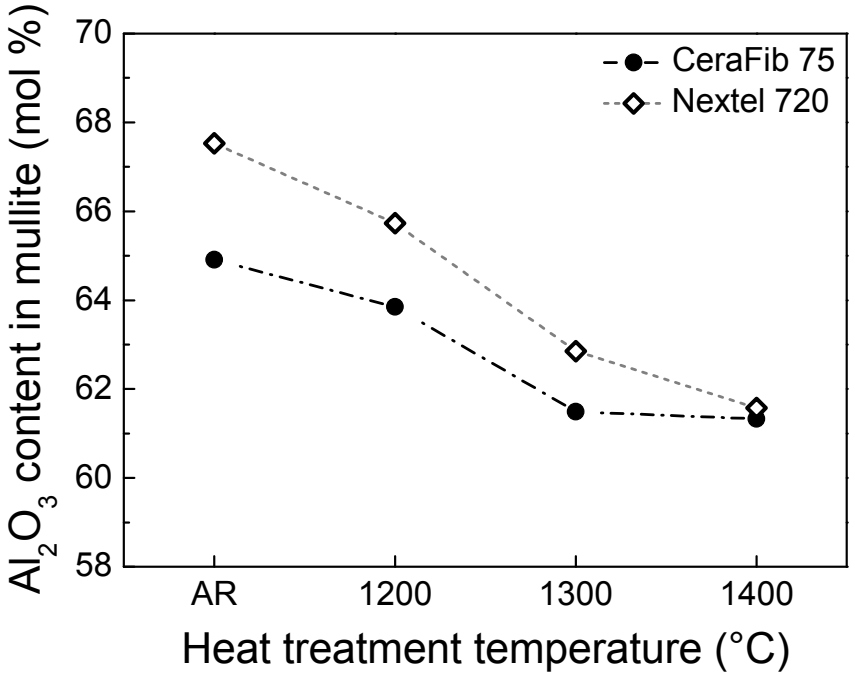

Figure 5.8: Alumina content in mullite phase of tested fibers determined from XRD results.

Parallel to phase transformation, grain growth was also observed after the treatments at 1200°C and higher. As-received fibers presented faceted mullite grains, which were more spherical in the case of CeraFib fibers, with smaller alumina grains. It is well known that the strength of small diameter fibers depends on this nanometer-sized grain structure. Crystallite growth after the treatments could be quantified with the XRD results, which were in accordance with observations made in the micrographs. As a result, both fibers showed a reduction in room-temperature strength following an inverse tendency to the crystallite size as seen in Figure 5.7. Alumina is known to start presenting grain coarsening at 1200°C [12]. Though, since the mullite structure is still stable at the same temperature, alumina grains mobility is reduced and only little coarsening took place. Higher mobility at 1300°C allows for changes in size, and also in morphology to more elongated grains. These observations are more drastic for Nextel 720 fibers at 1400°C, which could be attributed to the lower mullite content. In this case, attention should also be given to the dissociation phenomenon described above. Initial α-alumina content for Nextel 720 gradually increased from 41 wt.% to a final content of 48 wt.% due to thermal treatment. Thus, it is expectable that alumina grains will have more freedom. At the same temperature, the amorphous silica phase that might be present in as-received fibers can also enhance the abnormal grain growth [26], before phase

transformation takes place. As a result, Nextel fibers exhibited grains of 400 nm, and a few 1500 nm grains as seen in the micrographs. A different grain size evolution was found for CeraFib 75. Here, an uniform microstructure of 400 nm mullite grains and some alumina grains in the same order were found after heat treatment at 1400°C. The increase in α-alumina content was measured for this fiber as well, but the overall content was of only 11 wt.% after the treatment at 1400°C. Therefore, CeraFib 75 demonstrated a much better performance at such condition.

Strength retention measured on bundle tensile tests could be successfully related to the quantification of microstructure results. Yet, bundle tests can also offer interesting information about the mechanical behavior of the fibers and the resultant failure distribution determined for each condition. As-received samples presented a constant slope in the test curve until the first fiber failure was detected by the AE sensors. The tensile strength of the fibers is normally related to the presence of pre-existing flaws. Considering that each fiber in the bundle has its individual flaw distribution, which can be rather different from each other [27], each fiber will fail at a distinctive moment of the test. When a fiber fails, the total bundle area is reduced, and the load is then redistributed to the remaining fibers. During this load redistribution, if there is any fiber with a similar flaw density to the broken one, multiple fiber failure can occur resulting in steeper load drops. Nevertheless, only small load drops were detected showing that the fibers can withstand the load redistribution fairly well. Applying the AE methodology for data analyses, failure distributions could be determined with a high statistical significance. A–D test performed on results from as-received bundles showed that Weibull distribution was the best fit. This ratifies that the weakest link theory can be applied to fiber bundles. Hence, the Weibull distribution was used to compare the fibers. The results obtained, *e.g.*, σ_0 and m, are lower than the ones obtained by single filament because of the much higher sample size. Comparing both fibers, it can be seen that CeraFib presented lower values of characteristic strength and modulus. These results reflect the differences in chemical composition between Nextel and CeraFib, and the wider distribution of defects present in the new fiber [15].

Test curves showed the same shape for samples heat treated up to 1300°C in comparison to as-received fibers. A higher deviation pointed by A–D statistic was seen with the treatment at 1300°C, but Weibull distribution was still the best fit for this condition. It is also interesting to see that the fibers retained its Weibull modulus, indicating that the failure mechanisms

remained the same. Differences on mechanical behavior and failure distribution were observed only at 1400°C. As seen in the linearized Weibull plots from Figure 5.5 and Figure 5.6, the data set of both fibers did not follow properly the fitted line and the Weibull statistics could no longer describe the distribution. Instead, log-normal distribution was determined as the best fit for this condition. Fragile materials, like the ceramic fibers here studied, are normally related to the Weibull distribution. However, several examples in the literature showed that a log-normal or gamma distribution can be a better fit when there are more conditions that influence the failure of the material besides the presence of the biggest flaws [28, 29]. In the case of bundles treated at 1400°C, interactions between fibers can be then related with their deviation to Weibull distribution. Steeper load drops were observed for those bundles, which indicates multiple fiber failure resulted from a poor redistribution of stresses among the fibers of the bundle. This is mainly caused by the embrittlement of the fibers after the thermal exposure. Grain growth was measured with a significant extent at that temperature and, together with the increase in α-alumina phase, causes higher fragility in the fibers, *i.e.*, lower strength and higher E-modulus. In this state, when one fiber fails, the energy released to the others is too high causing a multiple fiber failure. This phenomenon was aggravated on Nextel 720 fibers at 1400°C also due to the fact that the fibers were sintered together, which could be related to the higher reactivity of the alumina phase at the given temperature. Nextel at 1300°C presented a Weibull distribution, but the higher A–D statics measured can be an indication of poor load redistribution.

Mechanical behavior observations raised during bundle tests have great relevance to the application of the fibers. In composites, fibers are applied as reinforcements in the form of bundles. Therefore, when a composite is loaded, the main part of the load is sustained by the fibers. To ensure that a CMC will present the desired pseudo-plastic behavior, different dissipating energy phenomena like fiber pull out or matrix cracking need to occur before significant fiber failure takes place [30]. In this sense, if the failure of the weakest fibers in the bundle promotes the consequent failure of the remaining fibers, the mechanical stability of the composite is compromised. This can be exemplified by the tests on Nextel fibers treated at 1400°C; when the first fibers broke, the bundle could not withstand load redistribution, which resulted in an overall much lower bundle strength. CeraFib treated at the same temperature demonstrated a less pronounced fragility. Thus, the bundle could undergo higher stresses, lower load drops were detected and it presented better load redistribution capability.

5.5 Conclusion

In the present work, the effects of different thermal exposures (1000-1400°C for 25 h) on the new mullite fiber CeraFib 75 were studied. For comparison, another mullite–alumina fiber was also tested: Nextel 720, which is known to offer the highest creep resistance and high-temperature stability of current commercial oxide fiber. Both fibers were characterized in relation to their microstructure and mechanical behavior to enable a direct comparison between them.

As-received microstructure revealed for CeraFib was of mullite grains with traces of α- and γ-alumina grains, while Nextel presented a higher amount of smaller corundum grains embedded in the larger mullite grains. Thermal exposure of the fibers resulted into two different phenomena starting at 1200°C: crystal phase transformation and grain growth. The first one occurred due to the dissociation of the metastable mullite phase into mullite plus α-alumina grains. In addition, phase transformation of γ- to α-alumina also occurred at 1200°C for CeraFib 75. The investigation of the grain size of the fibers after thermal exposure revealed that both fiber types showed a similar grain growth behavior up to 1300°C. Differences between CeraFib 75 and Nextel 720 were seen only at 1400°C, at which Nextel 720 presented some 1500 nm alumina grains. This abnormal growth was credited to the higher amount of alumina phase of Nextel 720 fibers.

Bundle tensile tests with AE sensors were applied to determine the failure distribution and the strength retention of the fibers. Both fibers showed a similar strength retention after treatments up to 1300°C of about 70%. With the thermal aging at 1400°C, however, CeraFib 75 presented a much higher strength of 623 MPa in comparison to Nextel 720, 118 MPa. These observations were in accordance to the microstructure and crystal phase quantification. The application of AE on bundle tensile tests was proved to be a relatively fast and precise method for the determination of the failure distribution. In addition, this test also provided important information regarding the behavior and load redistribution of bundles when they are loaded. It was observed that the Weibull statistic could describe the failure distributions measured for as-received samples and fibers treated at temperatures up to 1300°C. At 1400°C, the Weibull distribution could no longer trace the data points. This deviation was related to the poor load redistribution capability of the fibers, which was more expressed on Nextel 720 fibers. Nevertheless, CeraFib 75 bundle could still withstand fairly high loads at this condition, which proves the higher thermal stability of this novel fiber.

Therefore, one can conclude that CeraFib fibers can be used after such exposure depending on the level of stress applied to the component.

5.6 Acknowledgment

The authors thank the Brazilian Ministry of Science and Technology (CNPq) for the financial support through the program Science without Borders and the company CeraFib GmbH for the supply of testing materials. We also thank P. Witte from the University of Bremen for the SEM images. English proofreading performed by A. Almeida is also gratefully acknowledged.

5.7 References

This chapter was adapted, license no. 4183090052819, from:

R. S. M. Almeida, E. L. Bergmüller, B. G. F. Eggert, K. Tushtev, T. Schumacher, H. Lührs, B. Clauß, G. Grathwohl, K. Rezwan. “Thermal exposure effects on the strength and microstructure of a novel mullite fiber”. Journal of the American Ceramic Society, vol. 99 (5), pp. 1709-1716, 2016.

The article is mainly based on the work of the first author and author of this thesis Renato S. M. Almeida. The precise contributions of each author are listed below.

Table 5.4: Authors contributions for Chapter 5.

Author	Contribution
Almeida, R. S. M.	Conceptualized the work, planned the experiments, prepared the micrographs, analyzed the data of all experiments, wrote the manuscript
Bergmüller, E. L.	Performed experiments in the frame of Diploma thesis (cf. Supervised student projects)
Eggert, B. G. F.	Performed experiments in the frame of Diploma thesis (cf. Supervised student projects)
Tushtev, K.	Gave conceptual and scientific advices, helped in the scientific evaluation and editing of the manuscript
Schumacher, T.	Performed the XRD measurements and helped to evaluate and edit manuscript
Lührs, H.	Analyzed the XRD measurements and helped to evaluate and edit manuscript
Clauß, B.	Gave materials specific input and helped to evaluate and edit manuscript
Grathwohl, G.	Gave conceptual and scientific advices, helped in the scientific evaluation and editing of the manuscript
Rezwan, K.	Gave conceptual and scientific advices, helped in the scientific evaluation and editing of the manuscript

[1] R. C. Robinson, J. L. Smialek. “SiC recession caused by SiO_2 scale volatility under combustion conditions: I, experimental results and empirical model”. Journal of the American Ceramic Society, vol. 82 (7), pp. 1817-1825, 1999.

[2] R. A. Jurf, S. C. Butner. “Advances in oxide-oxide CMC”. Journal of Engineering for Gas Turbines and Power, vol. 122 (2), pp. 202-205, 2000.

[3] U. Trabandt, B. Esser, D. Koch, R. Knoche, G. Tumino. “Ceramic matrix composites life cycle testing under reusable launcher environmental conditions”. International Journal of Applied Ceramic Technology, vol. 2 (2), pp. 150-161, 2005.

[4] D. M. Wilson, L. R. Visser. “High performance oxide fibers for metal and ceramic composites”. Composites Part A: Applied Science and Manufacturing, vol. 32 (8), pp. 1143-1153, 2001.

[5] E. Volkmann, K. Tushtev, D. Koch, C. Wilhelmi, J. Göring, K. Rezwan. “Assessment of three oxide/oxide ceramic matrix composites: Mechanical performance and effects of heat treatments”. Composites Part A: Applied Science and Manufacturing, vol. 68 (0), pp. 19-28, 2015.

[6] M. L. Antti, E. Lara-Curzio, R. Warren. “Thermal degradation of an oxide fibre (Nextel 720)/aluminosilicate composite”. Journal of the European Ceramic Society, vol. 24 (3), pp. 565-578, 2004.

[7] D. M. Wilson. “New high temperature oxide fibers”, pp. 1-12 in *High Temperature Ceramic Matrix Composites*, W. Krenkel, R. Naslain, H. Schneider (Eds.). Wiley-VCH Verlag GmbH & Co. KGaA, 2002.

[8] M. D. Petry, T.-I. Mah. “Effect of thermal exposures on the strengths of Nextel™ 550 and 720 filaments”. Journal of the American Ceramic Society, vol. 82 (10), pp. 2801-2807, 1999.

[9] C. Milz, J. Goering, H. Schneider. “Mechanical and microstructural properties of Nextel™ 720 relating to its suitability for high temperature application in CMCs”, pp. 191-198 in *Proceedings of 23rd Annual Conference on Composites, Advanced Ceramics, Materials, and Structures*, E. Ustundag, G. Fischman (Eds.). John Wiley & Sons, Inc., 2008.

[10] F. Deléglise, M. H. Berger, D. Jeulin, A. R. Bunsell. “Microstructural stability and room temperature mechanical properties of the Nextel 720 fibre”. Journal of the European Ceramic Society, vol. 21 (5), pp. 569-580, 2001.

[11] R. S. Hay, E. E. Boakye, M. D. Petry, Y. Berta, K. Von Lehmden, J. Welch. “Grain growth and tensile strength of 3M Nextel 720™ after thermal exposure”, pp. 153-163 in *Proceedings of 23rd Annual Conference on Composites, Advanced Ceramics, Materials, and Structures*, E. Ustundag, G. Fischman (Eds.). John Wiley & Sons, Inc., 2008.

[12] M. Schmücker, F. Flucht, P. Mechnich. “Degradation of oxide fibers by thermal overload and environmental effects”. Materials Science and Engineering: A, vol. 557 (0), pp. 10-16, 2012.

[13] M. Schmücker, H. Schneider, T. Mauer, B. Clauβ. “Temperature-dependent evolution of grain growth in mullite fibres”. Journal of the European Ceramic Society, vol. 25 (14), pp. 3249-3256, 2005.

[14] S. Petzold, M. Morche, J. Taesler. “Oxide-ceramic continuous fibres and ceramic fibre reinforced composites – Innovative materials for the firing process”. ZI International, vol. 64, pp. 24-31, 2011.

[15] R. S. M. Almeida, K. Tushtev, B. Clauß, G. Grathwohl, K. Rezwan. “Tensile and creep performance of a novel mullite fiber at high temperatures”. Composites Part A: Applied Science and Manufacturing, vol. 76 (0), pp. 37-43, 2015.

[16] F. Deléglise, M. H. Berger, A. R. Bunsell. “Microstructural evolution under load and high temperature deformation mechanisms of a mullite/alumina fibre”. Journal of the European Ceramic Society, vol. 22 (9–10), pp. 1501-1512, 2002.

[17] K. G. Dassios, M. Steen, C. Filiou. “Mechanical properties of alumina Nextel™ 720 fibres at room and elevated temperatures: Tensile bundle testing”. Materials Science and Engineering: A, vol. 349 (1–2), pp. 63-72, 2003.

[18] V. Calard, J. Lamon. “Failure of fiber bundles”. Composites Science and Technology, vol. 64 (5), pp. 701-710, 2004.

[19] Y. Z. Pappas, A. Kontsos, T. H. Loutas, V. Kostopoulos. “On the characterization of continuous fibres fracture by quantifying acoustic emission and acousto-ultrasonics waveforms”. NDT & E International, vol. 37 (5), pp. 389-401, 2004.

[20] M. R’Mili, M. Moevus, N. Godin. “Statistical fracture of E-glass fibres using a bundle tensile test and acoustic emission monitoring”. Composites Science and Technology, vol. 68 (7), pp. 1800-1808, 2008.

[21] N. M. Razali, Y. B. Wah. “Power comparisons of shapiro-wilk, kolmogorov-smirnov, lilliefors and anderson-darling tests”. Journal of Statistical Modeling and Analytics, vol. 2 (1), pp. 21-33, 2011.

[22] D. M. Wilson, S. L. Lieder, D. C. Lueneburg. “Microstructure and high temperature properties of Nextel 720 fibers”, pp. 1005-1014 in *Proceedings of 19th Annual Conference on Composites, Advanced Ceramics, Materials, and Structures*, J. B. Wachtman Jr. (Ed.). John Wiley & Sons, Inc., 2008.

[23] S. Nohut. “Influence of sample size on strength distribution of advanced ceramics”. Ceramics International, vol. 40 (3), pp. 4285-4295, 2014.

[24] R. X. Fischer, H. Schneider, D. Voll. “Formation of aluminum rich 9: 1 mullite and its transformation to low alumina mullite upon heating”. Journal of the European Ceramic Society, vol. 16 (2), pp. 109-113, 1996.

[25] H. Schaper, L. Van Reijen. “A quantitative investigation of the phase transformation of gamma to alpha alumina with high temperature DTA”. Thermochimica Acta, vol. 77 (1), pp. 383-393, 1984.

[26] S. I. Bae, S. Baik. “Determination of critical concentrations of silica and/or calcia for abnormal grain growth in alumina”. Journal of the American Ceramic Society, vol. 76 (4), pp. 1065-1067, 1993.

[27] D. Wilson. “Statistical tensile strength of Nextel™ 610 and Nextel™ 720 fibres”. Journal of Materials Science, vol. 32 (10), pp. 2535-2542, 1997.

[28] B. Basu, D. Tiwari, D. Kundu, R. Prasad. “Is Weibull distribution the most appropriate statistical strength distribution for brittle materials?”. Ceramics International, vol. 35 (1), pp. 237-246, 2009.

[29] R. Danzer, P. Supancic, J. Pascual, T. Lube. “Fracture statistics of ceramics – Weibull statistics and deviations from Weibull statistics”. Engineering Fracture Mechanics, vol. 74 (18), pp. 2919-2932, 2007.

[30] F. W. Zok. “Developments in oxide fiber composites”. Journal of the American Ceramic Society, vol. 89 (11), pp. 3309-3324, 2006.

6 Thermal exposure effects on th e long-term behavior of a mullite fiber at high temperature

The behavior of an oxide fiber at elevated temperatures was analyzed before and after thermal exposures. The material studied was a mullite fiber developed for high-temperature applications, CeraFib 75. Heat treatments were performed at temperatures ranging from 1200-1400°C for 25 h. Quantitative high-temperature X-ray analysis and creep tests at 1200°C were carried out to analyze the effect of previous heat treatment on the thermal stability of the fibers. The as-received fibers presented a metastable microstructure of mullite grains with traces of alumina. Starting at 1200°C, grain growth and phase transformations occurred, including the initial formation of mullite, followed by the dissociation of the previous alumina-rich mullite phase. The observed transformations are continuous and occur until the mullite phase reaches a state near the stoichiometric 3/2 mullite. Only the fibers previously heat treated at 1400°C did not show further changes when exposed again to 1200°C. Overall, the heat treatments increased the fiber stability and creep resistance but reduced the tensile strength. Changes observed in the creep strain vs. time curves of the fibers were related to the observed microstructural transformations. Based on these results, the chemical composition of the stable mullite fiber is suggested.

6.1 Introduction

Over the past decades, ceramic matrix composites (CMCs) based on only oxide materials (Ox-CMCs) have been developed. Even though their development is considerably recent, these materials have already achieved a level of maturity for use in different industrial sectors, such as aerospace, power generation, hot gas filtration and metallurgical heat treatment [1, 2]. This growing interest in Ox-CMCs is due to their natural chemical stability, coupled with their high strength and considerable toughness, which is well known from CMCs [3, 4]. Logically, the development and production of such oxide systems was only possible due to the commercialization of high-strength oxide fibers. The first commercial oxide fibers were released in the 70s, but these fibers were rather fragile when handled and presented very low thermal stability [5]. Only in the 90s were suitable oxide fibers commercialized, which

allowed the further progress of Ox-CMCs [3]. The current development of Ox-CMCs is mainly related to fibers commercialized by the American company Minnesota Mining and Manufacturing (3M, Minnesota, USA): the alumina fiber Nextel 610, known as the strongest oxide fiber at room temperature, and the mullite-based fiber Nextel 720, credited to have the highest creep resistance [6].

Nevertheless, attention should be given to the high-temperature behavior of oxide fiber composites, since they are prone to creep and loss of strength when exposed to temperatures above 1000°C [7-10]. This indicates that used oxide fibers are subject to thermal degradation. Taking Nextel 720 as an example, several studies have been conducted on its creep performance, and it was shown that this fiber can exhibit high creep deformation at 1200°C [6, 11-13]. A decrease in strength was also reported after exposure to the same temperature [14], due to grain growth [15, 16] and grain boundary grooving [17]. Therefore, the development/improvement of fibers that can overcome these limitations is of great interest. Therefore, the Institute of Textile Chemistry and Chemical Fibers (ITCF, Denkendorf, Germany), together with the German company CeraFib GmbH (Olbersdorf, Germany), has produced the nearly pure mullite fiber CeraFib 75. At the current state of development, this fiber shows lower room-temperature strength than Nextel 720 but higher strength retention at temperatures above 1200°C [13, 18].

As discussed above, the exposure of oxide fibers to temperatures above 1000°C is of great concern. It should also be noted that such temperatures are normally reached during the processing of CMCs, as well as during their in-field usage. It is generally agreed upon in the literature that prolonged exposure to high temperatures should be avoided, since exposure leads to fiber grain growth and decreased tensile strength. Nevertheless, other microstructural changes, besides grain growth, also occur during the heat treatment of oxide fibers, especially in two-phase fibers such as Nextel 720 and CeraFib 75. In our previous study [18], it was shown that both mullite fibers undergo crystalline phase changes after heat treatment, leading to a more stable microstructure. It can thus be expected that the fibers will have higher thermal stability after exposure and, as a consequence, higher creep resistance. Studies on the creep behavior of heat-treated oxide fibers are quite rare and typically concern only alumina-based fibers [19, 20]. Hence, the objective of this work is to analyze the influence of previous thermal exposure on the long-term behavior of the fiber CeraFib 75 at high temperatures. To this end, the fibers were heat treated at temperatures between 1200°C and 1400°C for 25 h

and then characterized. The analysis was done in two steps. First, high-temperature X-ray diffraction (XRD) analyses were conducted to quantify the phase transformations over time at 1200°C. Second, the long-term behavior of the fibers under load was analyzed with several creep tests at the same temperature.

6.2 Experimental

6.2.1 Materials

All experiments were conducted on the mullite fiber CeraFib 75. This 10 μm fiber is produced by a dry-spinning process using a solution containing 72 wt.% alumina and 28 wt.% silica. Due to volatilization of the Si species, the fiber composition after pyrolysis is of approximately 75 and 25 wt.%, respectively. The fiber exhibits a microstructure of mullite grains with traces of γ-alumina. Further details/properties of the fiber have been published elsewhere [13]. For the methodology described below, fibers were tested before (as-received) and after heat treatment for 25 h at temperatures of 1200°C (HT 1200), 1300°C (HT 1300) and 1400°C (HT 1400). The heat-treatment duration of 25 h was set in accordance to previous studies, as microstructural changes were observed within this time [18]. All thermal exposures were conducted in a Nabertherm LHT 04/17 chamber furnace (Nabertherm GmbH, Lilienthal, Germany).

6.2.2 Characterization methods

To obtain an overview of the changes caused by thermal exposure, the as-received and heat-treated fibers were characterized in relation to their microstructure. Microstructural observations were obtained using scanning electron microscopy (SEM). For this, the fibers were initially embedded in epoxy resin to prepare the surface, *i.e.*, by grinding and polishing. Subsequently, the epoxy resin was thermally extracted, and the prepared fibers were thermally etched at 1300°C for 30 minutes. Micrographs of the fibers were taken using a ZEISS Supra 40 SEM (ZEISS, Oberkochen, Germany) with an acceleration voltage of 0.5 kV. Grain size measurements were done using the intercept line method with the help of the Lince software (TU Darmstadt, Germany). A total of five fibers per condition were analyzed.

6.2.3 High-temperature X-ray diffraction

To study the influence of the previous thermal exposure on the phase transformation at 1200°C, in situ high-temperature XRD experiments were performed on the as-received and

heat-treated samples. High-temperature XRD is a useful tool to study the kinetics of these transformations, which can also influence the creep performance of the fibers. Sample preparation consisted of crushing the fiber bundles to a fine powder. Measurements were performed using a Bragg-Brentano PANalytical X'Pert MPD PRO diffractometer (PANalytical GmbH, Kassel-Waldau, Germany), equipped with a high-temperature chamber HTK1200N (Anton Paar, Vienna, Austria), using $CuK_{\alpha 1,2}$ radiation, a Ni beta filter, and a X'Celerator detector system. Data were collected from $2\theta = 5$ to 120° with a total measuring time of 46 minutes for each scan. During the heating phase, scans were performed at constant temperatures of room temperature, 200, 400, 600, 800, and 1000°C. The samples were then kept at 1200°C for approximately 8 h with continuous collection of 11 diffraction patterns. Phase quantification was obtained by Rietveld refinements using the Diffracplus Topas 4.2 software (Bruker AXS GmbH, Karlsruhe, Germany). After careful refinement of the diffraction patterns recorded at room temperature, the resulting parameters were used as a starting model for the refinement of the patterns recorded at elevated temperatures. The following parameters were refined for all diffraction patterns: 6 background coefficients (Chebychev polynomial), zero-point error and sample displacement, in order to account for the thermal expansion of the sample holder. For all phases, the lattice parameters and scale factors were refined, and only for the major phase (mullite) were the Lorentzian crystallite size parameters optimized. For reference, R-values are given in Appendix A.5.

6.2.4 Creep tests

Single-filament tensile creep tests were performed to analyze the long-term behavior of the as-received and heat-treated fibers under load at 1200°C. To do so, the fibers were manually separated from the fiber bundle using surgical gloves. The fiber filaments were tested using a dead load system and a two SiC heating element oven. The specimens were heated at a rate of 1 °C/s, and the target temperature was held for approximately 15 minutes before the load was slowly released. The samples were tested until failure or until reaching the run-out time of 50 h. This run-out time was chosen based on previous studies, as the fibers reach the secondary creep stage within this time [13]. Three different weights were used to apply different creep loads. After the tests, the diameter of each tested fiber was measured on a SENSOFAR PLμ 2300 optical microscope (Sensofar Group, Terassa, Spain) to calculate the applied stress. To calculate the creep strain, an effective gauge length of 11.0 mm was determined, following the methodology proposed by Morrell [21]. Furthermore, the fracture surfaces of the tested fibers that failed before the run-out time were analyzed using SEM.

6.3 Results

6.3.1 Room-temperature properties

The effect of the heat treatments on the room-temperature properties of the fibers was examined by microstructural observations. Figure 6.1 presents the evolution of the microstructure of the fibers after the different heat treatments were performed. The microstructure of these fibers has been described previously [18]. With the improved grinding and polishing technique, the micrographs presented below show a much higher quality, allowing for a better interpretation of the fiber microstructure. In addition, the contrast of the figures was enhanced to identify the grain boundaries. The as-received CeraFib 75 fiber showed a microstructure of mostly equiaxial mullite grains of approximately 175 nm. Changes in the grain size were seen after exposure to 1200°C, at which the grains enlarged to 235 nm. Further changes were observed at 1300°C, with grains on the order of 260 nm and some being more elongated. After exposure to 1400°C, several elongated grains were detected, presumably of alumina, and the grains were on average 370 nm.

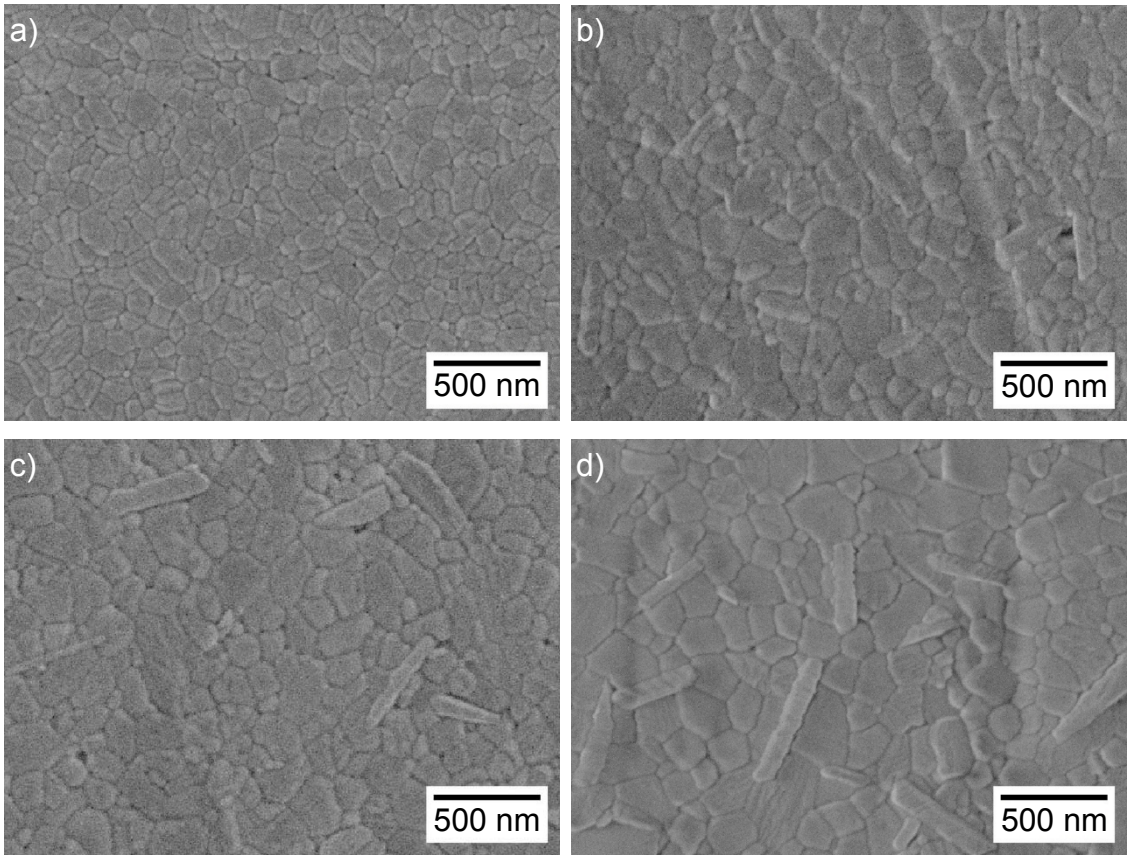

Figure 6.1: Microstructural evolution of CeraFib 75: as-received fiber (a) and fibers after heat treatment for 25 h at temperatures of 1200°C (b), 1300°C (c) and 1400°C (d).

Room-temperature XRD measurements gave further information regarding the microstructural changes caused by heat treatment. Quantification of the crystalline phases of the as-received and heat-treated fibers is given in Figure 6.2. These results were obtained with the same measuring parameters as used in the high-temperature XRD analysis for comparison and show the same tendency as seen in results published previously [18]. Before heat treatment, the fiber is mainly composed of mullite with traces of the γ-alumina phase. Again, changes were seen upon heat treatment at 1200°C, after which the amount of γ-alumina decreased, while the amount of both α-alumina and mullite slightly increased. At higher temperatures, HT 1300 and HT 1400, the ratio of the α-alumina phase increased, while that of the mullite phase decreased, indicating the dissociation of mullite, as discussed previously [18].

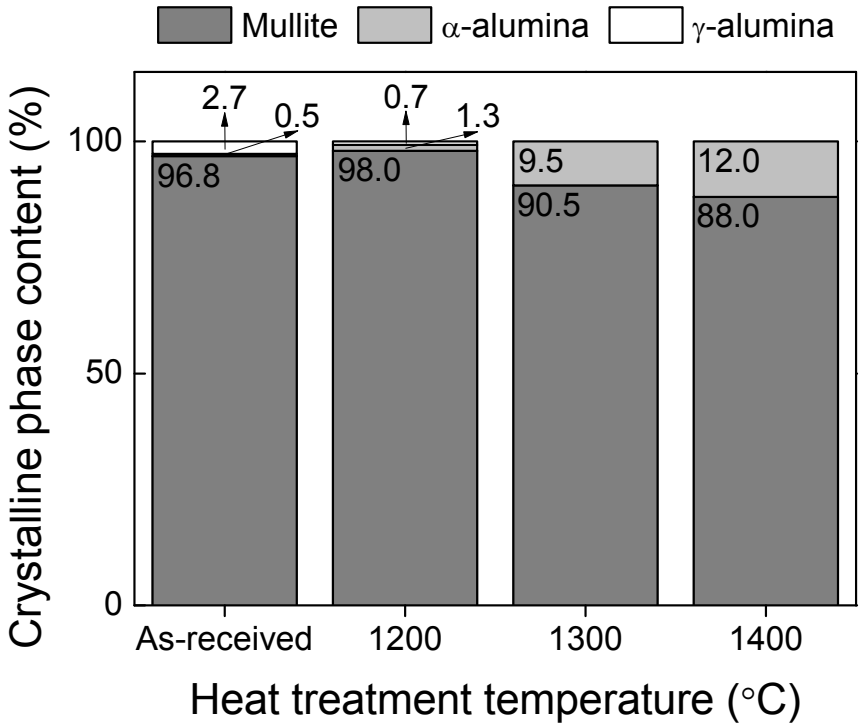

Figure 6.2: Crystalline phase quantification by XRD at room temperature for the as-received fibers and the fibers after heat treatment for 25 h at temperatures of 1200-1400°C.

6.3.2 High-temperature XRD analysis

Based on the quantitative phase composition obtained from Rietveld refinement of the in situ high-temperature XRD experiments, information about the phase transformation kinetics at 1200°C were gained. The phase quantifications of the as-received and HT 1400 samples at all applied temperatures are displayed in Figure 6.3, where the vertical line separates the heating phase (left) from the continuous measurements at 1200°C (right). It should be noted that since each sample yielded a different crystalline phase content (see Figure 6.2), different ranges were used in the graphs in Figure 6.3, but they have the same scale. The results for the HT 1200 and HT 1300 fibers are not presented, as their refinement resulted in relatively high data scattering and only small changes were observed. For instance, a small decrease in the mullite content was observed for both samples when comparing the measurements at room temperature to the ones at 1200°C: 98.0 wt.% to 97.2 wt.% and 90.5 wt.% to 89.9 wt.% for the HT 1200 and HT 1300 fibers, respectively. Then again, these changes are in the limit of the method, and a proper interpretation of the data cannot be made due to the scattering between the results.

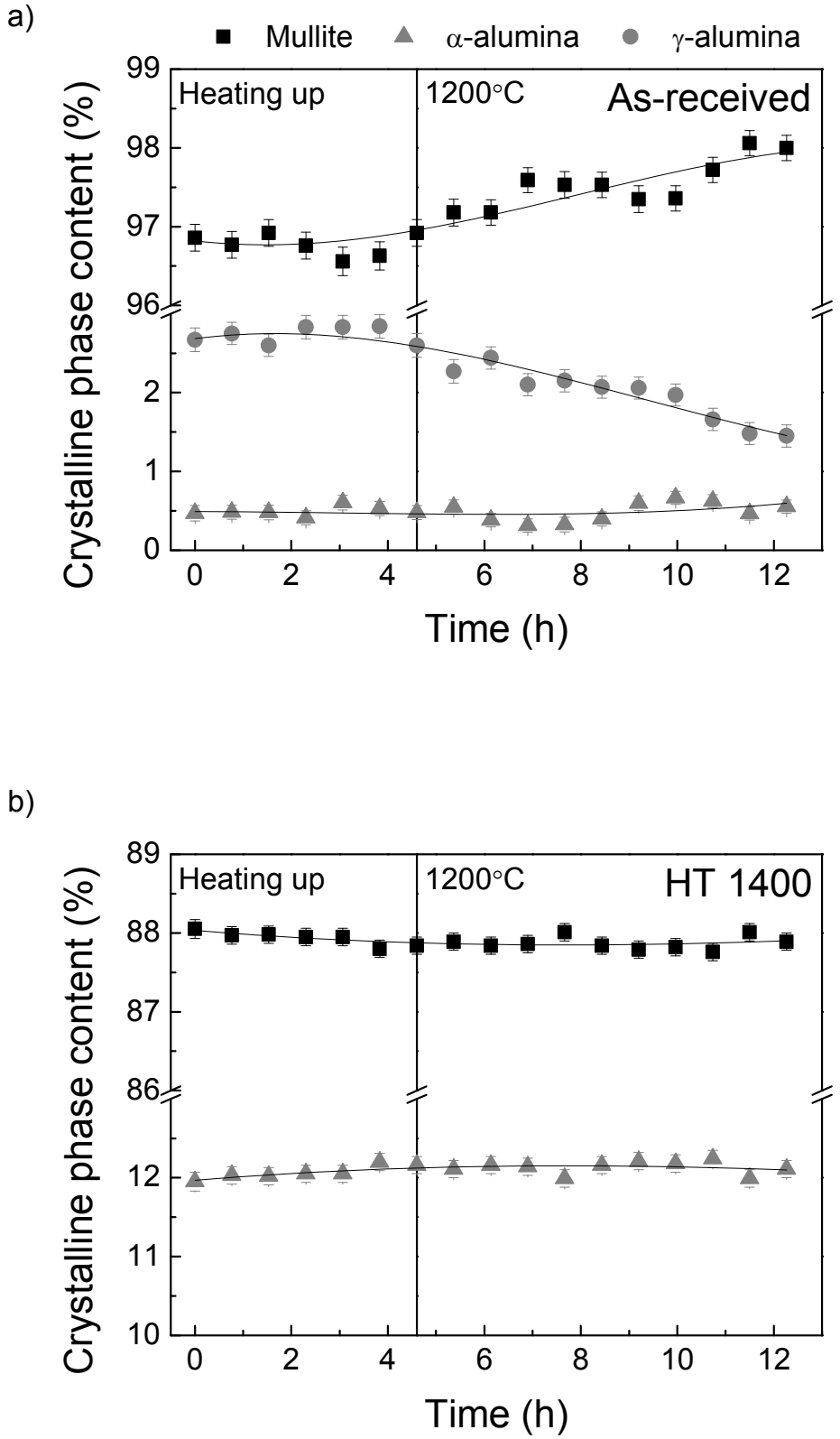

Figure 6.3: Crystalline phase quantification by XRD at high temperature for the as-received fibers (a) and the fibers after heat treatment for 25 h at the temperature of 1400°C (b). Measurements were performed at defined temperatures during heating to 1200°C (left) and continuously at the temperature of 1200°C (right). During the measurements, the temperature was kept constant.

The as-received CeraFib 75 fiber, shown in Figure 6.3a, was the most sensitive to crystalline phase transformation at 1200°C. During the heating phase, no significant changes of the phase composition were observed. In contrast, the diffraction patterns recorded during the 8 h period at 1200°C revealed distinct transformations of the crystalline phase. Considering the as-received state, the γ-alumina phase content decreased from 2.7 wt.% to 1.4 wt.%, while the mullite content increased from 96.8 wt.% to 98.1 wt.% after only 8 h at 1200°C. On the other hand, the amount of α-alumina phase remained constant at 0.5 wt.% within the duration of the scans. It can be expected that if the experiments were conducted for 25 h at 1200°C, the fiber would then present the composition of the HT 1200 fibers: 98.0 wt.% mullite, 1.3 wt.% α-alumina, and 0.7 wt.% γ-alumina. Unfortunately, as 1200°C represents the highest possible operating temperature of the equipment, an extension of the experiment was not considered.

For the samples heat treated at 1400°C, no significant differences were seen during the high-temperature measurements (Figure 6.3b). Hence, it can be concluded that the fibers achieved higher stability after exposure to 1400°C, and therefore, no crystalline changes were seen when the fiber was again exposed to a lower temperature of 1200°C.

6.3.3 Creep tests

Figure 6.4 presents examples of the creep tests of the as-received and heat-treated fibers under three different loads at 1200°C. The graphs are plotted until 20 h for better visualization of the tests with the highest creep load. It is important to note that the creep tests were performed at the same temperature as the high-temperature XRD measurements. In general, the tested fibers showed a non-linear region, primary creep stage, followed by a constant creep rate, secondary creep stage. A tertiary creep stage was not observed, which is expected given that the fibers are brittle. By comparing the results of the as-received fibers with the results of the heat-treated fibers, the effect of the previous thermal exposure was evident. In summary, a higher heat-treatment temperature results in fibers that are more creep resistant, *i.e.,* the fibers exhibit lower creep rate and longer creep lifetime. Nevertheless, this higher creep resistance comes at the expense of the tensile strength of the material. For instance, the HT 1400 fibers could not be tested with the highest load since they failed during loading, before the test began. In the same manner, the strain to failure decreased with an increase in the treatment temperature, *e.g.,* the HT 1300 specimen tested with 306 MPa broke with a strain to failure of only 0.11%, while the as-received and HT 1200 samples could undergo a creep deformation of 0.20% or more before failure. Another aspect of the creep tests that should be highlighted

is the duration of the primary creep stage. For stresses below 230 MPa, the as-received and HT 1200 specimens presented a much longer non-linear span of almost 4 h. The fibers heat treated at 1300°C showed a primary creep stage of approximately 2.5 h under the same conditions, while the creep rate of HT 1400 remained constant after only 1.5 h.

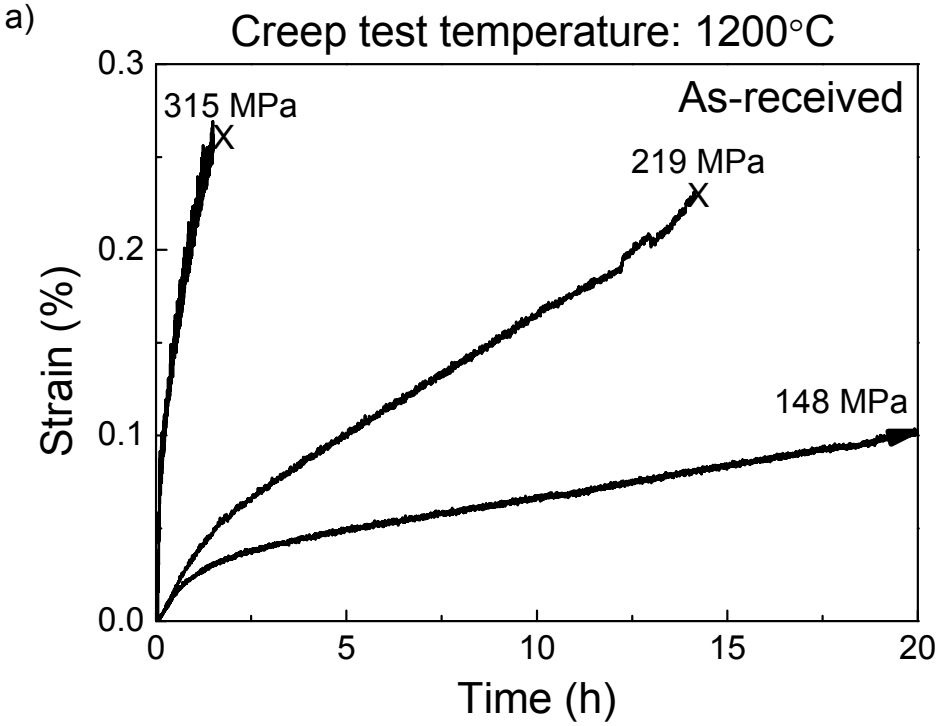

b)

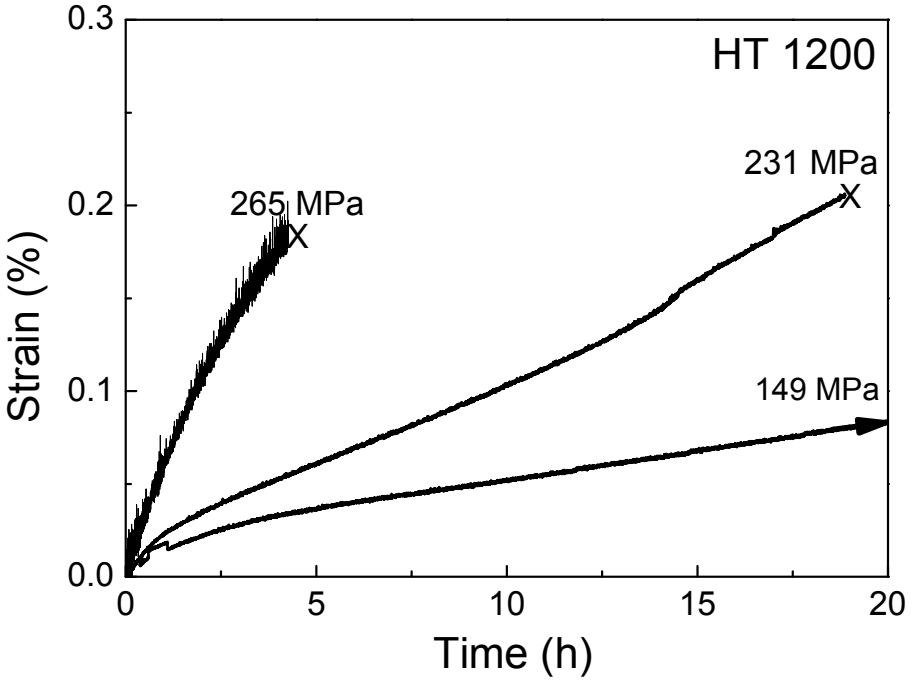
HT 1200
231 MPa
265 MPa
149 MPa
Strain (%)
Time (h)
0.0
0.1
0.2
0.3
0
5
10
15
20

c)

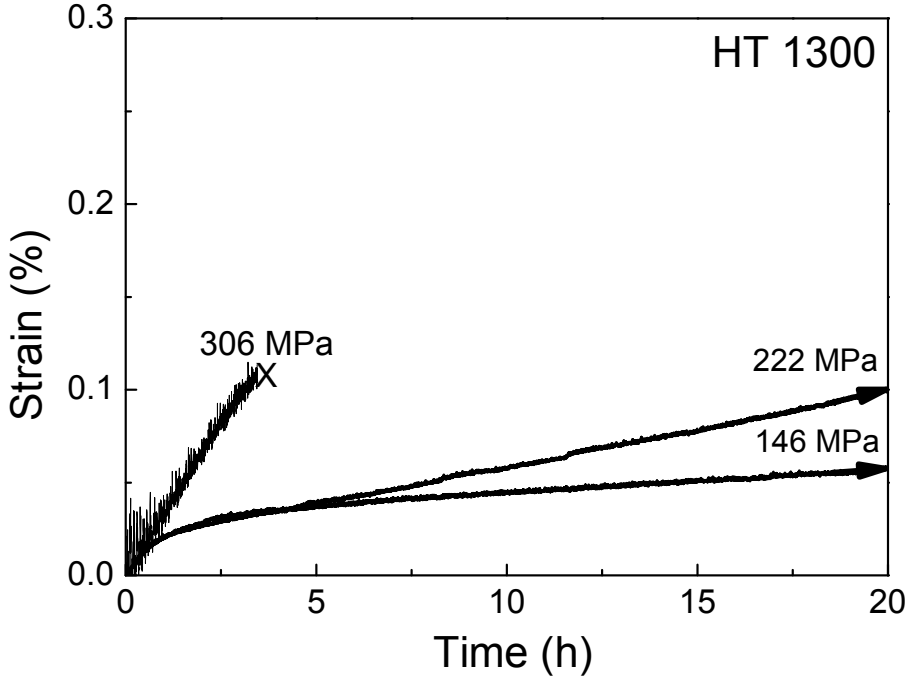
HT 1300
306 MPa
222 MPa
146 MPa
Strain (%)
Time (h)
0.0
0.1
0.2
0.3
0
5
10
15
20

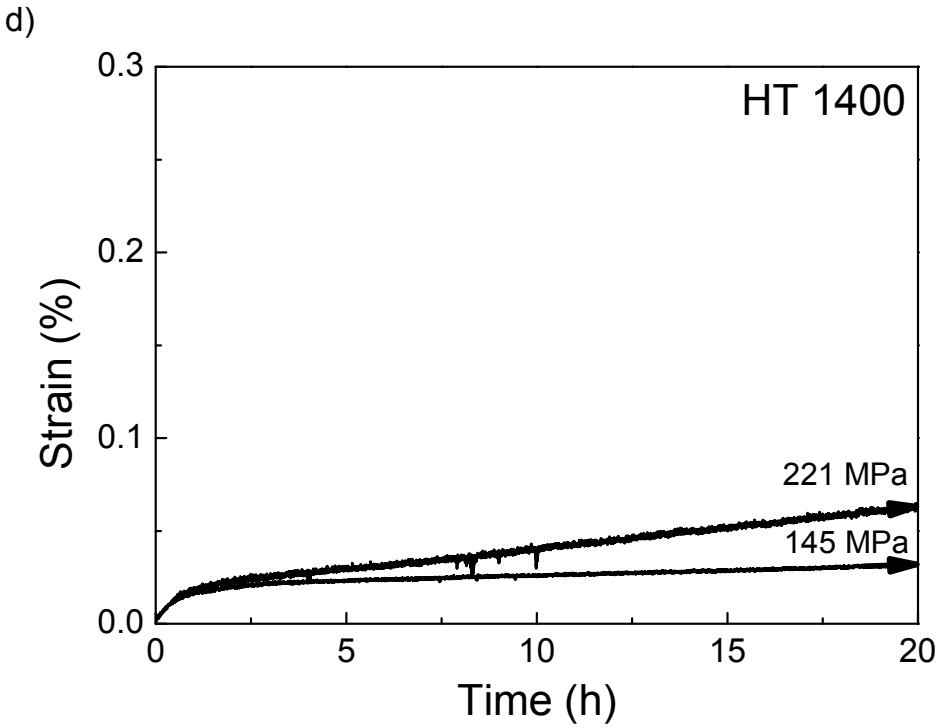

Figure 6.4: Creep deformation *vs.* time for the CeraFib 75 fibers tested at 1200°C under different applied stresses. Tests were performed on the as-received fibers (a) and the fibers after heat treatment for 25 h at temperatures of 1200°C (b), 1300°C (c) and 1400°C (d). Arrows indicate that the samples did not fail in the given run-out time.

Further differences were observed when analyzing the fracture surfaces of the crept fibers (Figure 6.5). The failure of the as-received fibers, as shown in Figure 6.5a, presumably began on the surface. In this region, crack propagation was initially intergranular, followed by a planar intragranular failure along the remaining portion of the fiber. The HT 1200 fibers failed in a similar manner, as shown in Figure 6.5b, although the depicted fiber has a larger intergranular region. In addition, the fiber also showed signs of cavitation, represented by the black dots in the figure. On the other hand, the fracture surface, shown in Figure 6.5c for an HT 1300 fiber, has a much different aspect. The fiber presents a considerable amount of cavities. Hence, it is suggested that the failure of the fiber began in the middle due to the coalescence of these cavities. As the remaining cross-section of the fiber could no longer sustain the creep load, a planar failure was then observed along the outer perimeter of the fiber. The fracture surface of HT 1400 fibers is not depicted in Figure 6.5 since the fibers survived the 50 h run-out time. For comparison, the fracture surface of an as-received Nextel 720 fiber tested is also given in Appendix A.5.

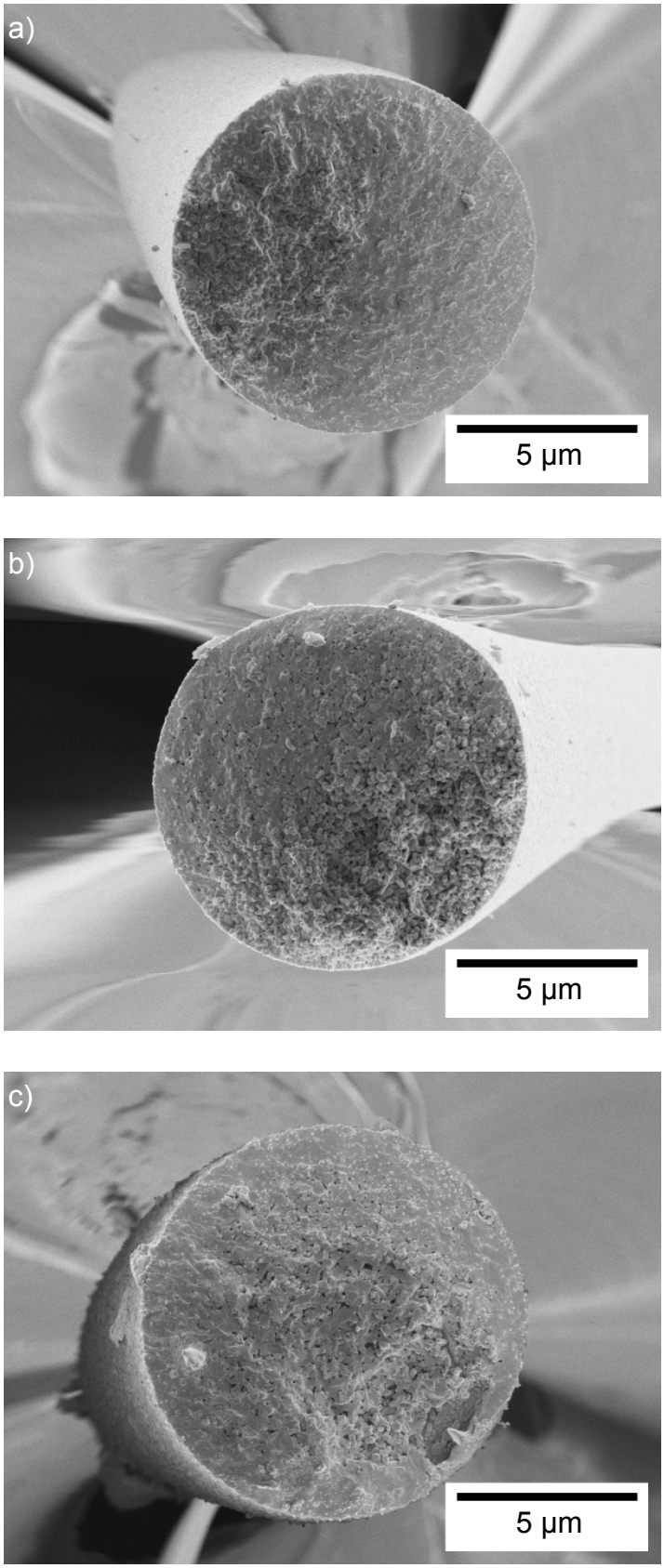

Figure 6.5: Fracture surface of the fibers tested under creep loading at 1200°C: as-received fiber tested with a stress of 315 MPa (a), HT 1200 fiber tested with a stress of 265 MPa (b) and HT 1300 fiber tested with a stress of 306 MPa (c).

6.4 Discussion

As discussed above, heat treatment caused different microstructural changes, which in turn affected the mechanical and long-term properties of the fibers. The main changes observed were grain growth and crystalline phase transformations. The grain growth kinetics of mullite fibers was studied in detail by Schmücker [14, 22]. In his works, it was shown that other mullite fibers also present grain growth starting at 1200°C but with overall slow kinetics at temperatures below 1600°C. In CeraFib 75, the low mobility of the mullite grains resulted in only slight grain coarsening at 1200°C, as shown in Figure 6.1b. At higher temperatures, the content of α-alumina grains increased significantly, as shown in Figure 6.2, and changes in the grain size and morphology were more evident, as shown in Figure 6.1c and d. As shown in our previous study on fiber bundles, this grain growth is responsible for the loss of room-temperature strength observed for the treated fibers [18].

The second microstructural change observed after heat treatment was related to crystal phase transformations, which were analyzed in more detail through the high-temperature XRD measurement of the as-received sample, as shown in Figure 6.3a. Because of the short pyrolysis time during its manufacturing, as-received CeraFib 75 fibers have a metastable microstructure of alumina-rich mullite and traces of γ-alumina. This microstructure is considerably stable up to 1200°C, at which it will gradually transform to the state of least energy. Within the first hours at 1200°C, the γ-alumina content decreased, and the mullite content increased. Previous studies have indicated that the fiber may contain an amorphous silica phase in amounts lower than 1 wt.% [18], which enables the formation of mullite in combination with the γ-alumina phase. This reaction occurs until the amorphous silica is completely consumed, which is likely to occur shortly after the 8 h at 1200°C, last XRD measurement in Figure 6.3a. From that point on, the remaining γ-alumina phase transforms into α-alumina, as this phase is the most stable one [23]. Although it is not evident from the high-temperature XRD measurements of the as-received fibers, the higher amount of α-alumina in the HT 1200 fibers suggests that the dissociation of mullite into α-alumina also occurs at 1200°C. As stated before, the mullite present in the as-received fibers is in a metastable state and rich in Al. Presumably after the formation of mullite from γ-alumina and free silica, the as-received mullite phase will dissociate into α-alumina and mullite with a lower content of Al. This dissociation is time-dependent, and the reaction is not completed

within the first 25 h of exposure to 1200°C. Thus, when the heat-treated fibers are heated again, the mullite further dissociates.

Since the phase transformations described above are thermally activated processes, they will occur faster at higher temperatures. Hence, the fibers heat treated for 25 h at 1300°C showed no trace of γ-alumina nor any amorphous silica phase, but instead showed a much higher content of α-alumina (Figure 6.2). The heat treatment at 1300°C was not performed for long enough to obtain the state of least energy, as can be seen by comparing the crystalline phase content of the HT 1300 and HT 1400 fibers (Figure 6.2). It is then expected that the mullite phase will dissociate until it achieves a state near the stoichiometric mullite structure: 72 wt.% alumina and 28 wt.% silica. This is the case for the HT 1400 fibers. The XRD measurements at elevated temperatures, shown in Figure 6.3b, showed that no transformation occurred during heating or after 8 h at 1200°C, proving that the microstructure of the fibers became stable after the heat treatment. The alumina content of the mullite phase of the HT 1400 fibers at room temperature was determined to be 72.6 wt.% based on the lattice parameters and the equation proposed by Fischer [24]. The microstructure of the HT 1400 fibers can be then considered to be the most stable.

Both aforementioned microstructural changes affected the creep behavior of the fibers, as shown in Figure 6.4. From the creep curves, it is possible to observe that the primary creep stage was shorter for the heat-treated fibers. During this stage, the initial strain rate is high and slowly decreases until reaching a constant value. Therefore, this stage is associated with the microstructural changes that occur under creep loading. The longer primary stage of the as-received fibers can then be related to their lower stability, *i.e.,* more pronounced phase transformation at 1200°C, as shown in Figure 6.3a. Following this argument, the HT 1400 fibers showed only a very short primary stage since no phase transformation was detected, as shown in Figure 6.3b. In fact, the HT 1400 fibers were the only fibers to really achieve a steady-state creep stage. When a load is applied, the as-received fibers might show different phase transformation kinetics in comparison to the results of Figure 6.3. Still, it is expected that their microstructure will slowly change during the greater part of the creep tests. The same is valid for the HT 1200 fibers and possibly for the HT 1300 fibers. Given these continuous phase changes, the term minimum creep rate is then more accurate than steady-state creep rate for the two-phase oxide fibers.

During the creep tests, the creep rate was observed to decrease for the previously treated fibers. Although grain growth caused strength loss, it had a positive influence on the creep resistance. It is well known that bigger grains have higher resistance against creep deformation [25]. Here, it should also be highlighted that the presence of the SiO_2 glass phase, even in small amounts, can also locally increase the creep deformation of the as-received fibers. This glassy phase is absent after thermal treatment [18]. As a consequence, the heat-treated fibers showed much smaller creep rates. For a better comparison, Figure 6.3 shows the minimum creep rates measured for the fibers under different applied stresses. The values of the as-received Nextel 720 fibers [13] are also given, since this oxide fiber is credited to have the highest creep resistance. The low creep rates of Nextel 720 are a result of its microstructure of 0.5 μm mosaic mullite grains [11]. Nevertheless, the CeraFib 75 fibers heat treated at 1300 and 1400°C showed even lower creep rates. However, it is expected that the Nextel 720 fibers would also show a decreased creep rate after similar thermal treatment. Moreover, the results could be fitted with the Arrhenius creep rate equation, Equation 2. At a constant temperature of 1200°C, the stress exponent n could be estimated for each fiber condition. The calculated n for the as-received CeraFib 75 was 2.9, and it changed to 3.2 for HT 1200 and 3.7 for HT 1300 and HT 1400. The inverse grain size exponent p was also estimated to be 3.0 by taking into account the grain size of the fibers before the creep tests (Figure 6.1) and the creep rates corrected for 150 MPa. Hence, the creep rate of the mullite fibers is rather dependent on the applied stress and grain size.

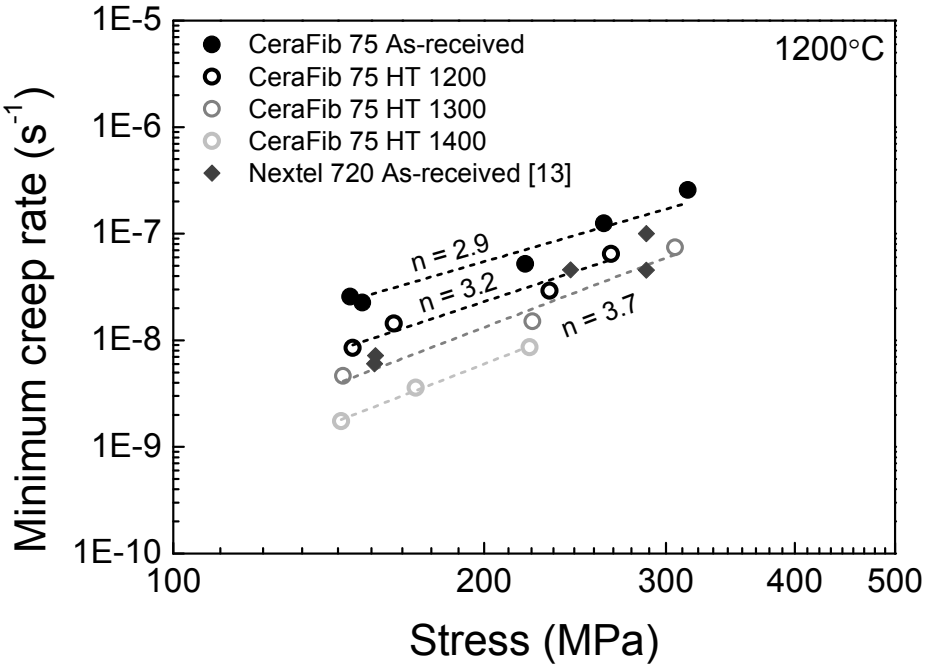

Figure 6.6: Minimum creep rate *vs.* applied stress for the as-received CeraFib 75 fibers and the fibers after heat treatment for 25 h at temperatures of 1200-1400°C. Data for the as-received Nextel 720 [13] were included for comparison.

Considering the presence of free SiO_2 [18], the metastable structure (Figure 6.3a), and the absence of cavitations in the fracture surface (Figure 6.5a), it is here suggested that the main creep mechanism for the as-received fibers is related to grain boundary sliding, assisted by the presence of the glassy phase. This conclusion agrees well with the observations of Nextel 720, which presents $n = 3$ at moderate stresses, and the creep mechanism is also related to grain boundary diffusion, controlled by diffusion [12]. The shift in the stress exponent observed for the heat-treated fibers can be related to different creep deformation mechanisms occurring when the fibers are loaded. For mullite fibers, the relation between the creep mechanisms and the creep exponents can be problematic, given the complexity of the structure of the fiber, which are two-phase and fine-grained [11, 12], and they normally present stress exponents higher than bulky mullite materials. Furthermore, care should be taken when making direct comparisons of the measured exponents with creep mechanism and models proposed for other polycrystalline ceramics, as they are described for steady-state creep. As mentioned before, steady-state creep may not be achieved with two-phase fibers. Nonetheless, the evaluation of the creep exponents n and p can still be used to give a general idea of the possible creep mechanisms. For instance, $n \approx 4$ and $p \approx 3$ are normally related to grain boundary sliding and

cavity growth, according to the literature for polycrystalline ceramics [26]. From the observed microstructural changes and absence of the glassy phase, the grain mobility is found to be lower after thermal treatment. In this sense, the formation and growth of cavities, as shown in Figure 6.5c, begins to play a larger role in creep deformation. Therefore, the creep rate of the fibers is more sensitive to the applied stress, *i.e.,* the increase in *n* observed for the HT 1300 and HT 1400 fibers.

In summary, the heat treatment of two-phase oxide fibers can be advantageous when a higher thermal stability is desired. In the literature, the effects of thermal exposure are normally only related to fiber degradation due to the strength decrease. However, heat treatments can be used to improve the fiber properties to a certain extent. Taking HT 1200 as an example, these fibers retained approximately 80% of the as-received strength but also showed a considerable improvement in creep resistance and creep lifetime, not to mention a more stable microstructure. It is important to highlight that the presented results can also be applied to other two-phase oxide fibers, such as Nextel 720, since it is expected that they will present similar microstructural changes after heat treatment due to their post-processing metastable microstructure [15, 16, 18, 27, 28]. On the other hand, when the heat-treatment temperature is too high or the duration is too long, the achievement of higher thermal stability is not justified, as the strength decrease is too pronounced. For instance, HT 1400 did not show any further transformation at 1200°C, but the grain growth and fiber degradation was so high that the fiber could not be tested with the highest creep load. Still, this analysis shows that the mullite structure containing 72.6 wt.% alumina is stable at 1200°C. Hence, it is suggested that a pure mullite fiber with this composition would have higher thermal stability than commercially available oxide fibers.

6.5 Conclusion

In this study, the effect of different thermal exposures on the subsequent high-temperature behavior of mullite fibers was studied in detail. The studied material was CeraFib 75, a fiber that shows a metastable microstructure containing 175 nm mullite grains with traces of γ-alumina. Upon 25 h of exposure to temperatures above 1200°C, grain growth and crystalline phase changes were detected. This led to a decrease in the room-temperature tensile strength

but an increase in the thermal stability. The latter was analyzed by high-temperature XRD measurements and creep tests at 1200°C.

The kinetics of the phase transformations that occur in the fibers at 1200°C were quantified through XRD analysis. Changes in the phase content of the as-received fibers occurred during the first hours of exposure to 1200°C. First, the present γ-alumina phase combines with free silica to form mullite, and the overall content of the mullite phase in the fibers increases. Afterwards, the previously metastable mullite structure slowly dissociates into α-alumina grains and a mullite structure with lower Al content. After 25 h of exposure to 1200°C, this reaction is not entirely complete, and therefore, the mullite phase content of the fiber further decreases when the fiber is heated again. These phase transformations occur at a faster pace at higher temperatures, *e.g.,* 1300 and 1400°C. Particular attention was given to the fibers heat treated at 1400°C, since they did not present further transformation when exposed to 1200°C. These fibers showed a mullite structure containing 72.6 wt.% alumina, which can then be considered stable at this temperature.

The effect of heat treatment on the creep behavior of the fibers was evident and could be related to the observed microstructural changes. In general, higher heat-treatment temperatures resulted in lower creep rates, a smaller primary creep stage, and an overall longer creep lifetime. This higher creep resistance of the fibers is due to the measured grain growth and higher thermal stability. In addition, since the fibers underwent phase transformation during the previous heat treatment, the overall creep deformation was considerably smaller. A possible change in the main creep mechanisms was also indicated in the fracture analysis. In this matter, it is suggested that the as-received fibers deformed mainly due to grain boundary sliding, while cavity growth was more prominent in the heat-treated fibers. Nevertheless, the improvement in the thermal stability and creep properties came at the expense of the tensile strength. For the fibers heat treated at 1400°C, grain growth and degradation were so prevalent that the fibers could not be creep tested with loads higher than 220 MPa. It is then suggested that a pure mullite fiber containing 72.6 wt.% alumina would present better performance than the current oxide fibers. Attention should be given to grain growth when achieving this composition.

6.6 Acknowledgments

The authors would like to thank the Brazilian Ministry of Science and Technology (CNPq) for the financial support through the program Science without Borders. Helpful discussions with Prof. Grathwohl from the University of Bremen are acknowledged. We also thank P. Witte from the University of Bremen for the SEM images.

6.7 References

This chapter was adapted, license no. 4183090220427, from:

R. S. M. Almeida, E. L. Bergmüller, H. Lührs, M. Wendschuh, B. Clauß, K. Tushtev, K. Rezwan. "Thermal exposure effects on the long-term behavior of a mullite fiber at high temperature". Journal of the American Ceramic Society, vol. 100 (9), pp. 4101-4109, 2017.

The article is mainly based on the work of the first author and author of this thesis Renato S. M. Almeida. The precise contributions of each author are listed below.

Table 6.1: Authors contributions for Chapter 6.

Author	Contribution
Almeida, R. S. M.	Conceptualized the work, planned the experiments, prepared the micrographs, performed the creep tests, analyzed the data of all experiments, wrote the manuscript
Bergmüller, E. L.	Performed experiments in the frame of Diploma thesis (cf. Supervised student projects)
Lührs, H	Analyzed the XRD measurements and helped to evaluate and edit manuscript
Wendschuh, M.	Performed the XRD measurements and helped to evaluate and edit manuscript
Clauß, B.	Gave materials specific input and helped to evaluate and edit manuscript
Tushtev, K.	Gave conceptual and scientific advices, helped in the scientific evaluation and editing of the manuscript
Rezwan, K.	Gave conceptual and scientific advices, helped in the scientific evaluation and editing of the manuscript

[1] K. A. Keller, G. Jefferson, R. J. Kerans. “Oxide-oxide composites”, pp. 236-272 in *Ceramic Matrix Composites*, N. P. Bansal, J. Lamon (Eds.). John Wiley & Sons, Inc., 2014.

[2] A. Noeth, A. Rüdinger, W. Pritzkow. “Oxide ceramic matrix composites – Manufacturing, machining, properties and industrial applications”. Ceramic Applications, vol. 3, pp. 48-54, 2015.

[3] F. W. Zok. “Developments in oxide fiber composites”. Journal of the American Ceramic Society, vol. 89 (11), pp. 3309-3324, 2006.

[4] D. Koch, K. Tushtev, G. Grathwohl. “Ceramic fiber composites: Experimental analysis and modeling of mechanical properties”. Composites Science and Technology, vol. 68 (5), pp. 1165-1172, 2008.

[5] A. R. Bunsell, M. H. Berger. “Fine diameter ceramic fibres”. Journal of the European Ceramic Society, vol. 20 (13), pp. 2249-2260, 2000.

[6] F. Deléglise, M. H. Berger, A. R. Bunsell. “Microstructural evolution under load and high temperature deformation mechanisms of a mullite/alumina fibre”. Journal of the European Ceramic Society, vol. 22 (9–10), pp. 1501-1512, 2002.

[7] E. Volkmann, K. Tushtev, D. Koch, C. Wilhelmi, J. Göring, K. Rezwan. “Assessment of three oxide/oxide ceramic matrix composites: Mechanical performance and effects of heat treatments”. Composites Part A: Applied Science and Manufacturing, vol. 68 (0), pp. 19-28, 2015.

[8] M. L. Antti, E. Lara-Curzio, R. Warren. “Thermal degradation of an oxide fibre (Nextel 720)/aluminosilicate composite”. Journal of the European Ceramic Society, vol. 24 (3), pp. 565-578, 2004.

[9] M. B. Ruggles-Wrenn, S. S. Musil, S. Mall, K. A. Keller. “Creep behavior of Nextel™610/Monazite/Alumina composite at elevated temperatures”. Composites Science and Technology, vol. 66 (13), pp. 2089-2099, 2006.

[10] M. Ruggles-Wrenn, P. Koutsoukos, S. Baek. “Effects of environment on creep behavior of two oxide/oxide ceramic–matrix composites at 1200 °C”. Journal of Materials Science, vol. 43 (20), pp. 6734-6746, 2008.

[11] D. M. Wilson, S. L. Lieder, D. C. Lueneburg. “Microstructure and high temperature properties of Nextel 720 fibers”, pp. 1005-1014 in *Proceedings of 19th Annual Conference on*

Composites, Advanced Ceramics, Materials, and Structures, J. B. Wachtman Jr. (Ed.). John Wiley & Sons, Inc., 2008.

[12] C. J. Armani, M. B. Ruggles-Wrenn, R. S. Hay, G. E. Fair. "Creep and microstructure of Nextel™ 720 fiber at elevated temperature in air and in steam". Acta Materialia, vol. 61 (16), pp. 6114-6124, 2013.

[13] R. S. M. Almeida, K. Tushtev, B. Clauß, G. Grathwohl, K. Rezwan. "Tensile and creep performance of a novel mullite fiber at high temperatures". Composites Part A: Applied Science and Manufacturing, vol. 76 (0), pp. 37-43, 2015.

[14] M. Schmücker, F. Flucht, P. Mechnich. "Degradation of oxide fibers by thermal overload and environmental effects". Materials Science and Engineering: A, vol. 557 (0), pp. 10-16, 2012.

[15] M. D. Petry, T.-I. Mah. "Effect of thermal exposures on the strengths of Nextel™ 550 and 720 filaments". Journal of the American Ceramic Society, vol. 82 (10), pp. 2801-2807, 1999.

[16] F. Deléglise, M. H. Berger, D. Jeulin, A. R. Bunsell. "Microstructural stability and room temperature mechanical properties of the Nextel 720 fibre". Journal of the European Ceramic Society, vol. 21 (5), pp. 569-580, 2001.

[17] R. S. Hay, E. E. Boakye, M. D. Petry, Y. Berta, K. Von Lehmden, J. Welch. "Grain growth and tensile strength of 3M Nextel 720™ after thermal exposure", pp. 153-163 in *Proceedings of 23rd Annual Conference on Composites, Advanced Ceramics, Materials, and Structures*, E. Ustundag, G. Fischman (Eds.). John Wiley & Sons, Inc., 2008.

[18] R. S. M. Almeida, E. L. Bergmüller, B. G. F. Eggert, K. Tushtev, T. Schumacher, H. Lührs, B. Clauß, G. Grathwohl, K. Rezwan. "Thermal exposure effects on the strength and microstructure of a novel mullite fiber". Journal of the American Ceramic Society, vol. 99 (5), pp. 1709-1716, 2016.

[19] J. C. Goldsby, H. M. Yun, G. N. Morscher, J. A. DiCarlo. "Annealing effects on creep of polycrystalline alumina-based fibers". Materials Science and Engineering: A, vol. 242 (1-2), pp. 278-283, 1998.

[20] V. H. Hammond, D. M. Elzey. "Comparing the creep response of alumina tows and single filaments". Scripta Materialia, vol. 46 (4), pp. 287-291, 2002.

[21] R. Morrell. “A tensile creep-testing apparatus for ceramic materials using simple knife-edge universal joints”. Journal of Physics E: Scientific Instruments, vol. 5 (5), pp. 465, 1972.

[22] M. Schmücker, H. Schneider, T. Mauer, B. Clauβ. “Temperature-dependent evolution of grain growth in mullite fibres”. Journal of the European Ceramic Society, vol. 25 (14), pp. 3249-3256, 2005.

[23] H. Schaper, L. Van Reijen. “A quantitative investigation of the phase transformation of gamma to alpha alumina with high temperature DTA”. Thermochimica Acta, vol. 77 (1), pp. 383-393, 1984.

[24] R. X. Fischer, H. Schneider, D. Voll. “Formation of aluminum rich 9: 1 mullite and its transformation to low alumina mullite upon heating”. Journal of the European Ceramic Society, vol. 16 (2), pp. 109-113, 1996.

[25] W. R. Cannon, T. G. Langdon. “Creep of ceramics – Part 1. Mechanical characteristics”. Journal of Materials Science, vol. 18 (1), pp. 1-50, 1983.

[26] G. Bernard-Granger, C. Guizard, R. Duclos. “Compressive creep behavior in air of a slightly porous as-sintered polycrystalline α-alumina material”. Journal Of Materials Science, vol. 42 (8), pp. 2807-2819, 2007.

[27] M. Schmücker, F. Flucht, H. Schneider. “High temperature behaviour of polycrystalline aluminosilicate fibres with mullite bulk composition. I. Microstructure and strength properties”. Journal of the European Ceramic Society, vol. 16 (2), pp. 281-285, 1996.

[28] Y. Wang, H. Cheng, H. Liu, J. Wang. “Microstructure and room temperature mechanical properties of mullite fibers after heat-treatment at elevated temperatures”. Materials Science and Engineering: A, vol. 578 (0), pp. 287-293, 2013.

BLANK PAGE

7 Conclusions

The mechanical behavior and the microstructural changes of four different oxide fibers were investigated at high temperatures. With the results of this work, it is possible to have a better understanding of the degradation mechanisms of oxide fibers at elevated temperatures, which is essential for the further development of Ox-CMCs. The investigations were conducted on two mullite fibers, Nextel 720 and CeraFib 75, and two alumina fibers, Nextel 610 and CeraFib 99. The fibers were characterized in relation to their microstructure and mechanical response under different conditions involving critical temperatures. The results discussed in this thesis, Chapter 4, 5 and 6, regard only the mullite fibers, given their importance to high-temperature applications. Nevertheless, the main results of the alumina fibers are depicted in Appendix A.1, and will be briefly discussed in this conclusion chapter.

In order to understand the mechanical properties of the fibers, their microstructure was investigated by electronic microscopy and X-ray diffraction. Nextel 720 is a two-phase fiber, and its microstructure consisted of several 160 nm mullite grains, which form a mosaic structure, and elongated α-alumina grains in-between. The microstructure revealed for CeraFib 75 was of 175 nm mullite grains and a small fraction of γ- and α-alumina grains. Both mullite fibers also showed traces of SiO_2 glass phase, but in amounts lower than 1 wt.%. CeraFib 99 and Nextel 610 presented a similar structure containing small alumina grains, *e.g.*, 100 nm for Nextel 610; although CeraFib 99 showed bigger grains and traces of spinel ($MgAl_2O_4$), possibly used as a dopant. These characteristics had a close relation to the measured mechanical properties of the fibers. In general, it was seen that the fibers with higher content of alumina were stronger at room temperature. In other words, the tensile strength of Nextel 720, 1650 MPa, was higher than CeraFib 75, 1420 MPa; while both were weaker than the alumina fibers CeraFib 99, 1700 MPa, and Nextel 610, 2610 MPa. Moreover, the strength was also influenced by the distribution of defects and the grain size of the fibers. For instance, the strength distribution of both CeraFib fibers was broader than the Nextel fibers, because of the occasional presence of large defects in the newer fibers.

The mechanical behavior of the fibers at elevated temperatures was evaluated by tensile tests at temperatures ranging 900-1400°C. A decrease in strength was measured for all fibers when tested at temperatures higher than 1000°C. At these temperatures, the fibers with lower

amount of alumina had higher strength retention. Hence, the strength of CeraFib 75 was higher than the other fibers above 1200°C. This fiber also showed a very interesting feature when tested at 1400°C. Under such conditions, most of the tested CeraFib 75 fibers exhibited an elastic–pseudo-plastic behavior, which was dependent on microstructure heterogeneities and related to creep mechanisms. To further study this behavior, creep tests were also carried out at the temperatures of 1000-1300°C. The mullite structure proved to have a much higher creep resistance, in which both mullite fibers showed creep rates three orders of magnitude lower than the alumina fibers. Contrary to the tensile tests, Nextel 720 exhibited the highest creep resistance within the fibers tested. The low creep rates measured for Nextel 720 are credited to its mosaic-like structure of mullite grains, which has low mobility even at high temperatures. The possible creep mechanisms of the mullite fibers were also investigated by analyzing their fracture surface, as well as comparing the calculated creep exponents. The main creep mechanism was related to grain boundary sliding, assisted by the presence of the glassy phase. In the case of Nextel 720, load-assisted grain growth was also detected in the fiber surface.

The thermal stability of the fibers was accessed by analyzing the fibers after exposure to temperatures of 1000-1400°C for 25 h. Grain growth was measured for all fibers after the heat treatments above 1200°C. At higher temperatures, *e.g.*, 1300°C, changes in grain shape were also observed. In this sense, the fibers also presented an abnormal grain growth at 1400°C, with the exception of CeraFib 75. Furthermore, crystal phase transformations were noticed for the mullite fibers after the heat treatments at 1200°C and above. The kinetics of these transformations could be studied in more detail by performing in situ XRD measurements on CeraFib 75 fibers at 1200°C. At first, mullite was formed by the combination of the γ-alumina phase and the free silica. After the glass silica was consumed, the as-received mullite structure started to dissociate into α-alumina grains plus mullite with a lower content of Al. This dissociation is a thermally activated process, and therefore, took place with a faster rate at higher temperatures. Hence, fibers that were heat treated at 1400°C were more thermally stable and presented a mullite structure close to the 3/2 stoichiometric mullite.

The microstructural changes observed during the heat treatments influenced the mechanical performance of the fibers. The measured grain growth was related to the decrease of room-temperature strength. In this matter, CeraFib 75 showed higher strength retention due to the higher stability of its mullite grains. On the other hand, Nextel 610 was the most susceptible

to degradation, and a decrease in strength was measured already with the treatment at 1000°C. In this case, the strength loss can also be associated with thermally induced defects. Moreover, it was also seen that the thermal treatments above 1300°C influenced the load-redistribution capability of the fibers. After the heat treatments, the fibers became more fragile, *i.e.*, higher E-modulus and lower strength. As the fibers of the bundle also interacted with each other during the heat treatment, and occasionally sintered together, the failure of the weakest fibers in the treated bundle promoted the consequent failure of the reaming fibers in a catastrophic way.

Even though strength loss was measured after the heat treatments, an improvement on the thermal stability of the fibers was also observed. Considering the metastable microstructure of the mullite fibers, crystal phase transformations take place at temperatures higher than 1200°C. Considering that these transformations happened during the previous exposures, the treated fibers were then less susceptible to further transformations. Particular attention was given to the fibers heat treated at 1400°C, since they did not present any changes when heated again to 1200°C. This increase of thermal stability, together with the measured grain growth, resulted in an increase of the fibers creep resistance. For instance, the heat treatment at 1400°C decreased the creep rates of CeraFib 75 up to one order of magnitude. Moreover, it was also observed that the fibers were more sensitive to the applied creep stress, which indicates a change in the main creep mechanism. Considering the measured creep exponents, and the microstructural observations made, it is suggested that the main creep mechanism of the treated fibers is related to the formation and growth of cavities.

In summary, this works shows that the mechanical properties of the fibers are rather dependent on their microstructure. However, these microstructures are prone to changes when exposed at temperatures higher than 1000°C. On the one hand, strength loss is observed due to grain growth and thermally induced defects. On the other hand, the crystal phase transformations increase the thermal stability and creep resistance of the fibers. Considering these transformations, it is here suggested that a mullite fiber containing 73 wt.% of alumina and 27 wt.% of silica would have higher thermal stability. Naturally, attention should be given to volatilization of the Si species and grain growth during fiber processing. Although, it should be highlighted that an increase of thermal stability in oxide fibers is normally followed by a decrease of strength.

BLANK PAGE

8 Outlook

Although the main objectives of this thesis were successfully achieved, other ideas for the continuation of the work appeared during this project. The main analyses and discussions performed were regarding the mullite fibers. In this sense, it is clear that the next step would be to further investigate the alumina fibers Nextel 610 and CeraFib 99. For this purpose, attention should be given to the effect of short-duration heat treatments on the mechanical properties of the fibers. As seen in the results of the 25 h heat treatments, these fibers are more susceptible to thermal degradation than the mullite fibers. Nevertheless, as the applications of alumina fibers are normally related to moderate temperatures, or short exposures to high temperatures, the evaluation of treatments with only a few hours of duration would be more pertinent. This analysis could also correlate well with the possible fiber degradations occurring during CMCs processing. Furthermore, a detailed analysis on the grain growth kinetics and the development of thermally induced defects should be carried out, as these two parameters are possibly the main reasons for the strength decrease seen for these fibers. For that, the measurement of the grain/crystallite size by SEM after different heat treatments, or in situ XRD at target temperatures, can be a viable option.

As seen on the high-temperature tests, crystal phase transformation plays a big role on the behavior of the mullite fibers. Above 1200°C, their metastable microstructure slowly changes towards the 3/2 stoichiometric mullite. Nonetheless, it is still unclear what can be considered a stable microstructure at each given temperature. Therefore, the formulation of a phase diagram for the mullite fibers would be of extreme importance for such investigations. This is not an easy task, especially considering the complex structure of these fibers. Hence, longer heat treatments should be performed in order to achieve stable microstructures at different temperatures. Particular attention should be given to the crystal phase content of the fibers, as well as the structure of the mullite phase. In situ XRD measurements can also help to identify if a stable microstructure was obtained. The formulation of a phase diagram would be very beneficial not only for the understanding of the long-term behavior of the fibers, but also to help on the development/improvement of new mullite fibers.

Furthermore, all the analyses here performed were done on fibers alone. In a composite however, the fibers are in contact with the matrix and reactions between them might happen at

elevated temperatures. Such reactions will depend on the type of matrix and fibers. Therefore, the study of the fiber microstructural evolution, while embedded in different matrices, is a very interesting topic for a new project. To analyze the effect of different matrix compositions, the most viable way would be by producing mini composites, *i.e.*, 1D composites containing only one fiber bundle. By characterizing the fibers microstructure before and after the processing of the mini composites, the actual impact of the processing conditions of CMCs on the fibers can be quantified. Moreover, the resulting strength of the fibers can be estimated by measuring the strength of the mini composites. This methodology can also be applied to evaluate the effect of long-term exposures on the fibers of a composite. In addition, the results of such analyses can be used to adjust/improve the current CMC processing techniques to account for fiber degradation.

Appendix

A.1. Results of CeraFib 99 and Nextel 610

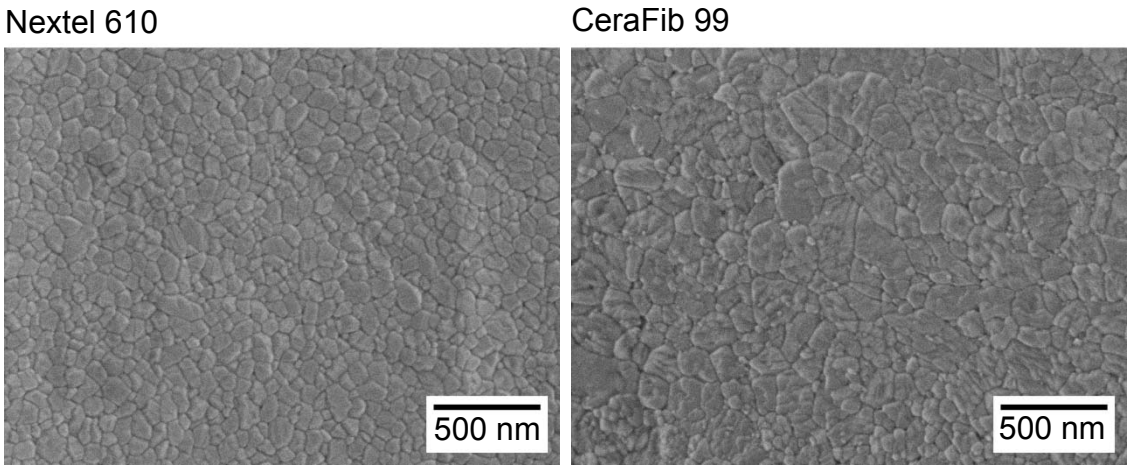

Figure A.1: SEM micrographs showing the microstructure of as-received CeraFib 99 and Nextel 610 fibers.

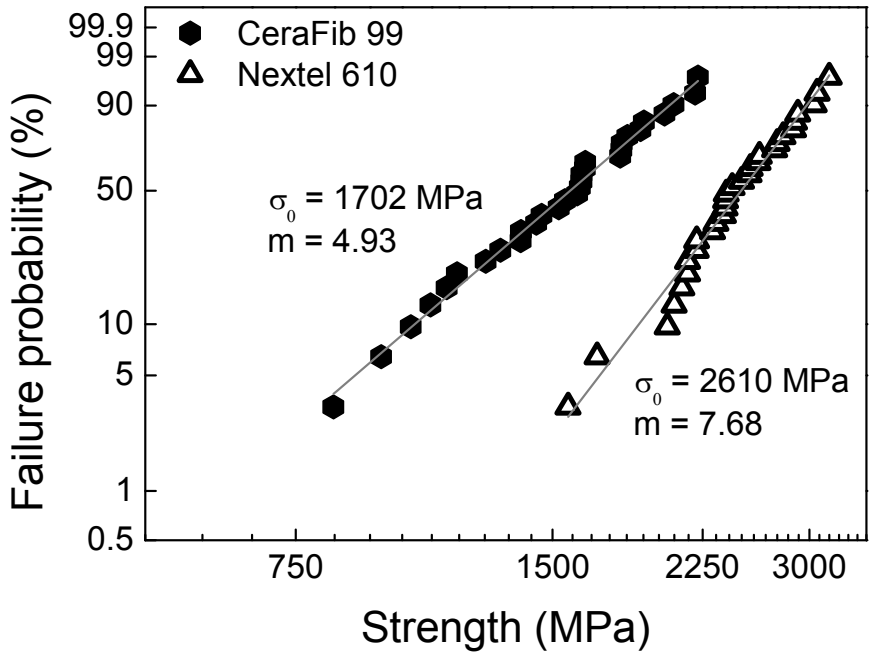

Figure A.2: Weibull failure distribution of tensile strength at room temperature of as-received CeraFib 99 and Nextel 610 filaments.

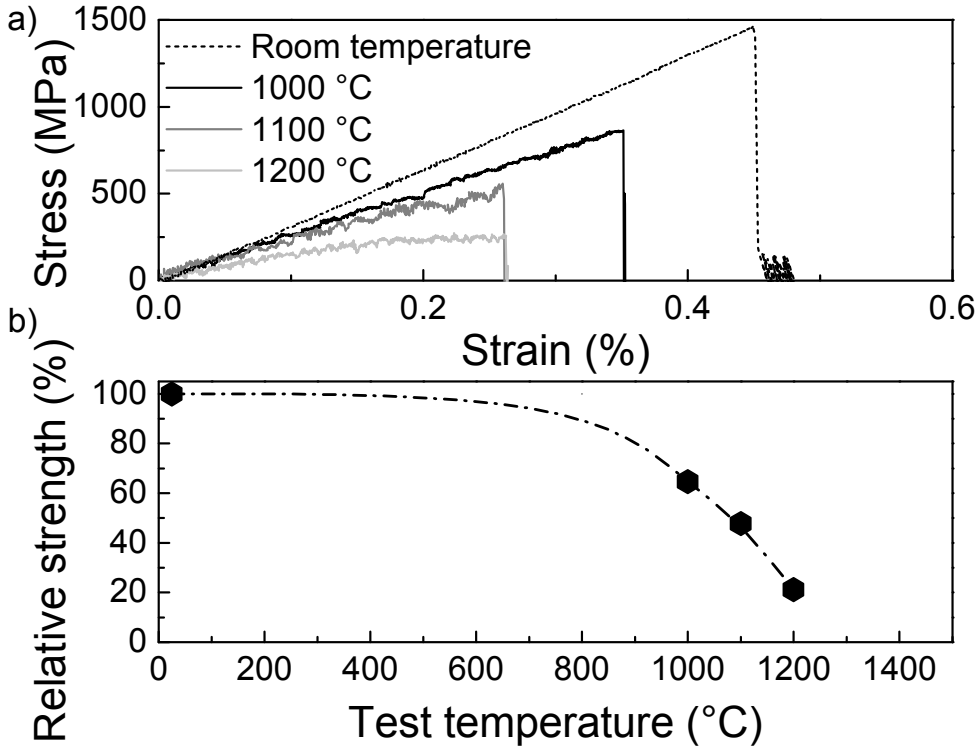

Figure A.3: (a) Stress–strain curves of CeraFib 99 filaments at different testing temperatures. (b) Strength retention of CeraFib 99 tested at different temperatures.

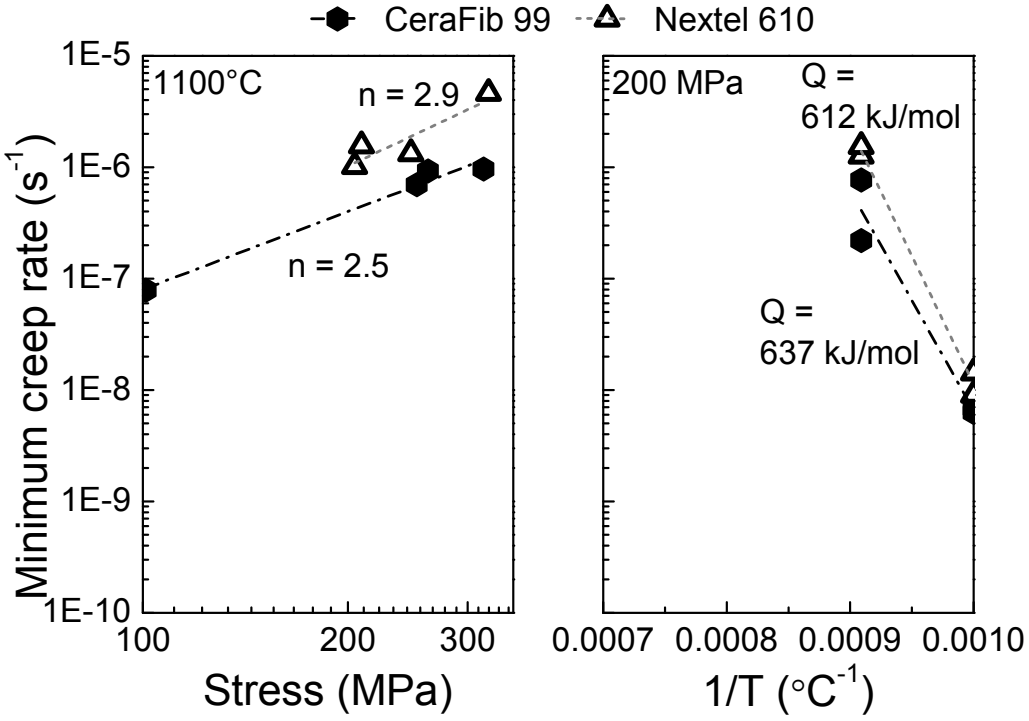

Figure A.4: Stress (left) and temperature (right) effects on creep of CeraFib 99 and Nextel 610 for the determination of n and Q.

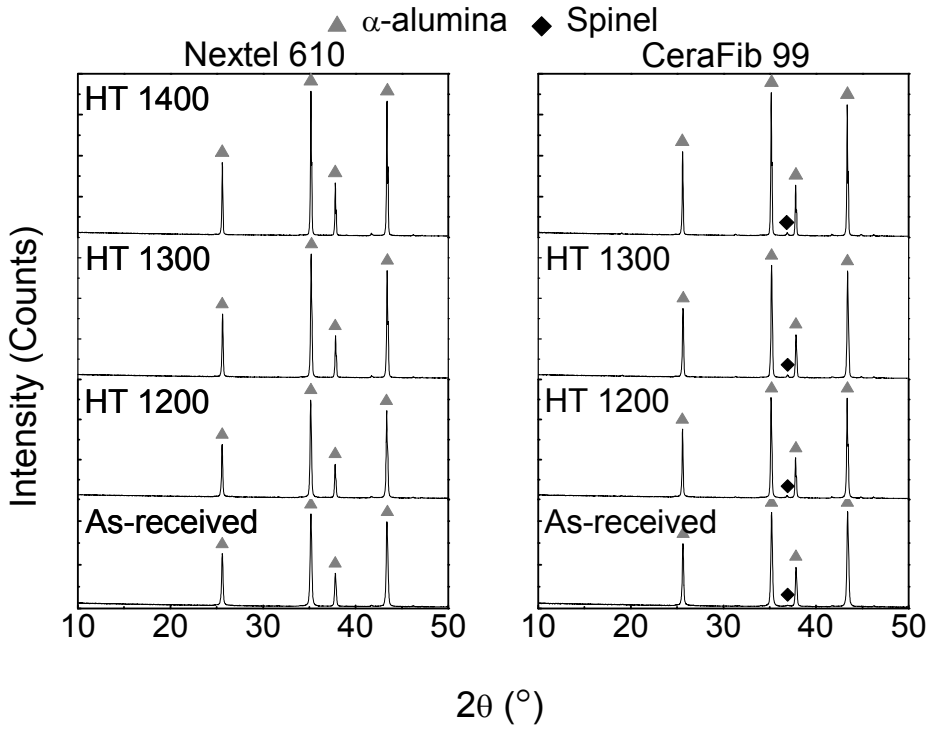

Figure A.5: Sections of X-ray diffraction patterns of CeraFib 99 and Nextel 610 as-received and after heat treatments for 25 h at temperatures of 1200-1400°C. α-alumina was the main phase detected, but CeraFib 99 also presented traces of spinel ($MgAl_2O_4$).

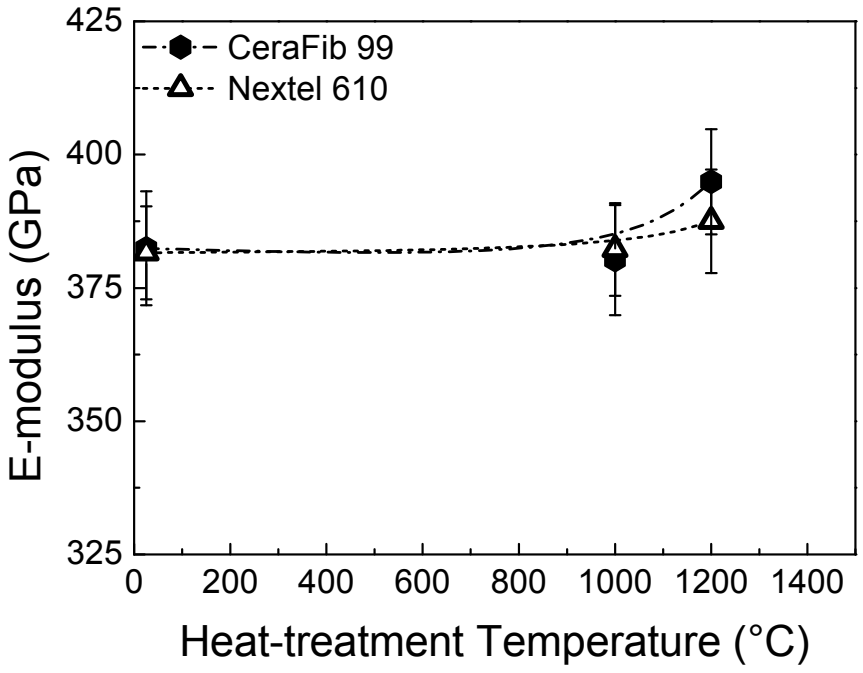

Figure A.6: Measured E-modulus of single filament CeraFib 99 and Nextel 610 as-received and after heat treatments for 25 h at temperatures of 1000-1200°C. Fibers heat treated at 1300°C and 1400°C could not be tested.

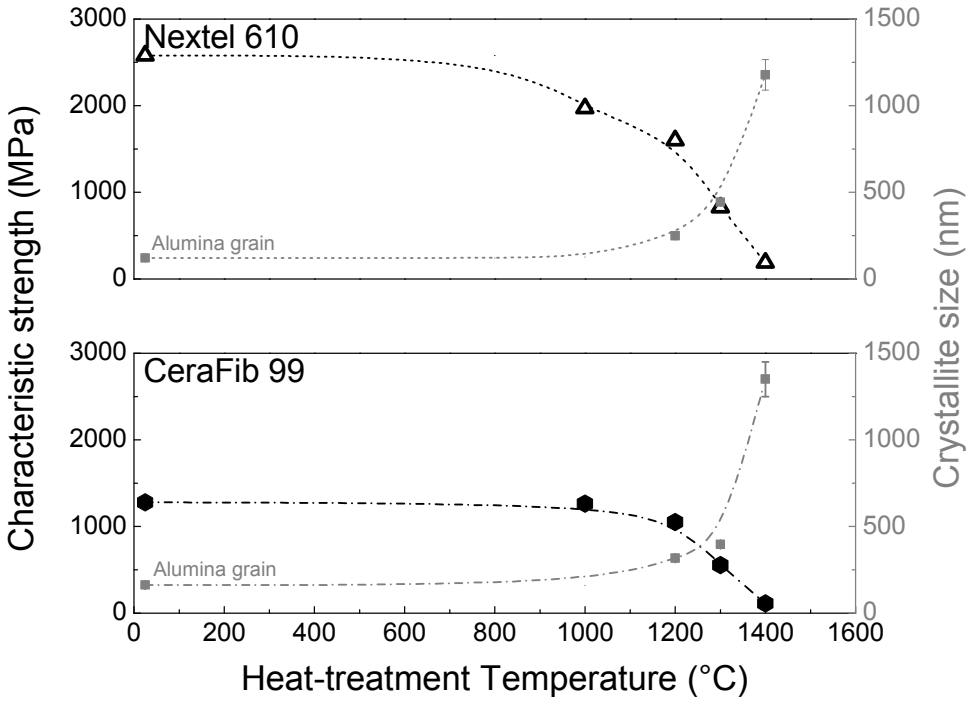

Figure A.7: Strength retention of CeraFib 99 and Nextel 610 as-received and after heat treatments for 25 h at temperatures of 1000-1400°C, and its relation to fiber crystallite growth measured by Rietveld refinements.

A.2. Supporting information for Chapter 2

Table A.1: Results of high-temperature tensile tests of Nextel 720 from different authors.

Author	Loading rate (mm/min)	Test temperature (°C)	Strength (MPa)	E-modulus (GPa)	Ref.
Wilson, 1995					
	0.5	Room temperature	1700		[1]
		1000	1710		
		1200	1450		
		1300	960		
Göring, 1997					
	1000 MPa/s	Room temperature	1510	270	[2]
		800		245	
		900		240	
		1000		235	
		1100		230	
		1200		210	
Milz, 1999					
	1000 MPa/s	Room temperature	1425		[3]
		900	1350		
		1000	1120		
		1100	895		
		1200	510		
Wilson, 2001					
	12.5	Room temperature	100%		[4]
		800	94.5%		
		900	94.0%		
		1000	94.5%		
		1100	88.5%		
		1200	99.0%		
		1300	93.8%		
		1400	87.3%		
Deléglise, 2002					
	1000 MPa/s	Room temperature	1740		[5]
		800	1730		
		900	1740		
		1000	1650		
		1100	1175		
		1200	450		

Dassios, 2003				
0.5	Room temperature	1117	257.7	[6]
	600	1182	128.2	
	800	1050	146.1	
	1000	950	151.1	
	1100	767	54.6	
	1200	646	25.7	

Table A.2: Room-temperature properties of Nextel 720 after thermal exposures measured by different authors.

Author	Exposure temperature (°C)	Exposure time (h)	Strength (MPa)	Grain size (nm)	Ref.
Das, 1995					
	As-received		2390		[7]
	982	250	2350		
		500	2110		
Göring, 1997					
	As-received		100%	320	[2]
	1200	2	103%	320	
	1300	2	89.9%	350	
	1400	2	57.7%	390	
	1500	2	44.0%		
Hay, 1999*					
	As-received		1995	63	[8]
	1000	100	1870		
	1100	2	1830		
	1200	2	1650		
		100	1040		
	1250	1	1550		
		10	1180		
		100	870		
	1300	1	1350	73	
		2	1590		
		10	1440	80	
		100	1180	104	
	1350	20 min		72	
		1	1410	84	
		3		101	
		10	1210	115	
		30		154	
		100	950	207	
		300		277	
	1400	1	1100	108	
		2	1170		
		3		120	
		10	980	142	
		30		236	
		100	730	267	
		300		286	

	1450	20 min		130	
		1	830	162	
		3		195	
		10		273	
		30		451	
		100		753	
Milz, 1999					
	As-received		1425		[3]
	1200	1	850		
Petry, 1999					
	As-received		1900		[9]
	1050	2	1700		
	1100	2	1830		
	1200	2	1650		
	1300	2	1590		
	1400	2	1170		
Deléglise, 2001					
	As-received		1620	300-500	[10]
	1200	5	1540		
		240		300-500	
	1300	5	1525	250-500	
		240		270-500	
	1400	5	1670	250-500	
		24	1360	300-500	
		96	1040	500-1000	
	1500	84		1000	
Wilson, 2002					
	As-received		2100		[11]
	1000	100	1945		
	1100	100	1900		
	1200	100	1750		
	1300	100	1790		
	1400	100	1190		
Schmücker, 2012					
	As-received		2150	270	[12]
	1200	1	1890	270	
	1300	1	1750	280	
	1400	1	1640	310	
	1500	1		500	

*Values of grain size are given as the inverse log-average [8].

A.3. Supporting information for Chapter 3

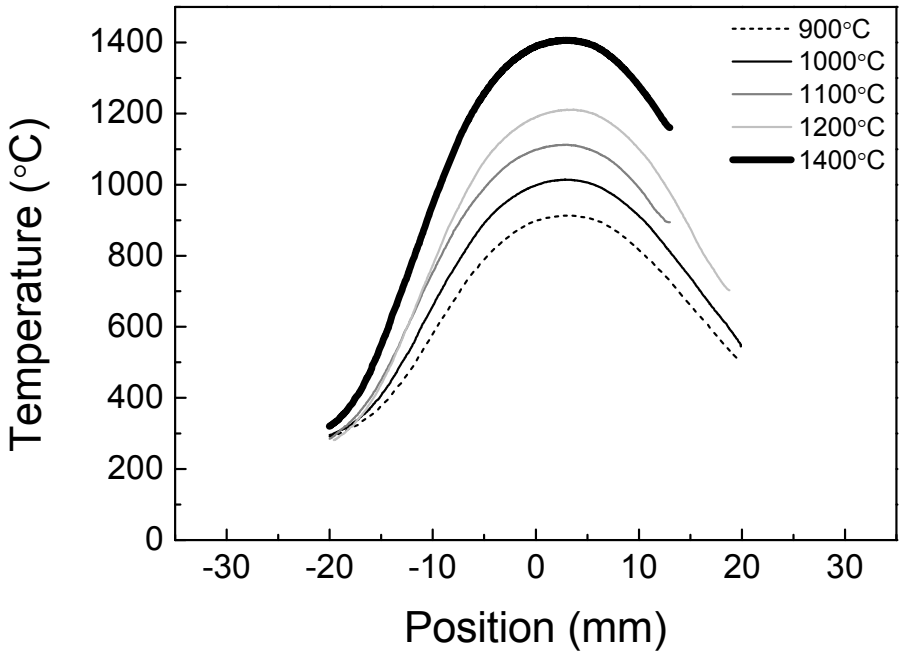

Figure A.8: Temperature profile of the oven used for single filament tensile tests at the tested maximum temperatures.

A.4. Supporting information for Chapter 5

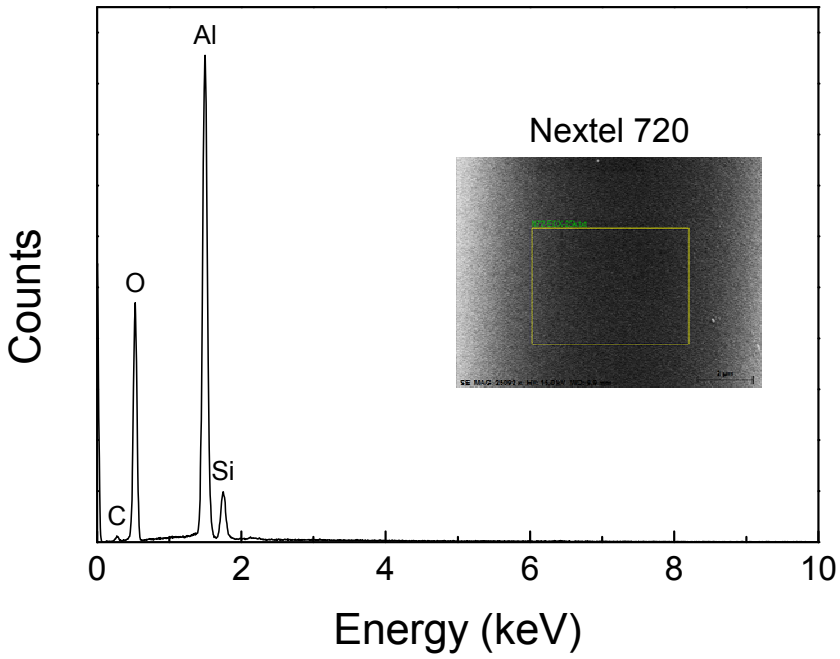

Figure A.9: EDX analysis of Nextel 720 fiber. Note that the fibers were coated with carbon for the analysis, and therefore, the content of C should be disregarded.

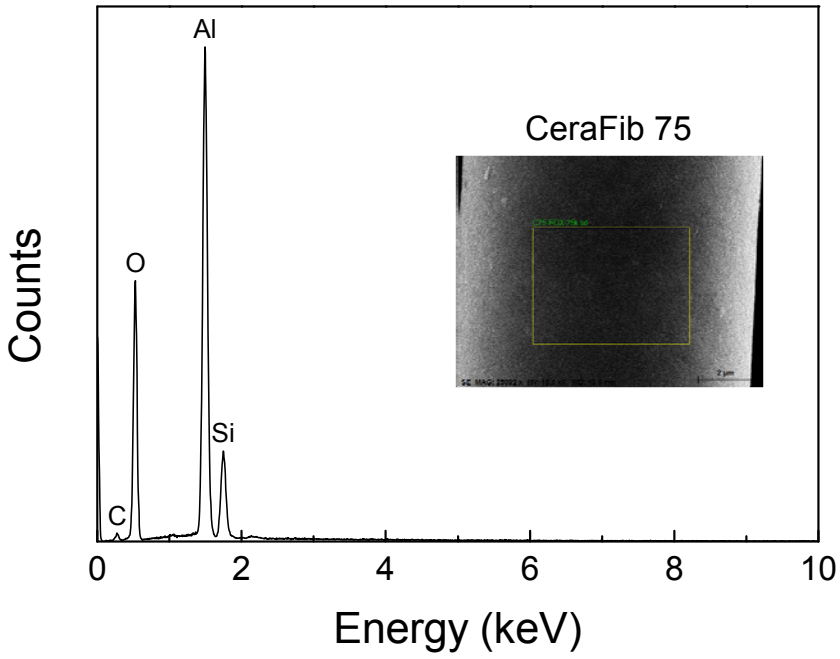

Figure A.10: EDX analysis of CeraFib 75 fiber. Note that the fibers were coated with carbon for the analysis, and therefore, the content of C should be disregarded.

A.5. Supporting information for Chapter 6

Table A.3: R-values of Rietveld refinements on as-received fibers.

Measurement	Rwp	Rp	RB (mullite)	RB (α-Al_2O_3)	RB (γ-Al_2O_3)
25°C	9.32	7.01	6.323	4.072	5.228
200°C	9.38	7.13	6.419	3.068	5.509
400°C	9.39	7.11	6.313	4.716	4.245
600°C	9.47	7.14	6.287	3.173	5.218
800°C	9.55	7.26	6.024	4.342	3.890
1000°C	9.59	7.23	5.832	3.446	3.591
1200°C, 1st	9.42	7.11	5.743	4.434	2.888
1200°C, 2nd	9.45	7.14	5.725	7.679	3.416
1200°C, 3rd	9.33	7.08	5.924	7.130	7.965
1200°C, 4th	9.29	7.07	5.896	4.811	6.725
1200°C, 5th	9.28	6.96	5.613	4.280	2.818
1200°C, 6th	9.22	7.07	5.848	4.869	7.280
1200°C, 7th	9.19	6.93	5.704	3.573	2.452
1200°C, 8th	9.21	6.93	5.634	3.387	2.839
1200°C, 9th	9.34	7.06	5.907	3.412	2.669
1200°C, 10th	9.20	6.98	5.750	6.008	2.685
1200°C, 11th	9.34	7.09	5.773	5.957	2.113

$Rwp = (\Sigma_i w_i(y_{io} - y_{ic})^2 / \Sigma_i w_i y_{io}^2)^{1/2}$;
$Rp = \Sigma_i|y_{io} - y_{ic}| / \Sigma_i y_{io}$;
$RB = \Sigma_k|I_{ko} - I_{kc}| / \Sigma_k I_{ko}$;
y_{io}/y_{ic} = observed/calculated step-intensity;
I_{ko}/I_{kc} = observed/calculated integrated intensity of reflection k;
w = weighting factor.

Table A.4: R-values of Rietveld refinements on HT 1400 fibers.

Measurement	Rwp	Rp	RB (mullite)	RB (α-Al_2O_3)
25°C	6,73	5.11	2.000	1.757
200°C	6.79	5.25	2.272	1.674
400°C	6.96	5.44	2.78	2.012
600°C	7.16	5.63	3.137	1.761
800°C	7.16	5.63	3.138	1.760
1000°C	7.64	6.09	4.461	2.003
1200°C, 1st	8.06	6.44	5.180	2.078
1200°C, 2nd	8.01	6.38	5.099	1.727
1200°C, 3rd	7.96	6.35	4.903	2.174
1200°C, 4th	8.14	6.45	5.051	2.396
1200°C, 5th	8.02	6.40	5.001	1.985
1200°C, 6th	8.06	6.42	5.016	1.883
1200°C, 7th	8.00	6.35	5.107	1.868
1200°C, 8th	8.10	6.44	5.216	2.251
1200°C, 9th	7.93	6.29	4.871	2.117
1200°C, 10th	8.04	6.43	4.999	2.140
1200°C, 11th	7.95	6.31	5.040	1.986

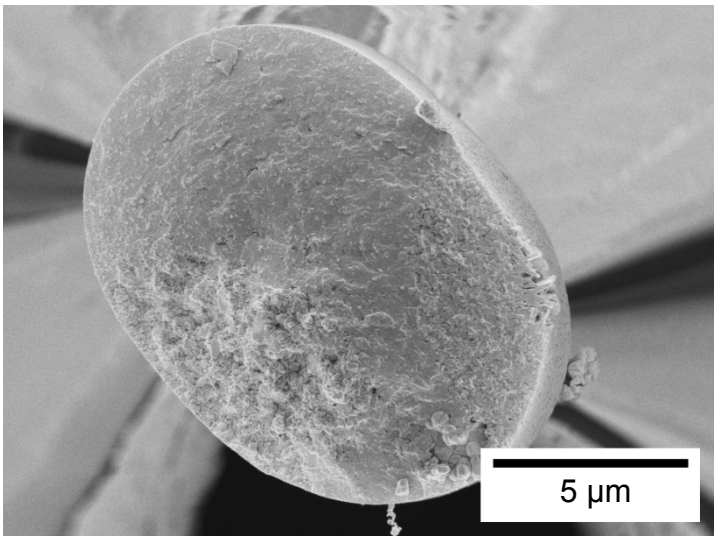

Figure A.11: Fracture surface Nextel 720 fiber tested under creep loading at 1200°C with the stress of 240 MPa. Fracture was first intergranular, and then planar intragranular. Grain growth was also detected in the surface.

A.6. References

[1] D. M. Wilson, S. L. Lieder, D. C. Lueneburg. “Microstructure and high temperature properties of Nextel 720 fibers”, pp. 1005-1014 in *Proceedings of 19th Annual Conference on Composites, Advanced Ceramics, Materials, and Structures*, J. B. Wachtman Jr. (Ed.). John Wiley & Sons, Inc., 2008.

[2] J. Göring, H. Schneider. “Creep and subcritical crack growth of Nextel 720 alumino silicate fibers as received and after heat treatment at 1300°C”, pp. 95-102 in *21st Annual Conference on Composites, Advanced Ceramics, Materials, and Structures*, J. P. Singh (Ed.). John Wiley & Sons, Inc., 2008.

[3] C. Milz, J. Goering, H. Schneider. “Mechanical and microstructural properties of Nextel™ 720 relating to its suitability for high temperature application in CMCs”, pp. 191-198 in *Proceedings of 23rd Annual Conference on Composites, Advanced Ceramics, Materials, and Structures*, E. Ustundag, G. Fischman (Eds.). John Wiley & Sons, Inc., 2008.

[4] D. M. Wilson, L. R. Visser. “High performance oxide fibers for metal and ceramic composites”. Composites Part A: Applied Science and Manufacturing, vol. 32 (8), pp. 1143-1153, 2001.

[5] F. Deléglise, M. H. Berger, A. R. Bunsell. “Microstructural evolution under load and high temperature deformation mechanisms of a mullite/alumina fibre”. Journal of the European Ceramic Society, vol. 22 (9–10), pp. 1501-1512, 2002.

[6] K. G. Dassios, M. Steen, C. Filiou. “Mechanical properties of alumina Nextel™ 720 fibres at room and elevated temperatures: Tensile bundle testing”. Materials Science and Engineering: A, vol. 349 (1–2), pp. 63-72, 2003.

[7] G. Das. “Thermal stability of single crystal and polycrystalline alumina fibers and 85% Al_2O_3-15 % SiO_2 fibers”, pp. 977-986 in *19th Annual Conference on Composites, Advanced Ceramics, Materials, and Structures*, J. B. Wachtman Jr. (Ed.). John Wiley & Sons, Inc., 2008.

[8] R. S. Hay, E. E. Boakye, M. D. Petry, Y. Berta, K. Von Lehmden, J. Welch. “Grain growth and tensile strength of 3M Nextel 720™ after thermal exposure”, pp. 153-163 in *Proceedings of 23rd Annual Conference on Composites, Advanced Ceramics, Materials, and Structures*, E. Ustundag, G. Fischman (Eds.). John Wiley & Sons, Inc., 2008.

[9] M. D. Petry, T.-I. Mah. “Effect of thermal exposures on the strengths of Nextel™ 550 and 720 filaments”. Journal of the American Ceramic Society, vol. 82 (10), pp. 2801-2807, 1999.

[10] F. Deléglise, M. H. Berger, D. Jeulin, A. R. Bunsell. “Microstructural stability and room temperature mechanical properties of the Nextel 720 fibre”. Journal of the European Ceramic Society, vol. 21 (5), pp. 569-580, 2001.

[11] D. M. Wilson. “New high temperature oxide fibers”, pp. 1-12 in *High Temperature Ceramic Matrix Composites*, W. Krenkel, R. Naslain, H. Schneider (Eds.). Wiley-VCH Verlag GmbH & Co. KGaA, 2002.

[12] M. Schmücker, F. Flucht, P. Mechnich. “Degradation of oxide fibers by thermal overload and environmental effects”. Materials Science and Engineering: A, vol. 557 (0), pp. 10-16, 2012.

Supervised student projects

This work could not have been accomplished without the help of several motivated and hard working students. Therefore, the following students are gratefully acknowledged.

Rech, M. B. R.	"Effect of matrix composition on the mechanical behavior of oxide mini-composites after processing and thermal exposure" Diploma thesis, 2016
Mainardi, J. C.	"Thermal degradation of oxide fibers during composites processing" Diploma thesis, 2016
Rescala, J. P.	"Microstructure evolution of oxide fibers during minicomposites processing" Internship, 2015
Chiedozie, A. E.	"Development and characterization oxide ceramic minicomposites" Internship, 2015
Bergmüller, E. L.	"Thermal aging effects on the mechanical behavior of oxide ceramic fibers" Diploma thesis, 2014
Eggert, B. G. F.	"Evaluation of different testing techniques on the mechanical properties of novel oxide fibers" Diploma thesis, 2014
Singh, A. **Zahn, D.** **Thomas, G.** **Cramer, L.** **Alghazawi, M.**	"Charakterisierung von neuen oxidkeramischen Fasern" *Lehrprojekt*, 2013

BLANK PAGE

Curriculum vitae

Surname:	Saint Martin Almeida
First name:	Renato
Date / Place of birth:	1. Sep. 1990 / Rio de Janeiro, Brazil
Nationality:	Brazilian

Education

09.2012	Diploma in Materials Engineering Universidade Federal de Santa Catarina (UFSC) – Florianópolis, Brazil
12.2007	High school Colégio Energia – Florianópolis, Brazil
12.2004	Elementary school Colégio Nossa Senhora de Fátima – Florianópolis, Brazil

Professional / Research Experience

03.2013 – Today	Ph.D. student Advanced Ceramics group, Universität Bremen – Bremen, Germany Scholarship from "National Counsel of Technological and Scientific Development" – CNPq, Brazil
05.2012 – 08.2012	Internship Intelbras S/A – São José, Brazil Topic: Injection molding of polymer components
05.2011 – 01.2012	Research assistant student / Diploma thesis Advanced Ceramics group, Universität Bremen – Bremen, Germany Topic: Mechanical properties of ceramic matrix composites
05.2010 – 05.2011	Research assistant student Heat Pipe Laboratory (LEPTEN), UFSC – Florianópolis, Brazil Topic: Characterization of mini heat pipes Scholarship from "National Counsel of Technological and Scientific Development" – CNPq, Brazil

02.2010 – 05.2010	Internship Metalúrgica Fey S/A – Indaial, Brazil Topic: Forming, heat treatments and quality control of fasteners
05.2009 – 09.2009	Internship Nitrion do Brasil Ltda. – Guaramirim, Brazil Topic: Ion nitriding (plasma nitriding) of metallic components

Awards / Additional qualifications

09.2012	Diploma of Merit - Best student of Materials Engineering Awarded by Ministry of Education – CAPES / UFSC, Brazil
Portuguese	Mother tongue
English	Fluent
German	Fluent
Spanish	Intermediary
IT knowledge	Maple, Matlab, Microcal Origin, Microsoft Office, Solid Works

List of publications

Peer-reviewed

P. Xiao, Y.-h. Lu, Y.-z. Liu, Z. Li, H.-c. Fang, W. Zhou, **R. S. M. Almeida** , Y. Li. "Microstructure and properties of Cu-Ti alloy infiltrated chopped C_f reinforced ceramics composites". Ceramics International, vol. 43 (18), pp. 16628-16637, 2017.

R. S. M. Almeida, E. L. Bergmüller, H. Lührs, M. Wendschuh, B. Clauß, K. Tushtev, K. Rezwan. "Thermal exposure effects on the long-term behavior of a mullite fiber at high temperature". Journal of the American Ceramic Society, vol. 100 (9), pp. 4101-4109, 2017.

Y. Li, P. Xiao, Y. Shi, **R. S. M. Almeida**, W. Zhou, Z. Li, H. Luo, F. Reichert, N. Langhof, W. Krenkel. "Mechanical behavior of LSI based C/C-SiC composites subjected to flexural loadings". Composites Part A: Applied Science and Manufacturing, vol. 95 (0), pp. 315-324, 2017.

Y. Li, P. Xiao, H. Luo, **R. S. M. Almeida** , Z. Li, W. Zhou, A. Brückner, F. Reichert, N. Langhof, W. Krenkel. "Fatigue behavior and residual strength evolution of 2.5D C/C-SiC composites". Journal of the European Ceramic Society, vol. 36 (16), pp. 3977-3985, 2016.

R. S. M. Almeida, E. L. Bergmüller, B. G. F. Eggert, K. Tushtev, T. Schumacher, H. Lührs, B. Clauß, G. Grathwohl, K. Rezwan. "Thermal exposure effects on the strength and microstructure of a novel mullite fiber". Journal of the American Ceramic Society, vol. 99 (5), pp. 1709-1716, 2016.

R. S. M. Almeida, K. Tushtev, B. Clauß, G. Grathwohl, K. Rezwan. "Tensile and creep performance of a novel mullite fiber at high temperatures". Composites Part A: Applied Science and Manufacturing, vol. 76 (0), pp. 37-43, 2015.

Book section

K. Tushtev, **R. S. M. Almeida** . "Oxide/oxide CMCs – Porous matrix composite systems; Composites with interface coatings", pp. 130-157 in *Comprehensive Composite Materials II*, P. W. R. Beaumont, C. H. Zweben (Eds.), vol. 5. Elsevier, 2017.

Conference presentation/proceedings

R. S. M. Almeida , M. B. R. Rech, J. C. Mainardi, K. Tushtev, K. Rezwan. "Microstructure evolution and property changes of oxide fibers during processing and thermal exposure of minicomposites". In *21. Symposium Verbundwerkstoffe und Werkstoffverbunde*, Bremen, Germany, 2017.

R. S. M. Almeida , K. Tushtev, K. Rezwan. "Microstructure evolution and long-term performance of a novel mullite fiber at high temperatures". In *9th International Conference on High Temperature Ceramic Matrix Composites*, Toronto, Canada, 2016.

J. P. M. Florez, G. G. V. Nuernberg, M. B. H. Mantelli, **R. S. M. Almeida** , A. N. Klein. "Effective thermal conductivity of layered porous media". In *Proceedings of 10th International Heat Pipe Symposium*, Taipei, Taiwan, 2011.

G. G. V. Nuernberg, J. P. M. Florez, K. Paiva, **R. S. M. Almeida** , M. B. H. Mantelli, A. N. Klein, F. Reis, J. B. Santos. "Experimental Permeability of Sintered Porous media Multilayer". In *Proceedings of 21st Brazilian Congress of Mechanical Engineering*, Natal, Brazil, 2011.